# Conversion of Microalgae into Hydrogen- or Methane-rich Syngas

*A Thesis*
*Submitted in partial fulfillment of the requirements*
*of the degree of*
***Doctor of Philosophy***
*of the*
*Indian Institute of Technology Bombay, India*
*&*
*Monash University, Australia*
*by*

**Pratik Vinayak Gholkar**
(144024003 and 26414643)

Supervisors:
**Prof Yogendra Shastri (IIT Bombay)**
and
**Prof Akshat Tanksale (Monash University)**

*The course of study was developed jointly by Monash University, Australia and the Indian Institute of Technology Bombay, India and was given academic recognition by each of them.*

*The programme was administrated by The IITB-Monash Research Academy*

May 2020

© *May 2020, by Pratik Vinayak Gholkar*

*All rights reserved*

# Acknowledgements

This thesis marks the end of my most cherished years as a research scholar at the IITB-Monash Research Academy. As I write the most crucial bit of my thesis, the acknowledgement, I feel blessed to have had such strong support from my advisers, my lab mates, my industrial collaborators, and my family. I want to express my sincere gratitude to all of those who helped me to complete this thesis.

First, I am indebted to my thesis advisers, Prof. Yogendra Shastri and Prof. Akshat Tanksale. They believed in me like nobody else and gave me endless support. It all started in June 2014 when I joined their group. They taught me what research is? Under their guidance, I learned how to identify and solve a problem. On a personal level, they have always motivated me by their passion for research. To summarise, I would give them most of the credit for becoming the kind of researcher I am today. Besides my advisor, I would like to thank my research progress committee members, Prof. Sharad Bhartiya (IIT B) and Prof. Meng Woo (Monash University). Their valuable feedback helped me to improve my thesis in many ways. I take this opportunity to gratefully acknowledge my industry parter JSW Group for supporting my project. I am also thankful to my industry mentor Dr Suman Majumdar (Chief Sustainability Officer, JSW Group) for his guidance and technical inputs during the project.

Special mention goes to my enlightening discussions with Prof. Murali Sastry, which taught me the subtlety of material characterisation techniques. I vividly remember all the technical and non-technical conversation I had with him, which shaped my perspective on life. I am also hugely appreciative to Dr Kyatanahalli Nagabhushana for his tremendous support and providing me with so many wonderful opportunities to learn chemistry and various instruments.

My time at Monash University was made enjoyable in large part due to many friends and groups that became a part of my life. I am grateful for time spent with roommates and friends; I have fond memories of cooking with Nikhil, Jhumur, Harini, Karan and Tushar. I cherish all the trips with my backpacking buddies, Ashwin and Aayush. A very special thank you to Fan Liang Chan (Frank) for his invaluable advice and feedback on reactive

flash volatilisation. I take this opportunity to thank Ms Sheryl Moh for introducing me to the lab and Ms Tig Yosef for helping me with catalyst synthesis. Also, I would like to give my sincere thanks to Mr Harry, Mr Ross and all the colleagues from G11, G12 and G13 (Monash University) for always being so supportive of my work.

I am grateful to all the staff of Sophisticated and Analytical Instrumentation Facility (SAIF) and Industrial Research and Consultancy Centre (IRCC) at IIT Bombay for allowing me to access various characterisation facilities. I would also like to thank all the lab mates from automation lab for supporting me unconditionally.

I would also like to thank...

Beena Ma'am for conducting a separate entrance exam for me. You made a special place for yourself in this effort of mine! Nancy Ma'am for all the prayers and appointments with prof Sastry. Jayasree Ma'am for resolving my candidature issues. Kuheli Ma'am for coordinating all the research finance. Kiran for helping me with academic facilities. Last but not least, Laya Ma'am, for all the discussions, special considerations, and unconditional help. I will cherish these memories for a lifetime.

Finally, I am thankful to my Aai, Mrs Medha Vinayak Gholkar, and Baba, Mr Vinayak Vasudeo Gholkar for believing in me and providing me with all the opportunities that they never had. You made me! Love you both.

***Pratik Vinayak Gholkar***
IITB-Monash Research Academy
May 2020

# List of Publications

## Indian Patents

- P. Gholkar, A. Tanksale, and Y. Shastri, Catalytic conversion of microalgae into hydrogen-rich syngas using reactive flash volatilization.2017; Indian Patent:201721042669
- P. Gholkar, A. Tanksale, and Y. Shastri, Catalytic conversion of microalgae into hydrogen-rich syngas using reactive flash volatilization.2017; Indian Patent:201721042668

## Journal Articles

- P. Gholkar, A.Tanksale, and Y. Shastri, Catalytic conversion of microalgae into hydrogen- and methane-rich syngas using catalytic reactive flash volatilization, Applied Catalysis B:Environmental, 251 (2019) 326 - 334
- P. Gholkar, Y. Shastri, and A.Tanksale, Renewable hydrogen and methane production from microalgae:A techno-economic and life cycle assessment. (Submitted to Journal of Cleaner Production)

## Conference Paper

- P. Gholkar, A.Tanksale, Y. Shastri and S. Majumdar, Catalytic conversion of microalgae into hydrogen- and methane-rich syngas using catalytic steam gasification, TOCAT 8, Japan, 2018.

# Abstract

The need for energy is increasing with the socio-economic development of an individual, and on the other hand, climate change concerns have led to an increasing push for cleaner energy options. To meet this increasing energy demands while transitioning from carbon-based energy to clean energy is one of the grand challenges for a sustainable future. Hydrogen is regarded as the clean source since it does not lead to the emissions of greenhouse gases (GHG). However, at present, 96% of the hydrogen is produced through non-renewable and non-environmentally friendly routes. Likewise, methane which is a starting chemical for a variety of chemical synthesis processes is produced mostly through natural gas extraction. Microalgae is the potential candidate to produce renewable hydrogen and methane. However, char- and tar-accumulation limits the current gasification technologies. Catalytic reactive flash volatilisation (RFV) is a single-step char- and tar-free alternative to the gasification process.

In this work, catalytic RFV of microalgae (*Scenedesmus sp.*) was performed using steam as a gasifying agent to produce hydrogen- or methane-rich syngas. *Scenedesmus sp.* was selected due to its high $CO_2$ tolerance. A downdraft, fixed bed quartz reactor was used to perform the RFV of microalgae. A vertical tubular furnace was used to heat the quartz reactor at the desired temperature. The flow rate of microalgae and steam was maintained at specific carbon-to-steam ratio (CSR) using a twin-screw feeder and a HPLC pump, respectively. The gases were analysed using gas chromatography.

The effect of temperature and steam content on the gasification efficiency and syngas composition was studied in presence of Ni-Rh/$\gamma$-$Al_2O_3$ catalyst which showed that at 650 °C and carbon-to-steam ratio (CSR) of 0.12, $H_2$ rich (65% (v/v)) syngas was generated, whereas, in presence of Ni-Cu-Pd/$\gamma$-$Al_2O_3$ catalyst at 600 °C and CSR of 0.12, $CH_4$ rich (16% (v/v)) syngas was generated. Gasification efficiency of 83% and 93%, respectively, was achieved without tar formation. Moreover, the molar ratio of $H_2$-to-CO in case of $H_2$-rich syngas was 10.9.

Furthermore, a detailed analysis of ash transformation characteristics of alkali and alkaline earth metals (AAEM) was performed to establish their catalytic properties. It

was observed that potassium and magnesium coated nanospheres of calcium phosphates were formed during the reaction. Depending upon the ash transformation characteristics, a novel reaction mechanism was proposed for RFV of microalgae.

The experimental results were used to develop a detailed ASPEN PLUS® flowsheet model to perform techno-economic assessment of hydrogen and methane production. A plant located in India, processing 12790 kg/h of microalgae to produce 1239 kg/h of $H_2$ or 3484.96 kg/h of $CH_4$ was considered. Process scale-up and heat integration principles were used to generate relevant data. Simultaneously, the experimental and simulation data are used to perform life cycle assessment (LCA). The results indicated that the payback period for hydrogen production was 3.78 years with 22% of IRR. Moreover, the life cycle climate change impact was 7.56 kg $CO_2$-eq./ kg $H_2$ produced, which was 36.47% lower than the steam reforming of methane. Methane production was not economically feasible. However, it was environmentally preferred with the life cycle climate change impact of 1.18 kg $CO_2$-eq./ kg $CH_4$ produced. Sensitivity analysis was performed to identify opportunities to achieve further reduction in costs and life cycle impacts.

# Table of Contents

**Acknowledgements** **ix**

**Declaration** **ix**

**List of Publications** **xi**

**Abstract** **xiii**

**List of Figures** **xix**

**List of Tables** **xxi**

**1 Introduction** **1**

**2 Literature Review** **5**

2.1 Renewable Hydrogen Production . . . . . 5

2.1.1 Hydrogen production using electrical energy . . . . . 6

2.1.2 Hydrogen production using solar energy . . . . . 6

2.1.3 Hydrogen production using thermochemical energy . . . . . 8

2.2 Renewable Methane Production . . . . . 14

2.3 Microalgae . . . . . 14

2.4 Microalgae processing . . . . . 15

2.4.1 Dry processing . . . . . 15

2.4.2 Wet processing . . . . . 16

2.4.3 Hydrogen production from microalgae . . . . . 16

2.4.4 Methane production from microalgae . . . . . 20

2.5 Catalyst selection . . . . . 21

2.6 Research Gaps . . . . . 23

**3 Materials and Methods** **25**

3.1 Catalyst preparation . . . . . 25

3.2 Catalyst Characterisation . . . 25
3.2.1 Nitrogen physisorption . . . 26
3.2.2 X-Ray fluorescence spectroscopy . . . 26
3.2.3 Temperature programmed reduction (TPR) . . . 26
3.2.4 Carbon monoxide temperature programmed desorption (CO-TPD) 27
3.2.5 Carbon monoxide chemisorption (CO-Chemisorption) . . . 27
3.2.6 Transmission Electron Microscopy (TEM) . . . 27
3.3 Biomass Feedstock and characterisation . . . 28
3.4 Slag Characterisation . . . 28
3.4.1 X-ray Computed Tomography (X-Ray CT) . . . 28
3.4.2 Scanning Electron Microscopy (SEM) . . . 28
3.4.3 X-ray Photoemission Spectroscopy (XPS) . . . 29
3.5 Reactor setup . . . 30
3.6 Approach . . . 31

**4 Results and Discussions 35**
4.1 Catalyst Characterisation . . . 35
4.1.1 Nitrogen physisorption and XRF analysis . . . 35
4.1.2 Temperature Programmed Reduction (TPR) . . . 36
4.1.3 Carbon monoxide temperature programmed desorption (CO-TPD) 37
4.1.4 Effect of steam content and temperature . . . 38
4.2 Ash transformation characteristics . . . 40
4.3 Reaction mechanism . . . 45
4.4 Catalyst Stability . . . 48

**5 Techno-Economic and Life Cycle Assessment 51**
5.1 Hydrogen production . . . 51
5.1.1 Area 100H: Reactive flash Volatilization of microalgae . . . 51
5.1.2 Area 200H: LT-shift and hydrogen purification . . . 54
5.2 Methane Production . . . 54
5.2.1 Area 100M: Reactive flash volatilization of microalgae . . . 54
5.2.2 Area 200M: CO-methanation and LT-shift . . . 56
5.2.3 Area 300M: Methane purification . . . 56
5.3 TEA Methodology . . . 60
5.4 LCA methodology . . . 62
5.5 Feasibility Assessment . . . 63
5.6 LCA analysis . . . 68

5.7 Scale-up challenges . . . . . 70
5.7.1 Microalgae cultivation . . . . . 70
5.7.2 $CO_2$ sequestration . . . . . 71
5.7.3 Process design . . . . . 71

**6 Conclusion and Prospects** **73**

**A Supporting Information** **75**

# List of Figures


2.1 Comparison of various thermochemical conversion processes . . . . . 11
2.2 Processing alternatives for algae . . . . . 15

3.1 Schematic diagram of TPR and TPD setup . . . . . 26
3.2 Reactor setup used to evaluate the catalytic activity during reactive flash volatilization of microalgae . . . . . 30
3.3 Approach towards reactive flash volatilization of microalgae . . . . . 31

4.1 TPR profile of the catalyst. a) Ni-Cu-Pd and b) Ni-Rh . . . . . 36
4.2 TPD profile of the tri-metallic catalyst. **a**: desorption of CO. **b**: desorption of $CO_2$ . . . . . 37
4.3 Effect of steam content on the distribution of the compounds in the syngas 38
4.4 Effect of temperature on the distribution of the compounds in the syngas . 38
4.5 Effect of temperature on the ratio of hydrogen to carbon monoxide ($H_2$/CO) 39
4.6 XRD pattern for ash and slag. (a) XRD of ash before reaction, (b) XRD of transformed ash (slag) . . . . . 41
4.7 XPS analysis of Phosphorus 2p to confirm a chemical shift after reaction. A) Phosphorus in ash and B) Phosphorus in slag . . . . . 42
4.8 XPS analysis of Potassium 2s to confirm a chemical shift after reaction. A) Potassium in ash and B) Potassium in slag . . . . . 42
4.9 XPS analysis of Magnesium 1s to confirm a chemical shift after reaction. A) Magnesium in ash and B) Magnesium in slag . . . . . 42
4.10 SEM Figures showing a morphological comparison of ash before reaction (A and B) and after reaction-slag (C and D). . . . . 43
4.11 SEM EDX Figure showing the presence of Phosphorus, Calcium, Potassium and Magnesium on the spherical nanoparticles present in the slag . . 44
4.12 SEM Figure showing a evolution of highly porous structure of a slag. A) Nanoparticle– a fundamental unit of a bead B) Agglomeration of nanoparticles to form a bead and C) Steps in the evolution of a porous structure. . 44

4.13 Proposed mechanism for reactive flash volatilization of microalgae. A shows the initial stages of RFV. B shows the formation of slag bed on top of the catalyst . . . . . 46
4.14 Image showing a slag bed formed in the reactor during RFV of microalgae. (a) Optical image of the slag bed formed during RFV and (b) X-Ray CT image of the slag bed formed during RFV . . . . . 47
4.15 STEM Figure of fresh and used Ni-Cu-Pd catalyst showing the presence of Nickel, Copper, and Palladium on the surface . . . . . 48
4.16 STEM Figure of fresh and used Ni-Rh catalyst showing the presence of Nickel, Rhodium, and Aluminium on the surface . . . . . 49
4.17 XRD pattern for fresh and used catalyst . . . . . 49
4.18 Rate of hydrogen and methane production (operating conditions: feeding rate 7 g/h, Temp 650 °C for hydrogen and 600 °C for methane, C/S 0.12) . 50

5.1 Area 100H Reactive flash volatilization of microalgae . . . . . 52
5.2 Area 200H LT shift and hydrogen purification . . . . . 55
5.3 Area 100M Reactive flash volatilization of microalgae . . . . . 57
5.4 Area 200M CO methanation and LT shift . . . . . 58
5.5 Area 300M Methane purification . . . . . 59
5.6 Boundary diagram for LCA analysis . . . . . 62
5.7 Distribution of revenue generation from hydrogen and methane production 66
5.8 Sensitivity analysis of hydrogen production . . . . . 67

A.1 Performance of the reactor . . . . . 75
A.2 ASPEN plus process flow diagram for hydrogen production . . . . . 77
A.3 ASPEN plus process flow diagram for methane production . . . . . 78

# List of Tables


2.1 Major reaction involved in RFV of biomass . . . . . 13

3.1 Elemental analysis of microalgae . . . . . 29

4.1 Nitrogen physisorption and XRF analysis . . . . . 35
4.2 XPS analysis . . . . . 43
4.3 XRD analysis of the catalyst . . . . . 50

5.1 LCA inventory to produce hydrogen and methane . . . . . 63
5.2 Cost of individual equipment involved in hydrogen production . . . . . 65
5.4 Comparison of renewable hydrogen production . . . . . 66
5.3 Revenue generation from hydrogen and methane production . . . . . 66
5.5 LCIA impacts for hydrogen and methane production . . . . . 68

A.1 Elements present in the slag after reaction . . . . . 76
A.2 Stream table for Area 100H . . . . . 79
A.3 Stream table for Area 200H . . . . . 80
A.4 Stream table for Area 100M . . . . . 81
A.5 Stream table for Area 200M and Area 300M . . . . . 82
A.6 Details of heat exchanger to produce hydrogen from microalgae using reactive flash volatilization . . . . . 83
A.7 Details of heat exchanger to produce methane from microalgae using reactive flash volatilization . . . . . 83
A.8 Direct costs involved in hydrogen production . . . . . 83
A.9 Indirect costs involved in hydrogen production . . . . . 84
A.10 Operating costs involved in hydrogen production . . . . . 84
A.11 Direct costs involved in methane production . . . . . 84
A.12 Indirect costs involved in methane production . . . . . 85
A.13 Operating costs involved in hydrogen production . . . . . 85

# Chapter 1

# Introduction

Since the first commercial coal mining started in 1750, fossil fuels have dominated the energy sector. According to the world energy consumption statics published by British Petroleum (2018), global coal and oil consumption is increasing with the annual rate of 1% and 1.2%, respectively. The coal and oil consumption of India is increasing with an annual rate of 4.87% and 5.2%, respectively. In Australia, the oil consumption rate is increasing with an annual rate of 1.1%, while the net production of oil is decreasing at an annual rate of 3.9%. This increased rate of coal and oil consumption is one of the major contributors to increased $CO_2$ emissions (British Petroleum, 2018). Chu *et al.* (2017) reported that in 2012, the total global annual consumption of the energy was 579 PJ, and 85% of it was contributed by non-renewable resources. It is projected that by 2020 we will need 664 PJ of energy annually, and by 2040 we will be consuming 858 PJ of energy annually. Moreover, if we continue the present trends of energy generation, the $CO_2$ emissions will triple in the next two decades (Chu *et al.*, 2017).

Currently, the major industrial sectors are relying on the thermal energy obtained from the direct combustion of coal. Bali *et al.* (2019) reviewed the global warming potential (GWP) of iron and steel industries in India. They noted that the iron and steel industry contributes to around 55% of the total industrial $CO_2$ emissions. Moreover, the $CO_2$ intensities ($MTCO_2$/MT of crude steel) are 50% higher than the world standards. While securing the energy demands, transitioning from carbon-based energy resources to clean energy resources, is one of the grand challenges for a sustainable future.

Hydrogen is a clean energy resource because it does not lead to the emissions of greenhouse gases (GHG) during the utilisation stage. Moreover, it is an essential industrial feedstock for petroleum, fertiliser and metal processing industries. According to the report of the National Hydrogen Strategy-Submission, Australia, global hydrogen demand is projected to increase up to 5,000 PJ by 2040 (Burdon *et al.*, 2019). However, at

present, steam reforming of methane is the primary route for hydrogen production, and hence, 96% of the hydrogen is produced from non-renewable and non-environmentally friendly routes (Dincer, 2012).

Methane– a starting chemical for a variety of chemical synthesis processes, is mainly produced through natural gas extraction. The international energy outlook 2016 predicted that the global annual consumption of natural gas would increase by 1.5% per year until 2040. This will result in the total consumption of around 200 trillion cubic feet of methane per year by 2040 (Conti *et al.*, 2016). At present, the majority of the methane is produced from non-renewable resources.

Renewable hydrogen can be produced using electrolysis of water and thermochemical transformations of biomass. Similarly, renewable methane can be produced from biomass using bio- or thermo-chemical transformations. In the case of hydrogen, although electrolysis of water is techno-economically feasible, it has 30% higher global warming potential than steam reforming of methane if conventional energy is used to drive the electrolysis (Bhandari *et al.*, 2014). Thermochemical transformation of biomass can be achieved by pyrolysis, gasification and reactive flash volatilisation. Gasification is limited by char- and tar- accumulation, whereas slow and low-temperature pyrolysis, is limited by low gas yield. Reactive flash volatilisation (RFV) – a char- and tar-free alternative to gasification was proposed by Salge *et al.* (2006). They observed that RFV needs smaller reactors and a lesser quantity of catalyst compared to gasification and pyrolysis. Therefore, reactive flash volatilisation was selected to produce renewable hydrogen and methane from biomass.

This thesis is organised as follows,

- **Chapter 2**: It compares various renewable hydrogen and methane production processes while highlighting the advantages of thermochemical transformation of biomass. It also highlights the key advantages of microalgae over lignocellulosic (LC) biomass and lays the objective of this research.

- **Chapter 3**: It summarizes various materials and methods used to perform RFV, catalyst synthesis and characterisation. It also highlights the approach towards RFV of microalgae.

- **Chapter 4**: It describes the effect of steam content and temperature on the distribution of gases and yield of hydrogen or methane. A novel reaction mechanism for reactive flash volatilisation of microalgae based on the ash transformation characteristics is also proposed in this chapter.

- **Chapter 5**: It describes the outcome of techno-economic and life-cycle assessment of hydrogen and methane production using RFV of microalgae.
- **Chapter 6**: It summarises the key outcomes while mentioning future prospects.

# Chapter 2

# Literature Review

Alternative fuels date back more than five decades and growing concerns of climate change have promoted the cleaner energy options (Liobikienė and Butkus, 2017; Taylor *et al.*, 2013). Sustainability of the feedstock is one of the major attributes for suitability of the alternative fuel. Sustainability can be defined in various ways. Here, it is defined as, a process to achieve human development goals while sustaining the ability of natural system and resources to continue their services towards ecosystems and economy on which society depends (Glavič and Lukman, 2007).

Hydrogen economy appears to be a sustainable energy solution. It is comprised of five major components such as a) production, b) delivery, c) storage, d) conversion, and e) application (Crabtree *et al.*, 2004). Hydrogen is advantageous over conventional fuels, because it has a) high conversion efficiency, b) higher HHV and LHV, c) no $CO_2$ emissions on combustion, and d) ease of transformation (Dincer, 2012). Dincer and Acar (2015) defined three parameters to rank the fuels in terms of their sustainability such as a) Environmental Impact factor (EIF)– kg of $CO_2$ produced per kg of fuel, b) Greenization Factor (GF) defined as global warming potential (GWP) potential compared to the coal, and c) Hydrogen Content Factor (HCF)– fraction of hydrogen in the fuel. Coal has very high EIF and as a consequence, it exhibits lower GF. With the increase in HCF, the fuel becomes greener, and the EIF is reduced. In terms of their sustainability, hydrogen is more sustainable compared to natural gas, oil, and coal.

## 2.1 Renewable Hydrogen Production

Forthwith, renewable hydrogen production is not accessible with commercial efficiencies due to the limitations of production technologies. Dincer (2012) classified renewable hydrogen production technologies depending on the energy that was used to drive the pro-

cess of hydrogen production. Additionally, based on the transformation, they are further classified as a) thermochemical transformation, and b) biochemical transformation (Dark and light fermentations). Only thermochemical hydrogen production processes driven by electrical-, solar-, and thermal-energy are considered here, because biochemical transformation to produce hydrogen is in a very nascent stage, and the scale-up potential of this technology is not yet fully understood (Tapia-Venegas *et al.*, 2015).

### 2.1.1 Hydrogen production using electrical energy

Electrolysis of water to produce pure hydrogen is the most widely reported method of renewable hydrogen production. Electrolysis of water can be performed using three different electrolysers– a) alkaline electrolyser (AE), b) proton exchange membrane (PEM) electrolyser and c) solid oxide electrolysers (SOE).

Alkaline electrolysers are the most mature and commercially viable electrolysis technology in which KOH or NaOH is used as an electrolyte solution, and negatively charged ions (hydroxyl ions) are used as the charge carriers. (Manabe *et al.*, 2013). Harrison *et al.* (2010) authored a report about wind energy based electrolysis of water at different locations. While designing and constructing a pilot-scale plant at West Beacon Farm, in Leicestershire, England, it was observed that the fluctuations in the wind energy resulted in the degradation of cell stacks. As a result, the overall efficiency of electrolyser was reduced. It is acknowledged in the literature that, the performance of AE is strongly dependent on the quality of the water. Ca and Mg ions from hard water get deposited on the surface of the electrode during electrolysis which creates an additional barrier layer for the charge carriers. Moreover, if small quantities of NaCl is present in the water, chlorine gas is produced on the electrode instead of oxygen, which is corrosive. Hence, the dedicated water deioniser is required to operate AE (Manabe *et al.*, 2013).

In the case of PEM and SOE, the technology is still at the research and development stage. PEM uses acidic electrolytes in which positively charged ions act as the energy carriers. The conversion efficiency of PEM is around 80% to 85% when operated in the temperature range of 60 °C to 80 °C . The bottleneck of the technology is the design of the membrane and electrodes. The commercial membranes are permeable to Ca and Cu, causing the problem of ion deposition. Moreover, since the medium is acidic, a Pd or Pt coating on the electrodes is required to avoid the corrosion (Kumar, 2019).

### 2.1.2 Hydrogen production using solar energy

Water splitting using photovoltaic (PV) solar cells and photocatalysts are the two ways to produce renewable hydrogen using solar energy. In the case of PV solar cell-

based water splitting, the energy required to split the water is generated from solar energy using PV cells. In contrast, a photocatalyst absorbs the energy of photons and releases it to split the water into hydrogen and oxygen.

Photocatalytic water splitting has received greater attention in the literature because it has the least global warming potential (GWP) compared to other renewable hydrogen production techniques (Acar and Dincer, 2014). Acar *et al.* (2016) reviewed various heterogeneous photocatalysts and concluded that a photocatalyst should exhibit some additional characteristics along with typical characteristics of a heterogeneous catalyst such as a) high crystallinity, b) recyclability, c) corrosion resistance, and d) appropriate valance- and conductance-band position. It is well reported in the literature that nano-photocatalysts show higher efficiency of hydrogen production. However, a contradicting result is reported by Deshpande and Gupta (2010). They evaluated the performance of nano Cadmium-Sulphate (CdS) catalysts for hydrogen production and concluded that 2.5 nm CdS catalyst performed better compared to 1.5 nm because the crystalline nature of CdS was retained at 2.5 nm. Their findings suggested that the activity of a photocatalyst is strongly dependent on the crystallinity. Nanomaterials tend to be amorphous, and often loose their crystallinity during the reaction as a consequence of thermal exposure. Synthesizing a stable nono-crystalline catalyst is one of the major limitations of the photocatalytic water splitting.

To generate the electron-hole pair, and split the water, it is necessary that the energy of the incident photon should be higher than that of the catalyst bandgap. This implies that most of the reported catalysts can function only under UV or near UV region of the solar radiations. Therefore, only 4% of the incident solar radiations is used to catalyze water splitting (Acar *et al.*, 2016). Additionally, Cowan *et al.* (2010) noted that the recombination of charges (electron and hole) during photo-radiation is responsible for reduced quantum efficiency. Development of a new catalytic material which has a lower bandgap, and can be excited with visible light is recommended. Although photocatalytic water splitting is environmentally preferable over other renewable hydrogen production process, the energy and exergy efficiency of this process is the least (<10%) compared to other hydrogen production processes (Acar and Dincer, 2014).

El-Emam and Özcan (2019) have reviewed various commercially viable water electrolysis technologies for renewable hydrogen production. They observed that the cost of hydrogen production is dependent on the source of electricity and the configuration of the electrolyzer. Depending on the configuration the cost of hydrogen varies between \$ 5 / kg of $H_2$ (grid-based AE electrolyser) to \$ 9/ kg of $H_2$ (wind energy based PEM electrolyser). PV solar cell-based water splitting has attracted significant attention in the literature over

the last decade due to increased efficiency of the PV solar cells. Shaner *et al.* (2016) performed the comparative techno-economic (TE) feasibility of current PV based water-splitting technologies assuming the efficiency of solar-to-hydrogen in the range of 12% to 17% (depending on the configuration). They observed that the gate price of hydrogen is in the range of $ 9/ kg of $H_2$ to $ 12/ kg of $H_2$, which is 45% higher than the current market price of the hydrogen. Furthermore, they reported that if 75% of the energy is supplied through the grid (fossil fuel-based), the cost of hydrogen production can be reduced by 33%.

Bhandari *et al.* (2014) evaluated the scenario of renewable hydrogen production using water electrolysis specific to Germany. They highlighted that the electrolysis of water is attractive only if renewable energy is used. In the case of renewable electricity, the GWP was calculated to be 5 kg $CO_2$-eq./ kg $H_2$, whereas, in the case of fossil fuel-based power generation the GWP was calculated to be 30 kg $CO_2$-eq./ kg $H_2$. Although renewable hydrogen production using electrolysis of water is a techno-economically feasible process, it has very high GWP. In such a scenario, thermochemical processes appear attractive compared to water electrolysis.

### 2.1.3 Hydrogen production using thermochemical energy

Hydrogen production using thermochemical conversion of lignocellulosic (LC) biomass has higher energy and exergy efficiency compared to the coal gasification and steam reforming of methane. Coal gasification and steam reforming of methane exhibit the energy and exergy efficiency in the range of 30% to 40%. In contrast, thermochemical biomass conversion exhibits the energy and exergy efficiency in the range of 60% to 65% (Acar and Dincer, 2014). Hydrogen production from LC biomass is extensively reported in the literature (Kalinci *et al.*, 2009; Tanksale *et al.*, 2010; Parthasarathy and Narayanan, 2014). Pyrolysis, gasification, supercritical water gasification and RFV can be used to produce renewable hydrogen from biomass using thermochemical energy. Pyrolysis and gasification are mature technologies compared to supercritical water gasification and RFV. The merits and demerits of these technologies are discussed in detail in the following subsections.

#### *2.1.3.1 Pyrolysis*

Pyrolysis is a thermochemical conversion of biomass into gas, oil and char in the absence of oxygen. In this process, oil is the main product. The yield of gas, oil and char depends on residence time, rate of heating, and the operating temperature.

Demirbaş (2002) performed catalytic pyrolysis of cotton cocoon shell, tea factory waste and olive husk in a downdraft pyrolyser. The reactor was heated externally using an electrical furnace in the range of 500 °C to 750 °C and $Na_2CO_3$, or $K_2CO_3$ was used as a catalyst. He reported that the gas yield increased by 28%, 14% and 28% for cotton cocoon shell, tea factory waste and olive husk, respectively, when the temperature was increased from 500 °C to 750 °C . $H_2$ composition in the produced gas was in the range of 40% (v/v) to 70% (v/v). They concluded that the higher operating temperature and longer residence time increases the yield of gases.

Yang *et al.* (2006) performed the pyrolysis of palm oil waste to produce hydrogen-rich gas. A countercurrent downdraft tubular quartz reactor was used to perform the pyrolysis. They observed that the yield of gas and composition of $H_2$ was increased by 43.23% and 89.37%, respectively, as the temperature was increased from 500 °C to 900 °C . Furthermore, they noted that the $H_2$ composition increased to 37.56% from 14.52% as residence time was reduced to 7.5 s from 26 s. They hypothesised that a longer residence time favours the direct hydrogenation of char, resulting in the higher $CH_4$ composition compared to $H_2$.

Bakhtyari *et al.* (2017) have summarised the effect of various catalysts on the pyrolysis of LC biomass. They have reported that the overall gas yield increased by 50% in the presence of Ni catalysts compared to $Na_2CO_3$ and $K_2CO_3$ catalyst. However, the composition of $H_2$ remained unchanged (35% to 45%). Moreover, they reported that in pyrolysis, around 40% carbon (depending on the operating conditions) is converted to oil. Therefore, the overall yield of gases and carbon conversion efficiency (amount of carbon in the gas phase/amount of carbon in the feedstock) is low compared to gasification.

#### *2.1.3.2 Gasification*

Gasification is a thermochemical process in which biomass is transformed into gaseous products along with char- and tar-formation (depending on operating conditions) using a gasifying agent ($O_2$, steam or $CO_2$). Gasification is the most matured technology to produce syngas (CO and $H_2$). Kalinci *et al.* (2009) reported that, in 1970, first gasification technology was demonstrated to produce syngas from coal, and thereafter, the technology was adapted for LC biomass to produce hydrogen. Turn *et al.* (1998) performed dry and ash-free biomass gasification using steam to produce hydrogen. They observed that 62 g of $H_2$/kg of biomass could be produced at 850 °C . Arregi *et al.* (2018) have reviewed gasification of non-woddy biomass. They noted that non-woody biomass is devoid of lignin and can be gasified at a lower temperature. However, the gasification efficiency is in the range of 50% - 70% and tar formation is one of the major reasons for lower

gasification efficiency.Tar accumulation deactivates the catalyst; hence, the selection of the catalyst for gasification is the crucial step.

Fraga *et al.* (1991) have reported that the constituents of tar were dependent on the feedstock composition. Moreover, Milne *et al.* (1998) and Kiel *et al.* (2004) have classified the tars based on their chemical composition and condensability, respectively. Tar can be eliminated by either operating the gasifier at high temperature (1000 °C to 1400 °C ) or by reforming it *in-situ* in the presence of a primary or secondary catalyst (Milne *et al.*, 1998). Among all the proposed approaches, *in-situ* steam reforming of tar in the presence of the catalyst is a promising solution (Sutton *et al.*, 2001).

The detail TE analysis of hydrogen production using pyrolysis was performed by Spath *et al.* (2003). They have reported that the cost of hydrogen production is $ 1.56/ kg of $H_2$ when the biomass cost is $ 30/ tonne. Sarkar and Kumar (2010) performed the TE analysis of hydrogen production from LC biomass. They observed that the cost of hydrogen is strongly dependent on the cost of feedstock. Depending on the feedstock, the cost of hydrogen production varies between $ 2.4/kg of $H_2$ to $ 4.32/kg of $H_2$. Ruth (2011) performed the predictive analysis of the TE feasibility of hydrogen production using biomass gasification. They predicted that by 2020, the cost of hydrogen production would be $ 5.46/ per kg of $H_2$ when the cost of biomass is $ 38/ tonne. Furthermore, they observed that if the capacity of the plant is increased by 4 times, the cost of hydrogen production would be reduced by 50%. IEA Bioenergy (2019) published a critical report on the technology development for LC biomass gasification. The report articulates that most of the gasification plants are not successful because a) there exists a gap in the communicated results and the implemented technology, and b) fluctuating costs of the LC biomass. Furthermore, they noted that gasification is techno-economically not feasible for distributed operating systems.

#### *2.1.3.3 Supercritical water gasification*

The difference in the moisture content and ash properties of coal and LC biomass was one of the major shortcomings of using LC biomass as a feedstock for gasification (Kirubakaran *et al.*, 2009). LC biomass can have a moisture content as high as 40%. The heat of evaporation of liquid dominates the heat of combustion of solids if the wet (moisture content > 40%) biomass is used as the feedstock. Supercritical water gasification (SCWG) was proposed to gasify the high moisture contenting biomass. Okolie *et al.* (2019) have presented a critical review on biomass SCWG to produce hydrogen. During SCWG, biomass is treated at 250-280 bar pressure and 300 °C to 500 °C temperature in the presence or absence of the catalyst.

Although high moisture containing biomass can be gasified directly using SCWG, the material of construction for the reactor is expensive. Ni-containing alloys such as Hastelloy or Inconel are used to provide corrosion resistance to the reactor (Ou *et al.*, 2015). Additionally, Kirkels and Verbong (2011) have noted that the gasification is advantageous compared to SCWG because it generates a product without any ringed or double bond structures. However, tar cleaning remains a challenge in the commercialisation of the gasification technology (Swanson *et al.*, 2010).

#### 2.1.3.4 *Reactive flash volatilization*

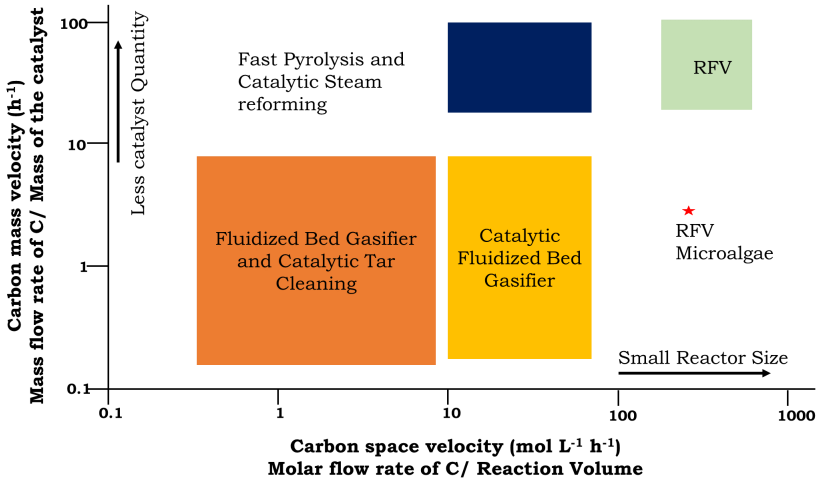


Figure 2.1: Comparison of various thermochemical conversion processes based on the carbon mass- and space-velocity (Adapted and modified from Colby *et al.* 2008)

Reactive Flash volatilisation– a char- and tar-free alternative to gasification, was proposed by Salge *et al.* (2006) to produce hydrogen-rich syngas from bio-oil and cellulose. They observed that RFV was able to convert non-volatile feed hydrogen-rich gas, and they assumed this process to be a combination of gasification reactions (Table 2.1). Colby *et al.* (2008) compared RFV with pyrolysis and gasification on the basis of two parameters, viz. space velocity and mass flow rate of carbon, as shown in Figure 2.1. Size of the reactor is related to carbon space velocity, and the amount of catalyst required is related to the mass flow rate of carbon. Their analysis clearly shows that RFV needs smaller volume and lesser catalyst when compared to gasification and pyrolysis. They observed that, maximum 0.8 – 0.9 (mass flow of C. mass of catalyst$^{-1}$ h$^{-1}$) of carbon mass velocity can be achieved in conventional gasifier whereas, RFV can be operated at carbon mass velocity of 50-80 (mass flow of C. mass of catalyst$^{-1}$ h$^{-1}$). Dauenhauer (2008) articulated that the possible reasons for 95% carbon conversion in RFV, and no accumulation of char and tar

can be attributed to the high surface temperature of the catalyst, which rapidly oxidises the decomposed products to form gases. Additionally, the exothermic reactions prevent the condensation reactions responsible for carbon and tar formation. 60% hydrogen selectivity was reported without catalyst whereas, increased selectivity of 95%, was observed towards hydrogen during catalytic RFV.

Salge *et al.* (2006) performed RFV of soy oil and glucose water in the presence of Rhodium-Cesium (Rh-Ce) catalyst to produce $H_2$ and CO. Soy oil and glucose are ash-free feedstocks, and they are easy to gasify compared to LC biomass. Moreover, Rh-Ce catalysts are expensive. Hence, the activity of nickel catalyst with a promoter metal was analysed by Chan and Tanksale (2016). They have reported, that nickel catalysts can be a better alternative for an expensive rhodium-cesium catalyst. Colby *et al.* (2008) performed, RFV of pure crystalline cellulose in the presence of Rh-Ce/Al as a catalyst at 600-800 °C temperature. Space time for the reaction was reported to be 24 ms. Chan and Tanksale (2014a) have performed similar reactions using Ni based catalyst supported on alumina in the temperature range of 700-800 °C. Higher space time of 50 ms was observed with no char and tar formation. Nickel- Rhodium (Ni-Rh) supported on alumina was reported to show higher selectivity towards gases compared to other catalysts.

Table 2.1: Major reaction involved in RFV of biomass

| | | | | |
|---|---|---|---|---|
| Pyrolysis Reactions | | | | |
| Biomass | $\longrightarrow$ | Primary tar ($CH_xO_y$)<br>$CH_4$, $C_2H_4$, $H_2O$, CO, $CO_2$<br>Carbon and Oil | | (1) |
| Homogeneous gas-phase-reactions | | | | |
| $CH_4 + CO_2$ | $\longrightarrow$ | $2\,CO + 2\,H_2$ | Dry reforming reaction | (2) |
| $CO + 3H_2$ | $\longleftrightarrow$ | $CH_4 + H_2O$ | CO methanation reaction | (3) |
| $CH_4 + 0.5O_2$ | $\longrightarrow$ | $CO + 2H_2$ | $CH_4$ combustion | (4) |
| $CH_4 + H_2O$ | $\longleftrightarrow$ | $CO + 3\,H_2$ | Steam reforming methanation | (5) |
| $CO + H_2O$ | $\longleftrightarrow$ | $CO_2 + H_2$ | Water-gas-shift reaction | (6) |
| $H_2 + 0.5O_2$ | $\longleftrightarrow$ | $H_2O$ | $H_2$ combustion | (7) |
| $CO + 0.5O_2$ | $\longleftrightarrow$ | $CO_2$ | CO combustion | (8) |
| Heterogeneous reactions | | | | |
| $C + CO_2$ | $\longleftrightarrow$ | $2\,CO$ | Boudoard equilibrium | (7) |
| $C + H_2O$ | $\longrightarrow$ | $CO + H_2$ | Steam reforming of carbon | (8) |
| $C + 2H_2$ | $\longrightarrow$ | $CH_4$ | Methane production reaction | (9) |
| $C + O_2$ | $\longrightarrow$ | $CO_2$ | Complete oxidation of carbon | (10) |
| $C + 0.5O_2$ | $\longrightarrow$ | CO | Partial oxidation of carbon | (11) |

To summarise, renewable hydrogen can be produced from electrolysis of water and thermochemical transformation of biomass. Electrolysis of waster driven by conventional energy is techno-economically feasible. However, the GWP is 60% higher compared to the steam reforming of methane. On the other hand, photocatalytic water splitting has the least GWP; however, it is limited by TE feasibility. In such a scenario, hydrogen production through a thermochemical transformation of biomass appears to be an attractive option. Thermochemical transformation of biomass can be achieved through pyrolysis, gasification and RFV.

The slow and low-temperature pyrolysis of biomass is not favourable for hydrogen production because the yield of gaseous products is less compared to liquid products. Conventional gasification is limited by char- and tar-accumulation in the reactor. Moreover, it also needs large reactors with a high amount of catalyst compared to RFV. RFV is advantageous compared to gasification and pyrolysis mainly because char- and tar-free conversion of biomass can be achieved. Furthermore, it also needs small reactors with less amount of catalyst. Considering the pros and cons of the various processes, RFV was chosen for the producing hydrogen.

## 2.2 Renewable Methane Production

Biogas production using anaerobic digestion of LC biomass is the most sought after renewable fuel production technology. Biogas is mostly composed of around 65% to 70% $CH_4$, 30% to 35% $CO_2$ and some small amount of $H_2S$, and $NH_3$ (Homs *et al.*, 2018). Anaerobic digestion is a techno-economically viable technology, because a) it can process high moisture containing feedstocks with pretreatment, b) valorisation of the produced biogas is easy since mostly it is coupled with combined heat and power generation plant, c) waste generated through anaerobic digestion is rich in nitrogen and can be used in agriculture as fertiliser or soil amendment, and d) the process can be scaled up or scaled down easily (Appels *et al.*, 2011).

Although anaerobic digestion has proven its commercial value for a household and community uses, industrial suitability is challenging due to waiting time. It takes around 20 to 25 days for LC biomass to digest anaerobically (Homs *et al.*, 2018). Additionally, high nitrogen-containing feedstocks can inhibit the anaerobic digestion due to the accumulation of ammonia (Fricke *et al.*, 2007).

Renewable $H_2$ and $CH_4$ production from LC biomass is extensively reported in the literature. However, microalgae is one of the leading alternative feedstock. The advantages of microalgae and various processing alternatives of microalgae are highlighted in the following section.

## 2.3 Microalgae

Microalgae is one of the leading alternative feedstocks because, compared to lignocellulose, it provides a) higher $CO_2$ fixation efficiency, b) higher growth rate, c) higher photosynthetic efficiency, d) higher energy density ($J/m^3$), and e) ability to grow in brackish water (Brennan and Owende, 2010; Rittmann, 2008; Rosenberg *et al.*, 2008a; Chisti, 2008; Grima *et al.*, 2003; Mata *et al.*, 2010).

Wijffels (2008) noted that plants could fix up to 6% of the incident light. In contrast, microalgae could fix up to 9% - 11% of the incident light. Dismukes *et al.* (2008) have compared various biofuel feedstocks based on their ability to convert absorbed sunlight into fuels. They have noted that only 0.05% and 0.5% of the incident sunlight was converted into ethanol by corn and switchgrass, respectively. In contrast, 0.75% to 1.0% of the incident light was converted into biofuel by microalgae. Furthermore, this higher conversion can be correlated with higher areal productivity.

One of the most noted advantages of microalgae is the ability to grow in brackish water. Farm-based fuels, for example, food-based ethanol draws a significant share of

freshwater for irrigation. Murali and Shastri (2019) have noted that the water footprint of LC biomass-based ethanol is in the range of 232 and 672 L/L of ethanol. These advantages strongly support the selection of microalgae as the feedstock. However, the choice of processing technology plays an important role. The following section describes and compares various processing alternatives for microalgae.

## 2.4 Microalgae processing

In spite of the advantages, to date, commercialisation of microalgae-based biofuel production has not yet been realised due to a) low concentration of biomass (0.5 g/L to 1.5 g/L in the case of open pond system), b) requirements of cost-intensive pre-treatment processes (Brownbridge *et al.*, 2014), and c) focus towards biodiesel production from microalgal lipids (Sen Gupta *et al.*, 2016). Depending on the requirement of dewatering and drying the processing alternatives are divided into two groups such as a) wet processing, and b) dry processing, as shown in Figure 2.2.

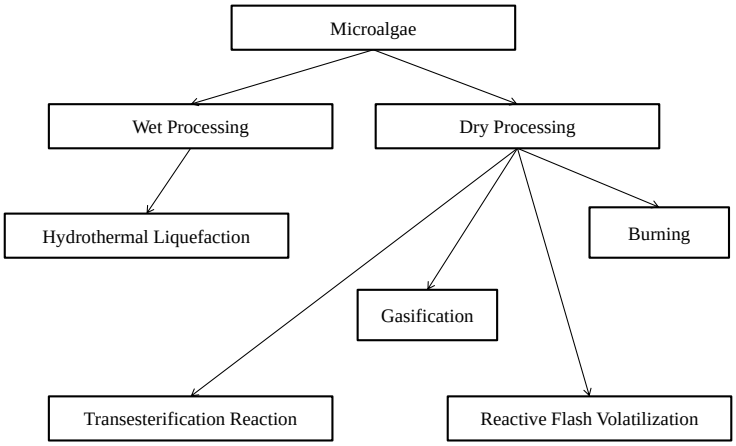


Figure 2.2: Processing alternatives for algae

### 2.4.1 Dry processing

Dried microalgal biomass can be processed to obtain fatty acid methyl esters (FAME) or syngas using transesterification reaction or thermochemical routes, respectively. Transesterification of microalgal oil in the presence of various catalysts is extensively reported in the literature. Drapcho *et al.* (2008) articulated that, transesterification has its own merits and demerits. Although conversion efficiency of oil to ester is high (>98%), low (<20%) efficiency of oil extraction from microalgae using chemical

or mechanical means leads to overall low process efficiency. Additionally, high molar requirements of methanol impose more constraints on its scale-up. (Grima *et al.*, 2003)

Benemann and Oswald (1996) have performed the detailed TE analysis of microalgae to FAME production. They noted that around 70% of the total cost is contributed by microalgae growth, harvesting and drying. Out of which, 32% is contributed by drying. Similar observations were reported by Sen Gupta *et al.* (2016). They noted that the minimum annualised life cycle cost (ALCC) of biodiesel to produce 30,000 kg/d biodiesel from *Chlorella*, was \$13.3/l of biodiesel. Moreover, the cost of biodiesel was reduced to \$8.52/l after considering the revenue generated through the co-production of proteins and secondary metabolites. (Sen Gupta *et al.*, 2017) The effect of renewable energy on the TE analysis of FAME production was assessed by Taylor *et al.* (2013). In a hypothetical scenario where electricity is produced using PV cells and microalgae was harvested and dried using solar power, the cost of biodiesel was estimated to be \$114/barrel. Brownbridge *et al.* (2014) have reported the sensitivity ranking for the parameters. They have noted that the lipid content of microalgae is the most sensitive parameter whereas, the carbon price for $CO_2$ sequestration is the least sensitive parameter towards final biodiesel cost. While indicating the economic infeasibility of FAME production, they highlighted the need for technology development to produce a value-added product from microalgae.

### 2.4.2 Wet processing

Studies have reported that harvesting followed by drying of microalgae consumes most of the process energy and economy. (Biller *et al.*, 2011; Davis *et al.*, 2011; Sen Gupta *et al.*, 2017) Hence, wet processing is advantageous mainly, because hydrothermal liquefaction uses water as one of the reactants (Johnson and Tester, 2013). Wet algal biomass is treated at 250 – 280 bar pressure and 300 °C – 350 °C temperature in the presence or absence of the catalyst. Lipids, carbohydrates and proteins get converted to saturated fatty acids, alkanes, $CO_2$, $H_2$, char, aldehyde and amines (Tsukahara and Sawayama, 2005; Fu *et al.*, 2010; Gao *et al.*, 2012). However, the material of construction for a reactor is expensive since Ni containing alloys such as Hastelloy or Inconel is used to provide corrosion resistance (Ou *et al.*, 2015). The utilization of microalgae for hydrogen and methane production appears attractive when compared with other routes of microalgae utilization.

### 2.4.3 Hydrogen production from microalgae

Two-step conversion of microalgae, i.e. pyrolysis followed by steam reforming of oil and gasification of char is reported in the literature. Miao *et al.* (2004) performed fast

pyrolysis of *C. protothecoides* and *M. aeruginosa* using continuous fluidised bed reactor. The final temperature of the reactor was 500 °C , and it was heated externally with a heating rate of 600 °C /s, in which sand was used as the fluidising media. They observed that all of the microalgae was not pyrolysed with a residence time of 2 to 3 s. Moreover, the gas yield of around 30% and 50% was observed in the case of *C. protothecoides* and *M. aeruginosa*, respectively. The proximate analysis of *C. protothecoides* and *M. aeruginosa* showed that *M. aeruginosa* contains 50% more ash–mainly composed of alkali and alkaline earth metals (AAEM), compared to the *C. protothecoides*. The increased yield of gases can be attributed to the catalytic effect of AAEM to transform the oil into gaseous compounds. Although, they have analysed the yields of gas, oil and char, the composition of gaseous products was not analysed.

Similar experiments were performed by Wang *et al.* (2013) with *C. vulgaris*. They observed that the yields of oil, char and gas are comparable with the LC biomass pyrolysis. However, the elemental analysis of char showed the presence of AAEM. It was observed that only 40% of the yield was attributed to gaseous products. Moreover, the oil was rich in nitrogen (12%). This suggests that microalgal proteins transform into oil when exposed to pyrolytic conditions. To understand the devolatilisation characteristics of microalgae in pyrolytic and combustion conditions, Agrawal and Chakraborty (2013) performed TGA experiments with *C. vulgaris* and observed that microalgae disintegrate in two different zones. Protein and carbohydrates decomposed at around 200 °C to 300 °C , whereas, lipids decomposed at around 400 °C to 500 °C . They noted that a minimum 450 °C temperature is required to devolatilise 75% of microalgae. Similar observations were reported by Sanchez-Silva *et al.* (2013) and Rizzo *et al.* (2013) for *Nanochloropsis sp.* It was observed that the gas yield improved at higher temperature due to secondary cracking of oils. Low gaseous yield from slow and low-temperature pyrolysis is not favourable for hydrogen production. Hence, gasification is preferred over pyrolysis.

Krishnan *et al.* (2016) performed SCWG of three species of microalgae viz. *B. braunii*, *N. oculata* and *T. chuui* to evaluate the performance of Ni catalyst and saline water on the yield of $H_2$. *B. braunii* is a freshwater species, whereas, *N. oculata* and *T. chuui* are saline water species. SCWG was performed in the small tubular reactor made up of stainless steel, having 9.53 mm OD and 6.53 mm ID. The reactor was heated externally to reach 400 °C using a salt bath. The composition of microalgae and water was adjusted such that 250 bar pressure was developed inside the reactor. They reported that in the presence of Ni catalyst around 35% (v/v) $H_2$ was produced and the yield of $H_2$ was increased in the presence of salts. This indicates that the presence of Na ions from saline water catalyses the water-gas shift reactions in SCWG. The carbon-to-water ratio

was predetermined to reach the 250 bar pressure. Hence, the effect of water content on the reaction was not evaluated. This is important because water acts as a reactant at elevated temperature and pressure and can affect the product distribution.

Tiong *et al.* (2016) performed SCWG of *Chlorella vulgaris* and *Scenedesmus quadricauda* in the presence of Ni/alumina and Raney Ni/alumina catalysts at around 400 °C . They evaluated the performance of both the catalysts by varying the residence time of the reaction and observed that the yield of $H_2$ in the case of SCWG of *Chlorella vulgaris* was less compared to *Scenedesmus quadricauda*, irrespective of the holding time and the catalyst used. They noted that the protein content of *Chlorella vulgaris* was 58% higher compared to *Scenedesmus quadricauda*. As a consequence, the nitrogen content in the reaction mixture of *Chlorella vulgaris* was higher in comparison to *Scenedesmus quadricauda*. Therefore, the incomplete conversion of nitrogen resulted in tar formation and catalyst deactivation.

To overcome the limitations of SCWG, and convert unreacted char, air gasification of microalgae was proposed by Raheem *et al.* (2017). They performed thermogravimetric analysis (TGA) of microalgae to understand the devolatilisation characteristics of microalgae. Depending on the devolatilisation characteristics, bench-scale experiments were performed in a horizontal tube reactor using *Chlorella vulgaris*. A quartz reactor was used to perform pyrolysis, and the composition of tar and gases was evaluated using inline GC. They observed that with a holding time of 20 min., the weight percentages of gas, char and tar were 75.8 %, 11.6 % and 12.6 %, respectively. Furthermore, they evaluated the effect of biomass loading on $H_2$ production and concluded that as biomass loading increases, $H_2$ percentage decreases and $CH_4$ percentage increases. They attributed this behaviour to the mass- and heat-transfer limitations caused by excess biomass. This resulted in localised pyrolytic conditions responsible for lower $H_2$ percentages. Another plausible explanation could be the enhancement of CO-methanation reaction. Increased biomass caused the heat transfer limitations resulting in the local low-temperature spots in the reactor. Therefore, CO-methanation, which is an exothermic reaction, was favoured locally, resulting in the higher $CH_4$ and lower $H_2$.

Steam content in the gasifier has a significant effect on the $H_2$ composition. Steam gasifies char and reforms the tar *in-situ*. López-González *et al.* (2014) performed steam gasification of *Scenedesmus almeriensis*, *Nannochloropsis gaditana* and *Chlorella vulgaris* in the absence of catalyst using a TGA. They observed that the rate of char gasification using steam is not constant. Their observations highlighted the catalytic role of AAEM in char gasification. Initially, the rate of char gasification was higher because Ca,

Mg and K were evenly distributed, and as the reaction proceeded Ca, Mg and K sintered. As a consequence, the rate of the reaction decreased.

Chemical looping combustion (CLC) of *Chlorella vulgaris* was reported by Liu *et al.* (2017). $Fe_2O_3$ was used as an oxygen carrier, and steam was used as a gasifying agent. A copper crucible containing U-shaped quartz reactor was used to gasify the microalgae. A predetermined quantity of $Fe_2O_3$ powder and microalgae was mixed in the copper crucible, and it was loaded into a preheated reactor. The gases were measured using a gas analyser. They observed that the yield of $H_2$ increased with increased $Fe_2O_3$ concentration and temperature. However, after 900 °C , the yield decreased due to the agglomeration of $Fe_2O_3$ particles. Furthermore, they concluded that the average carbon-to-gas conversion efficiency of the process was only 77%. Duman *et al.* (2014) have performed microreactor gasification experiments on macro- and microalgae to study the tar conversion characteristics. They have reported that, in the case of microalgae, only 70 % of tar was converted into gaseous form, at 700 °C in the presence of the $Fe_2O_3/CeO_2$ catalyst.

To understand the interplay between carbon conversion and operating conditions (steam content and temperature), the gasification process was modelled by Azadi *et al.* (2015), Li (2019) and Adnan and Hossain (2018). Azadi *et al.* (2015) simulated the gasification of microalgae under oxy-steam gasification environment using ASPEN Plus, and Peng-Robinson thermodynamic model was used for the process simulation. The process was split into different zones, such as pyrolysis and char gasification. Pyrolysis was modelled using yield reactor, and gasification reactions were modelled using Gibbs reactor. They assumed that the lipid content in the microalgae is predominantly reformed in the gasification process. Hence, they analysed the effect of lipid content on $H_2$ production. It was observed that the $H_2$ composition in the produced gas increased by 30.89% when lipid content increased by 40%. The results of global sensitivity analysis were in agreement with the simulation results. Li (2019) modelled the oxy-steam gasification of *Chloropsis sp.*, *Chlorella vulgaris* and *Dunaliella tertiolecta* using the similar approach mentioned earlier. He observed that the $H_2$ composition increased by 30% when the temperature was increased to 900 °C from 700 °C . Adnan and Hossain (2018) have also adopted the similar approach to model the $CO_2$ gasification of *Nanochloropsis Oculata* and predicted that 30.45% (v/v) $H_2$ will be produced, at 800 °C temperature with $CO_2$-to-carbon ratio of 0.5.

Although efforts were made to model the microalgae gasification, it was assumed that the rate of char gasification remains constant. However, López-González *et al.* (2014) proved that it varies as the reaction progresses. Furthermore, the effect of nitrogen content

on the reaction mechanism was not captured because reactions schemes and kinetics were extrapolated from LC biomass gasification.

### 2.4.4 Methane production from microalgae

Anaerobic digestion of microalgae to produce methane is extensively noted in the literature (Santos *et al.*, 2014; Cavinato *et al.*, 2017; Klassen *et al.*, 2017). Both saline water and freshwater microalgal species are reported in the literature. It was observed that the yield of methane in the produced gas was in the range of 170 $ml \cdot g^{-1}$ to 550 $ml \cdot g^{-1}$.

Although, anaerobic digestion has excellent performance in the case of LC biomass, it shows characteristic limitations in the case of microalgae processing such as, a) possibility of bacterial washout, b) resistance of microalgal cell walls and requirement of additional pretreatments, c) high nitrogen content, and d) high lipid toxicity (Ward *et al.*, 2014). The anaerobic reactors are designed for high hydraulic retention to avoid the dewatering step. However, excess water can cause bacterial washout resulting in the inhibition of anaerobic digestion. The effect of the microalgal cell wall on the amount of biogas produced is extensively reported in the literature (Mussgnug *et al.*, 2010). It was observed that amount biogas produced was higher in the case of microalgal species which exhibit either protein-rich cell wall or no cell wall. However, cellulose and hemicellulose rich cell wall tend to be resistive to bacterial degradation (Mussgnug *et al.*, 2010; González-Fernández *et al.*, 2012). A pretreatment step to disrupt the cell wall is necessary to achieve higher gas yields. Three types of pretreatment processes are described in the literature; a) thermal, b) ultrasonic, and c) enzymatic. Ward *et al.* (2014) have reported that pretreating microalgae at 100 °C for 8 h while maintaining the pH in the range of 7 to 9 using NaOH increased the yield of methane by 57%. Moreover, they have reported that in the case of untreated microalgal biomass, 60% of the microalgae had an intact cell wall resulting in the lower yield of $CH_4$. Ultrasonication and mechanical disruption of the cell wall is energy consuming, and hence, it is not extensively reported in the literature. Lü *et al.* (2013) explored the option of enzymatic hydrolysis of cell wall before fermentation. They observed that the addition of cellulase increased the yield of biogas up to 24%.

González-Fernández *et al.* (2012) have reported that the fermentation of microalgae to produce methane is suitable where transesterification of lipids is the main objective of microalgae processing because the cell wall is disrupted during the lipid extraction. Additionally, defatted microalgae exhibit less lipid toxicity during fermentation. However, defatted microalgae propose another processing challenge by forming ammonia during the fermentation. Ammonia is formed as a result of microalgal protein degradation, and

it has detrimental effects on methane formation. Firstly, it changes the overall pH of the reaction to basic where methanogenic bacteria cannot survive, and secondly, it inhibits the enzymatic activity of the intracellular enzyme responsible for methane generation (Kayhanian, 1999; Sialve *et al.*, 2009).

Microalgae dewatering is the most intensive (energetically and economically) unit operation of microalgae processing (Sen Gupta *et al.*, 2016; Benemann and Oswald, 1996). Therefore, microalgae processing using SCWG was considered as a promising processing alternative in the literature. Although the intrinsic water content of microalgae can be used as the reactant, it is techno-economically challenging to commercialise the process due to the expensive material of construction of the reactor. Similarly, dry microalgae gasification has the operational limitations of tar accumulation.

Reactive flash volatilisation using steam as a gasifying agent appears to be an appealing alternative because it is tar-free and the intrinsic water content of microalgae can be used to generate steam, which will act as a gasifying agent. However, the selection of the process parameters, especially catalyst, is critical. The criteria for catalyst selection is discussed in the following section.

## 2.5 Catalyst selection

Tar formation in the microalgal gasification is well reported in the literature. Moreover, it is observed that most of the nitrogen was getting transformed into tar. Hence, a need for *in-situ* tar reforming catalyst during RFV has been observed. Tar reforming catalysts are divided into two groups based on their chemical composition such as a) natural minerals and b) synthetic catalysts (Abu El-Rub *et al.*, 2004). Dolomite and olivine are categorised as the natural mineral catalyst, whereas, AAEM or transition metals are categorised as synthetic catalysts. Wang *et al.* (2005) have noted that, although the quality of gas was improved using dolomite as the primary catalyst, additional gas cleaning steps were required to meet the end-use specifications.

Synthetic catalysts, specifically Ni-based catalysts, are extensively reported in the biomass gasification literature. Ni is acknowledged for its performance in tar elimination and its ability to improve the gas quality. Chan and Tanksale (2014b) have reviewed Ni-based catalysts for biomass gasification. They have noted that commercially Ni-based catalysts have been used as a primary catalyst for steam reforming, water-gas shift, whereas, very few studies have reported commercial Ni-based catalysts as the primary catalyst for biomass gasification. Although Ni improves the gas quality and catalyses the tar reforming, it suffers from rapid deactivation due to surface carbon deposition and sintering (Se-

hested, 2006). On the other hand, commercial Ni-based secondary catalysts are excellent in tar elimination. It was reported in the literature that more than 90% tar was converted using commercial catalysts obtained from BASF, Haldor Topsoe, ICI Katalco and Sud Chemie (Caballero *et al.*, 1997; Aznar *et al.*, 1998; Caballero *et al.*, 2000; Corella *et al.*, 1998). Deactivation of Ni can be minimised by doping it with promoters such as noble metals, AAEM or another transition metal.

The effect of the noble metal such as Pd, Pt, Rh and Ru on biomass gasification using steam as a gasifying agent was analysed by Nishikawa *et al.* (2008). They noted that the gasification efficiency – the percentage of carbon getting converted into the gas phase, was enhanced in the presence of Pt compared to other promoters. Similar observations were reported by Chaiprasert and Vitidsant (2009) in the case of coconut shell gasification. They have reported that 1% (wt) Pt promoter and 10% (wt) Ni improved the hydrogen yield by enhancing the water gas shift reaction. Huber *et al.* (2004) have reported the effect of Pd on aqueous phase reforming of biomass-derived oxygenates. They observed that the selectivity of Pd towards alkane production is higher compared to Pt. They argued that the Pd acts as a bifunctional catalyst which has a higher rate of hydrogenation and a lower rate of C-C bond cleavage. Similar observations were reported by Van Druten and Ponec (2000) in the case of competitive hydrogenation of propanol and acetone. Nisamaneenate *et al.* (2012) performed the steam reforming of benzene as a model compound for tar. They noted that Pd enhances the steam reforming resulting in higher yields of $H_2$.

In the case of transition metal effect of Cu on the activity of Ni-based catalysts is extensively reported in the literature. Kitayama *et al.* (1997) performed hydrogenation of $CO_2$ in the presence of $SiO_2$ supported Ni and Ni-Cu alloy. They observed that the reduction efficiency of $CO_2$ was increased significantly in the presence of Cu. Moreover, they articulated that the selectivity of Ni-Cu catalyst is differential. CO exhibits a higher selectivity over $CH_4$ in Cu-rich regions of the catalyst, and $CH_4$ exhibits a higher selectivity in the Ni-rich regions of the catalyst. Similar observations were reported by Liu and Liu (1999). They articulated that $CO_2$ and $H_2$ have a strong affinity towards Cu and Ni, respectively. This facilitates the partial reduction of $CO_2$ to CO on Cu sites and complete reduction of CO to $CH_4$ on Ni sites.

Depending on the reported literature, we decided to develop a supported catalyst comprising of alumina as a support, and Nickel, Copper and Palladium as the active sites for tar reforming and gas-phase reactions.

## 2.6 Research Gaps

The aim of this study was to enhance the selectivity of methane and hydrogen in the syngas using reactive flash volatilisation of microalgae. Thus, using oxygen as a gasifying agent was not preferable since it reduces the selectivity of both via oxidation. Altering selectivity of the hydrogen and methane in the reducing environment was challenging mainly because of a) short resident time of 2 sec, b) the sequence of the reactions is unknown, c) complete conversion of char in the absence of oxygen was doubtful, and d) selection of the gasifying temperature, gasifying agent along with appropriate space and mass velocity of carbon, was critical.

Single-step, tar-free conversion of microalgae into hydrogen- or methane-rich syngas was not reported in the literature. Furthermore, Microalgae has around 10% (w/w) to 12% (w/w) ash, which is rich in Phosphorus. Unlike silica-rich ash, the ash transformation characteristics of phosphorus-rich ash are not extensively reported in the literature (Boström *et al.*, 2010). It is well known in the literature that, AAEM can catalyse gasification reactions. However, the understanding behind the catalytic activity and their role in reaction mechanism were briefly mentioned in the literature (Arnold and Hill, 2019). This research is an effort to understand the ash transformation characteristics of phosphorus-rich ash during steam gasification.

Reactive flash volatilisation is in its nascent stage. Detail TE assessment is necessary to establish commercial competitiveness. Moreover, a detailed life cycle assessment (LCA) is required to assess environmental sustainability. In the microalgae to fuel literature, detailed TEA and LCA studies have mostly been performed for the biochemical routes to produce biodiesel and co-products formation and they have indicated that harvesting and drying of microalgae is the cost and energy-intensive step. (Benemann and Oswald, 1996; Brownbridge *et al.*, 2014; Sen Gupta *et al.*, 2016; Rizwan *et al.*, 2013, 2015) We have performed RFV of microalgae using steam as the gasifying agent and have proposed to use excess water after sedimentation as the gasifying agent. Therefore, it is no longer required to dry the microalgae completely, and hence the GHG emission will be lower compared to the dry microalgae gasification. Although Azadi *et al.* (2014) have reported the GHG values for microalgae gasification, they have not considered the scenario of complete microalgae steam gasification. This work addresses this knowledge gap by performing detailed TEA and LCA studies for the proposed hydrogen and methane production from microalgae using catalytic RFV.

# Chapter 3

# Materials and Methods

## 3.1 Catalyst preparation

The bimetallic– Nickel-Rhodium (Ni-Rh) and trimetallic– Nickel-Copper-Palladium (Ni-Cu-Pd) catalyst was developed using a wet impregnation method explained by Chan and Tanksale (2014a). Alumina ($Al_2O_3$) was used as a support and Nickel nitrate ($Ni(NO_3)_2.6H_2O$), Rhodium chloride ($RhCl_3$), Cupric nitratetrihydrate ($CuN_2O_6.3H_2O$) all obtained from Sigma Aldrich were used as a source for nickel, rhodium and copper, respectively.

To prepare the catalyst, nickel nitrate was dissolved in the deionised water, and then alumina was added to the solution followed by the precursors. The final concentration of nickel and rhodium in the bimetallic catalyst was 10% (w/w) and 1% (w/w), respectively. On the other hand, the final concentration of nickel, copper and palladium was 20% (w/w), 1% (w/w) and 1% (w/w), respectively. Homogeneity of the mixture was ensured by continuous stirring at 65 °C for 5 hours. The solution was dried at 100 °C , and the precipitate was calcinated at 600 °C for 6 hours. The resultant catalysts were reduced *in-situ* before analysing their catalytic activity.

## 3.2 Catalyst Characterisation

Catalysts were characterized to know the surface area, active metal sites and reducibility, using nitrogen physisorption, carbon monoxide temperature programmed desorption (CO-TPD) and temperature programmed reduction (TPR) respectively.

### 3.2.1 Nitrogen physisorption

Nitrogen physisorption was used to measure specific area, pore volume and distribution of the catalyst. Brunauer, Emmett and Teller (BET) method of analysis was used to measure the specific surface area. Whereas, pore volume was analysed using BJH method. 500 *mg* of catalyst was degassed at 350 °C for 10 hours.

### 3.2.2 X-Ray fluorescence spectroscopy

Ultimate analysis of ash and elemental composition of catalyst was measured using Ametek Spectro iQ II XRF.

### 3.2.3 Temperature programmed reduction (TPR)

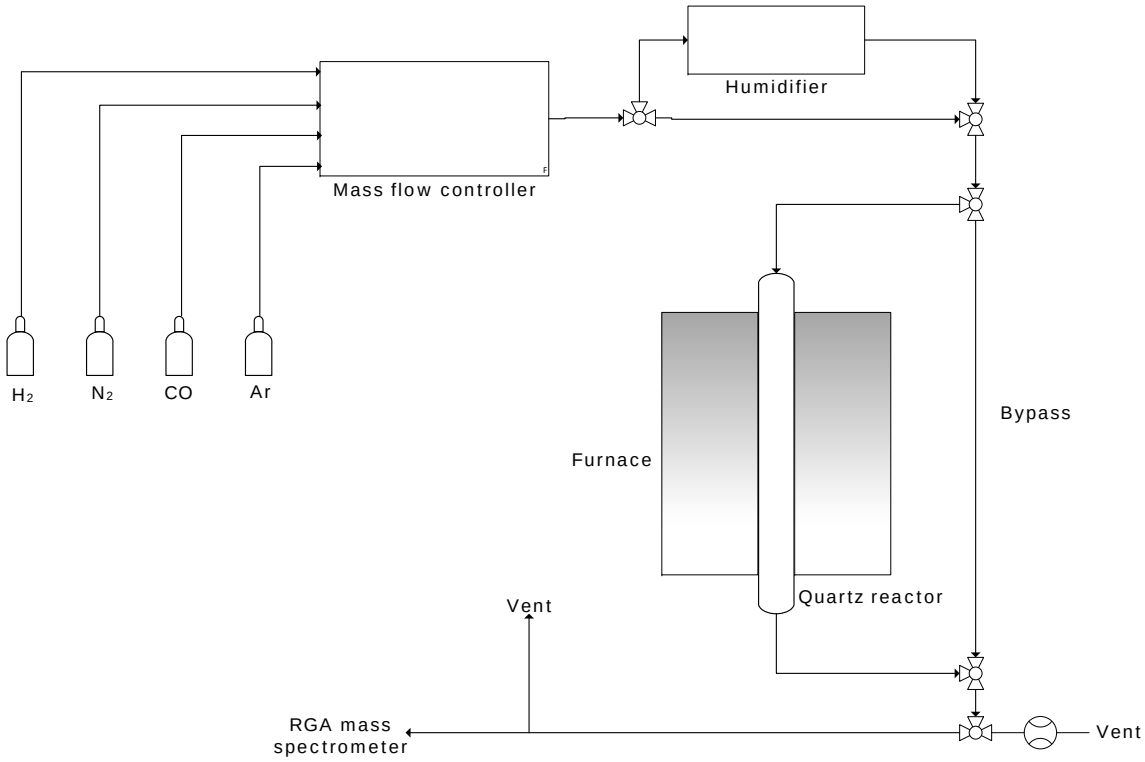


Figure 3.1: Schematic diagram of TPR and TPD setup

To investigate, the temperature required for onset of catalyst reduction and effect of promoters on the reducibility, TPR analysis was performed. Figure 3.1 shows the schematic diagram of custom build instrument for TPR analysis. Mainly; it consisted of Aglient Technology's compact vacuum pump, a Stanford Research Systems Residual Gas

Analyser (RGA) 300 and a vertical tube furnace manufactured by Labec Equipments. To perform TPR analysis, 500 mg of catalyst was loaded into a quartz reactor fitted with a frit. The reactor was then placed into the furnace. Heating profile for the furnace was programmed to reach 800 °C with the ramping of 10 °C/min. 5% hydrogen in nitrogen was fed to the reactor continuously with the flow rate of 50 ml/min during heating. A small fraction of the gas coming out of the reactor was introduced to the RGA via a capillary tube. Partial pressure of the gas was recorded for further analysis.

### 3.2.4 Carbon monoxide temperature programmed desorption (CO-TPD)

To investigate, the strength and number of metal active sites; CO-TPD analysis was performed with the help of a instrument described in Figure 3.1. 500 mg of catalyst was reduced at 400 °C by 5% $H_2/N_2$ mixture for 4 hours. The reactor was then purged with argon for 1 hour at 400 °C. In the presence of inert atmosphere reactor was allowed to cool down to room temperature. CO doping of the catalyst surface was achieved by flowing 10% CO/Ar gas mixture through the reactor for 15 min. Then, to ensure monolayer adsorption of CO, reactor was purged with Ar gas for 2 hours. Furnace was then programmed to reach 800 °C with the ramping of 10 °C/min. Gas coming out of the reactor was then analysed using RGA 300.

### 3.2.5 Carbon monoxide chemisorption (CO-Chemisorption)

CO Chemisorption was performed to analyse the active sites using Thermo Scientific TPDRO 1100 instrument. To perform CO chemisorption, a quartz reactor was loaded with 500 mg of catalyst and assembled in the furnace. Then, the catalyst was reduced with 5% $H_2$/Ar gas mixture at 400 °C for 4 hours. The reactor was cooled down to 21 °C under inert atmosphere. At 21 °C, pulse injection of CO was performed. 0.34 ml of 99.999% pure CO was injected during each injection. TCD detector was used to quantify the adsorbed CO. Depending on the CO-chemisorption, turnover frequency (TOF) was calculated as,

$$\text{TOF} = \frac{\text{Rate of the reaction (mol}\cdot\text{ g catalyst}^{-1}\cdot\text{ min}^{-1})}{\text{Moles of CO (mol}\cdot\text{ g catalyst}^{-1})} \tag{3.1}$$

### 3.2.6 Transmission Electron Microscopy (TEM)

Scanning Tunneling Transmission electron microscopy (STEM) of catalyst was performed using JEOL HR-TEM 300 kV to analyse the size and morphology of the catalyst, and to map the elemental distribution on the surface of a catalyst. To prepare a sample, a

small quantity of catalyst was ground in presence of n-butanol, and it was then sonicated for 15 min. The suspension was then loaded onto a holey carbon copper grid, and was dried using IR lamp for 20 min. Ni, Cu, Rh, and Pd were mapped using STEM-EDX methodology.

## 3.3 Biomass Feedstock and characterisation

*Scenedesmus sp.* – henceforth referred as microalgae,, obtained from South Australia Research and Development Institute (SARDI) was used as the biomass feedstock. *Scenedesmus sp.* was chosen due to its higher tolerance for $CO_2$. Microalgae was characterized using European standards (EN) for its chemical properties. EN14774, EN14775 and EN15148:2009 were used to analyse moisture, proximate and ultimate content of the microalgae, respectively. LECO TruMac analyser was used to identify CHNS content and Ametek Spectro iQ II was used for analysing elemental content.

## 3.4 Slag Characterisation

Slag was characterised to understand its elemental composition, porosity, morphology and chemical shift in the constituent elements.

### 3.4.1 X-ray Computed Tomography (X-Ray CT)

X-ray computed tomography (CT) was performed using Zeiss Xradia Versa 520, to analyse the porous structure of the slag. A 0.5 cm $\times$ 0.5 cm $\times$ 0.5 cm sample of slag was used for the CT scan.

### 3.4.2 Scanning Electron Microscopy (SEM)

The slag sample was collected from the reactor at the end of the experiment. It was ground to fine powder, and sprinkled on the sticky carbon tape. The sample was non-conducting, and hence, was sputter coated with platinum for 150 s. A sputter coated sample was then observed under JSM-7600F Field Emission Gun-Scanning Electron Microscope (FEG-SEM), to observe the changed morphology and particle size. Energy Dispersive X-ray Spectroscopy (EDX) was performed to map the alkali and alkaline earth elements (AAEM).

Table 3.1: Elemental analysis of microalgae

| Ultimate analysis | (% db) |
|---|---|
| C | 40.29 |
| H | 7.0 |
| N | 8.1 |
| S | 1.22 |
| Ash | 10.86 |
| O* | 32.53 |
| Ash | (%) |
| MgO | 15.55 |
| $Al_2O_3$ | 1.83 |
| $SiO_2$ | 5.84 |
| $P_2O_5$ | 51.93 |
| $SO_3$ | 0.68 |
| Cl | 0.062 |
| $K_2O$ | 12.62 |
| CaO | 8.6 |
| $TiO_2$ | 0.16 |
| MnO | 0.11 |
| $Fe_2O_3$ | 2.57 |
| CoO | 0.09 |
| NiO | 0.01 |
| CuO | 0.03 |
| ZnO | 0.04 |

* Calculated by difference

### 3.4.3 X-ray Photoemission Spectroscopy (XPS)

The powdered sample was analysed using AXIS Supra Surface Analysis Instrument, by Shimadzu. Monochromatic Al K-$\alpha$ at 600 W, with 1486.6 eV energy was used as a X-ray source, and C1s peak from surface adsorbed carbon was calibrated at 284.7 eV. XPS peaks were analysed by fitting a mixed Gaussian-Lorentzian function with 30% contribution of Lorentzian. The contribution of Lorentzian function was decided based on the instrument setting.

## 3.5 Reactor setup

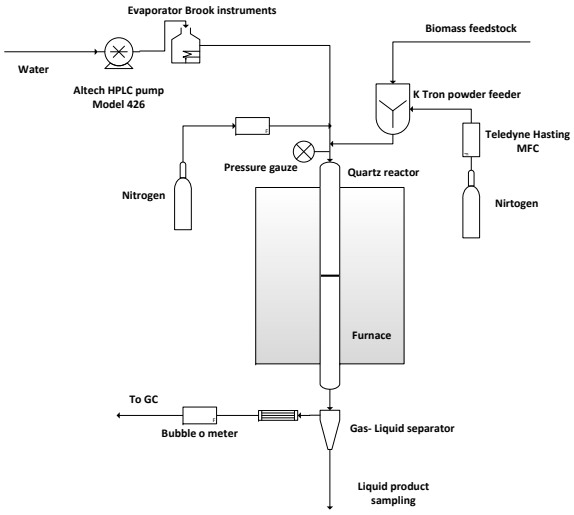


Figure 3.2: Reactor setup used to evaluate the catalytic activity using reactive flash volatilization of microalgae (Adapted and modified from Chan and Tanksale 2014a)

To evaluate the catalytic activity of the catalysts, reactive flash volatilization (RFV) of microalgae was performed in the bench scale reactor shown in the figure 3.2. It consists of a 25 mm X 700 mm quartz tube reactor, a K-Tron twin screw powder feeder (K-MV-KT20), an Alltech HPLC pump (model 426), three Teledyne Hasting mass flow controllers for nitrogen and oxygen, a Labec vertical split tube furnace, a Brooks Instrument DLI Series evaporator and a custom built gas-liquid separator.

To perform RFV, reactor was loaded with 1 g of the fresh catalyst and assembled in the furnace. Then, the catalyst was reduced with 5% $H_2/N_2$ gas mixture at 400 °C for 4 hours. Furnace was then programmed to reach the desired operating temperature with the ramping of 10 °C /min. Carbon to steam ratio in the range of 0.12 to 0.8 was maintained by using the flow rate of the water. The gas hourly space velocity was maintained in the range of 10000 $h^{-1}$ to 11000 $h^{-1}$ using the flow rate of nitrogen. 7 g/h of microalgal biomass having 5% moisture was fed to the reactor using twin-screw feeder. The feeding rate of microalgae was decided based on the carbon space- and mass-velocity. The carbon mass velocity was maintained in between 2.5 $h^{-1}$ to 3 $h^{-1}$. Product gas was sampled periodically after gas-liquid separator and injected into GC for analysis. Shimadzu gas chromatograph GC-2014; equipped with a molecular sieve 5A column, Thermal Conductivity Detector (TCD) and a Flame Ionisation Detector (FID) was used for gas analysis. Bubble-O-Meter was used to measure the flow rate of product gas. Carbon content of condensate and

slag, produced after RFV was analysed using LECO TruMac CHNS analyser. Depending on the individual carbon content and distribution of the gases, selectivity and yield was calculated using equation 3.2 and 3.3, respectively. Experiments with gas phase carbon selectivity of more than 85% were performed in triplicates to evaluate the performance of the reactor.

$$\text{Selectivity} = \frac{\text{Moles of carbon in particular phase}}{\text{Moles of carbon in product}} \times 100 \tag{3.2}$$

$$\text{Yield} = \frac{\text{Amount of hydrogen or methane produced}}{\text{Total amount of gaseous products}} \times 100 \tag{3.3}$$

## 3.6 Approach

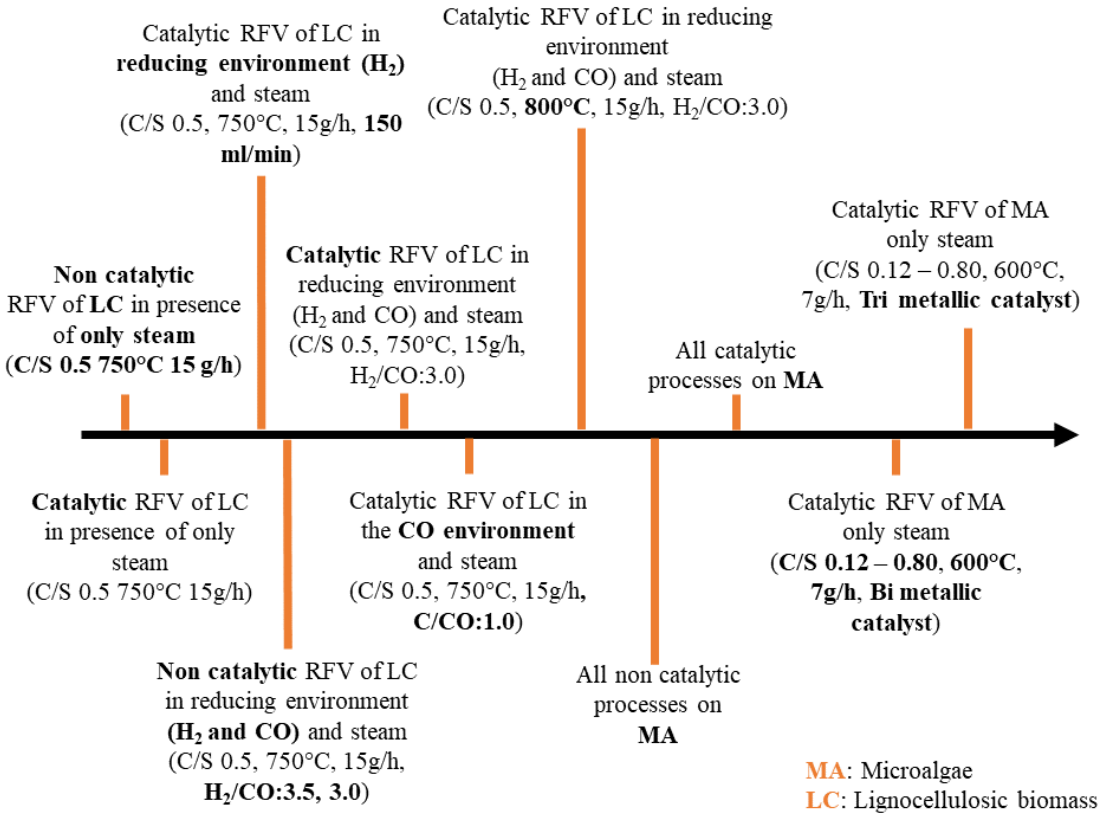


Figure 3.3: Approach towards reactive flash volatilization of microalgae [1]

To enhance the methanation reaction, we performed our preliminary experiments in the reducing environment with *Eucalyptus regnans* (LC biomass). *Eucalyptus regnans* was selected as the feedstock because, a) it had around 7% ash composed of alkali and alkaline

[1] Operating conditions are specified in the brackets and changes in the operating parameters w.r.t. the previous experiment are denoted in the bold characters

earth metals (AAEM), which is similar to that of microalgae, b) we had the understanding of its behaviour in oxidative environment (Chan and Tanksale, 2016), and c) the precedent of microalgae gasification in the reducing environment was not reported in the literature. Figure 3.3 shows our approach towards reactive flash volatilisation of microalgae.

At first, the non-catalytic experiments were performed to evaluate the catalytic performance of AAEM present in the ash. The operating conditions explained by Chan and Tanksale (2016) were used to perform the experiments. We observed that the reactor was clogged due to accumulation of unreacted char and tar. We concluded that the catalytic activity of AAEM was not enough to gasify and reform the char and tar, respectively.

To enhance the catalytic activity, Ni-Rh supported on alumina was selected as the catalyst based on the observations reported by Chan and Tanksale (2016). Although the overall catalytic activity in the reactor was improved and higher selectivity towards CO was observed, the reactor was clogged with tar and char accumulation. To hydrogenate the tar and increase its reactivity, firstly; the hydrogen was introduced in the RFV along with steam, and secondly; a mixture of CO and $H_2$ was introduced in the reactor as suggested by Sirdeshpande and Preston (2011). We observed that regardless of the reaction environment; in both the cases, initially, the methanation reaction was promoted on the surface of fresh catalyst; however, tar and char formation clogged the reactor resulting in a decline in the methane composition over the period. A similar observation was noted by Jüntgen (1981). He noted that the reactivity of hydrogen differs depending upon the structure of the char. Moreover, it inhibits the steam gasification of char in some cases. Therefore, to enhance the gasification rate, we increased the operating temperature to 800 °C and substituted $H_2$ with CO. However, the reactor was clogged. Based on the observations, we postulate that not only the hydrogen but also the pyrolysates of lignin inhibit the steam gasification of the char during RFV of lignocellulosic biomass in the reducing environment. Here, we concluded the experiments with lignocellulosic biomass and moved on to microalgae.

Microalgae has a very different composition compared to LC biomass. It is devoid of lignin and mostly composed of cellulose, hemicellulose, lipids and proteins (Chisti, 2007; Rosenberg *et al.*, 2008b). The behaviour of these individual compounds during the gasification process was well established. However, the synergistic effect of the compounds in the reactor was missing in the literature. To analyse the behaviour of microalgae, and establish the base case, we performed oxidative RFV of microalgae using the operating conditions specified by Chan and Tanksale (2014a); Colby *et al.* (2008). We observed that 16% of methane was formed in the produced gas. However, the reactor was clogged due to tar accumulation.

The ultimate analysis of tar revealed that it was mainly composed of nitrogenous compounds. Moreover, we realised that the operating zone for RFV was fixed based on nitrogen-deficient feedstocks. Whereas, microalgae is rich in nitrogen mainly due to its protein content. It has around 8% of nitrogen on a dry weight basis. The operating conditions and catalysts were modified to account for the difference in the composition. The effects of operating parameters and promoters on the composition of the syngas produced are described in the following chapter.

# Chapter 4

# Results and Discussions

## 4.1 Catalyst Characterisation

### 4.1.1 Nitrogen physisorption and XRF analysis

Table 4.1: Nitrogen physisorption and XRF analysis

| | Catalyst | | |
|---|---|---|---|
| Characterization | Alumina | Ni-Rh | Ni-Cu-Pd |
| Surface Area ($m^2/g$) | $1.02 \times 10^2$ | $8.70 \times 10^1$ | $8.20 \times 10^1$ |
| Pore volume ($cm^3/g$) | $1.80 \times 10^{-1}$ | $1.70 \times 10^{-1}$ | $1.50 \times 10^{-1}$ |
| XRF characterisation | | Ni :11.90% ± 0.8%<br>Rh*: 0.92 % | Ni: 21.5% ± 0.8%<br>Cu: 1.33% ± 0.23%<br>Pd*: 1.20% |
| Ni Dispersion (%) | | 1.03 | 0.01 |
| Turnover Frequency ($min^{-1}$) | | $3.31 \times 10^2$ | $3.69 \times 10^3$ |

* Calculated by difference

Table 4.1 shows the results of nitrogen physisorption and XRF analysis. It was observed, that the surface area of alumina was reduced while pore volume remained the same. XRF analysis was used to confirm the metal loading. The values reported in the Table 4.1 match with the theoretical calculated metal loading. CO chemisorption was conducted using pulse titration method which showed that Ni-Rh had a CO coverage of 22.3 $\mu$mol/g-catalyst whereas Ni-Cu-Pd catalyst had a CO coverage of only 0.3 $\mu$mol/g-catalyst. The pulse titration method might underestimates the CO coverage on Pd catalysts. Moreover, it is also possible that the formation of Ni-Cu alloy resulted in the

modification of Ni active sites. This is in coherence with the observation reported in TPR and XRD analysis.

### 4.1.2 Temperature Programmed Reduction (TPR)

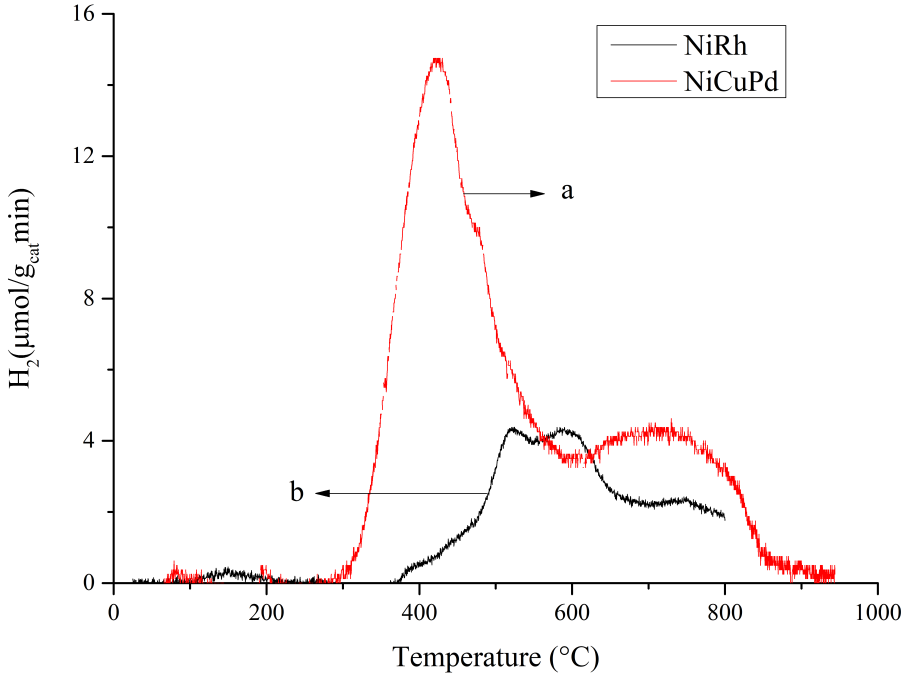


Figure 4.1: TPR profile of the catalyst. a) Ni-Cu-Pd and b) Ni-Rh

Figure 4.1 shows the TPR profiles of Ni-Cu-Pd (curve a) and Ni-Rh (curve b) catalysts. The onset of reduction for Ni-Cu-Pd and Ni-Rh catalyst was observed at 300 °C and 362 °C , respectively. It has been extensively reported in the literature, that the reducibility of Ni catalysts is promoter dependent, and it is governed by the hydrogen spill over effect attributed by the individual promoter (Profeti *et al.*, 2009). Curve a shows a major peak at 400 °C , a broad peak between 600 °C to 800 °C and a shoulder peak around 480 °C . Whereas, curve b exhibits four peaks at 400 °C , 520 °C , 600 °C and 750 °C , respectively. Monometallic Ni on alumina support reduces at temperatures in excess of 700 °C (Tanksale *et al.*, 2008). A peak at 750 °C in curve a and a broad peak between 600 °C to 800 °C in curve b is attributed to the strong interaction of Ni with the support forming Nickel Aluminate. It is well known in the literature that the interaction of Ni with alumina is strongly depended on the Ni loading. At <12% Ni interacts with the tetrahedrally coordinated sites present on alumina. In contrast, above 12% it forms NiO as a bulk phase due to alumina surface saturation (Li and Chen, 1995). A major peak at 400 °C in curve a is attributed to the bulk NiO and a shoulder peak at 480 °C is likely to be the Ni-Cu alloy reduction. Moreover, two TPR peaks at 520 °C and 600 °C in curve b

can be attributed to the Nickel-alumina interaction at tetrahedrally coordinated sites. Furthermore, the phases observed during reductions are in coherence with the observations of XRD analysis.

### 4.1.3 Carbon monoxide temperature programmed desorption (CO-TPD)

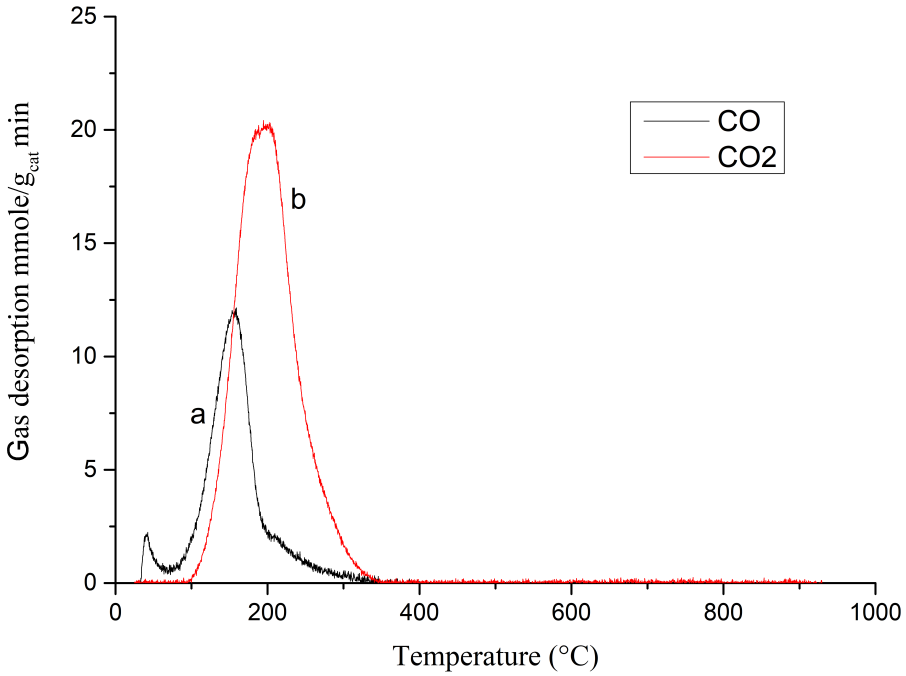


Figure 4.2: TPD profile of the tri-metallic catalyst. **a**: desorption of CO. **b**: desorption of $CO_2$

CO desorption at elevated temperature is a complex process. The entire mechanism of CO desorption is not always fully understood. The desorption is mainly dependent on a) activation energy and b) surface area coverage by CO (Hayward and Trapnell, 1964). Figure 4.2 shows the TPD profile for Ni-Cu-Pd catalyst and the TPD profile for Ni-Rh catalyst can be found in our earlier work (Chan and Tanksale, 2014a). Curve (a) in Figure 4.2 indicates desorption of CO and curve (b) in Figure 4.2 denotes the evolution of $CO_2$. $CO_2$ is formed on the surface of the alumina catalyst by reacting with the hydroxyl groups on the surface of alumina (Hayward and Trapnell, 1964). Weak multilayer adsorption of CO on the catalyst surface resulted into the early low temperature peak at 50 °C. However, strong single layer CO adsorption resulted into the dominant peak at approximately 160 °C.

### 4.1.4 Effect of steam content and temperature

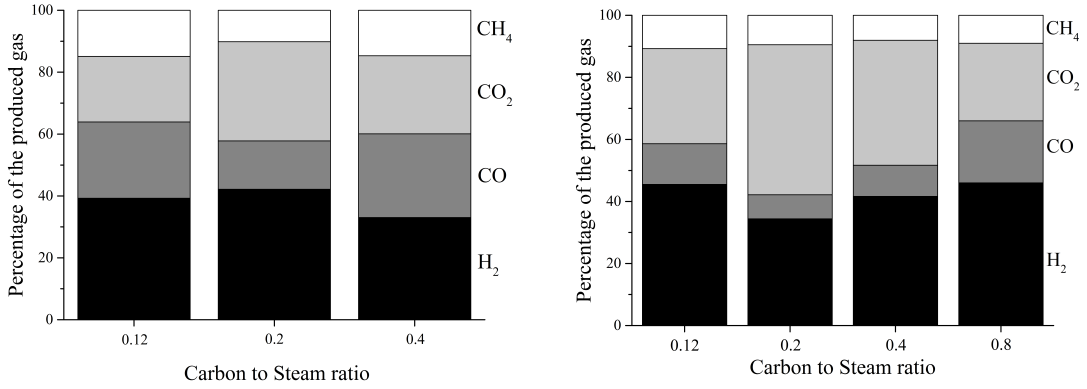


(a) Ni-Cu-Pd (b) Ni-Rh

Figure 4.3: Effect of steam content on the distribution of the compounds in the syngas (Operating conditions :– Temp: 600 °C , feeding rate: 7g/h, Tri-metallic catalyst: Ni-Cu-Pd/$Al_2O_3$, Bi-metallic catalyst: Ni-Rh/$Al_2O_3$)

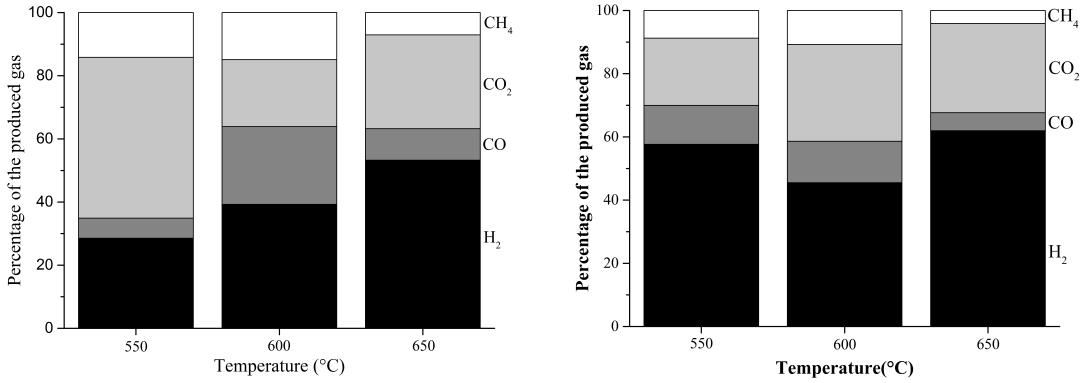


(a) Ni-Cu-Pd (b) Ni-Rh

Figure 4.4: Effect of temperature on the distribution of the compounds in the syngas (Operating conditions :– C/S: 0.12, feeding rate: 7g/h, Tri-metallic catalyst: Ni-Cu-Pd/$Al_2O_3$, Bi-metallic catalyst: Ni-Rh/$Al_2O_3$)

Figure 4.3 and 4.4 show the effect of steam content and temperature on the composition of gases in the produced gas. The results obtained using fresh catalyst are reported in this study. We have not evaluated the catalytic effect of a recycled catalyst. Figure 4.3 shows that at 600 °C and in presence of Ni-Rh catalyst the composition of $H_2$ and CO decreased, and the composition of $CO_2$ increased with decreasing the carbon-to-steam ratio (CSR) which is likely due to the competing reaction equilibria of water gas shift and CO methanation reaction. Although, at CSR of 0.8 the composition of $CH_4$ and $H_2$ was high (16% and 45%) the reactor clogged after 3 hours of operation because of char

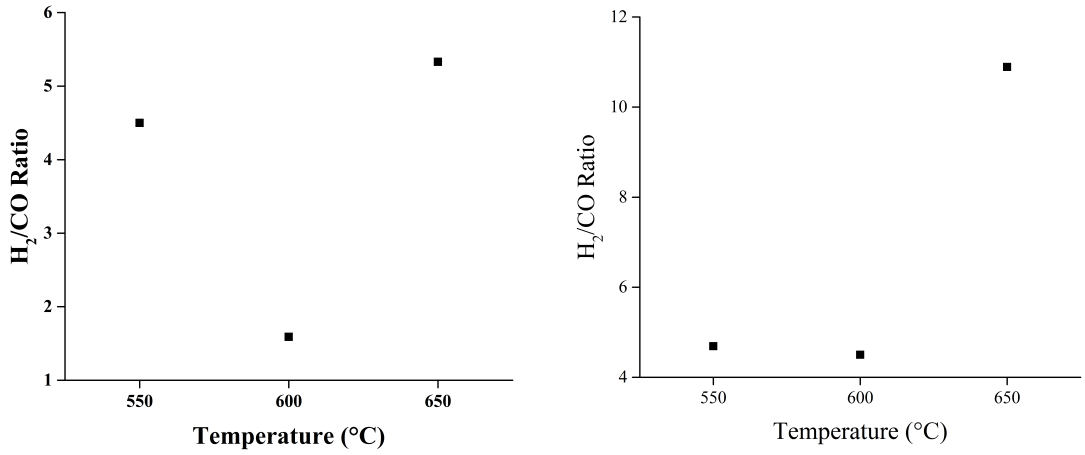


(a) Ni-Cu-Pd (b) Ni-Rh

Figure 4.5: Effect of temperature on the distribution of the ratio of hydrogen to carbon monoxide ($H_2$/CO) (Operating conditions :– C/S: 0.12, feeding rate: 7g/h, Tri-metallic catalyst: Ni-Cu-Pd/$Al_2O_3$, Bi-metallic catalyst: Ni-Rh/$Al_2O_3$)

and tar accumulation. The steam content was not enough for char gasification and tar reformation. Similarly, as shown in Figure 4.4 at CSR of 0.12 and temperature 550 °C , although the composition of $H_2$ and $CH_4$ was high (55% and 15%, respectively) the reactor clogged after 2.5 hours of operation. The operating temperature was not enough for char gasification and tar reformation. Although, the gasification efficiency was improved when CSR was changed from 0.8 to 0.2 the operational time was limited to 4 hours due to tar accumulation. As shown in Figure 4.4, at 650 °C in presence of Ni-Rh catalyst and CSR of 0.12, 65% (v/v) $H_2$ was produced with the gasification efficiency of more than 95%. The performance of the reactor was evaluated for the reproducibility of the results. In the case of hydrogen production, an experiment performed at 650 °C and a carbon to steam ratio of 0.12 was selected, Whereas, in the case of methane production, experiment performed with 600 °C and a carbon to steam ration of 0.12 was selected. These experiments were selected because a) the gas phase carbon selectivity was more than 85%, and b) yield of hydrogen and methane was 65% and 16%, respectively. Figure A.1 shows the performance evaluation for $H_2$ and $CH_4$ production. A constant reactor performance was observed during for three different runs. The composition of $H_2$ is 60% more than the hydrogen composition reported by Xie *et al.* (2019) during hydrothermal gasification. The reactor was operational for 9 hours with an average rate of reaction of 7.38 mmol$\cdot$ $min^{-1} \cdot$ g-$catalyst^{-1}$, giving a turn over frequency (TOF) of 330.94 $min^{-1}$ based on the CO-coverage measured using pulse titration method. The yield of hydrogen was calculated to be 59.23 mol of $H_2$/ kg of microalgae. Moreover, the overall yield of gas, char and tar on

condensate and ash free basis was calculated to be 95%, 3% and 1%, respectively. The yield of hydrogen obtained is 97% higher compared to catalytic HTL process reported in the literature (Cherad *et al.*, 2016). The monometallic Ni catalyst was not stable in the reaction conditions, leading to quick deactivation before stable operating conditions could be achieved, and hence it was not possible for us to estimate the TOF of the reaction over Ni/alumina catalyst. The effect of the promoter is to keep the Ni surface clean by promoting tar reforming and preventing coke deposition. The composition of $H_2$ was enhanced most likely due to enhancement of water gas shift and methane steam reforming reactions (Wheeler *et al.*, 2004; Wang and Ruckenstein, 2000; Guo *et al.*, 2004). In presence of Ni-Cu-Pd catalyst (Figure 4.3), composition of $CH_4$ was observed to be 16% at 550 °C and 600 °C . However, at 550 °C the reactor clogged after 3.5 hours, whereas, at 600 °C the reactor was operational for 13 hours with the gasification efficiency of 85%. Based on the CO-coverage measured using pulse titration method, the TOF of the catalyst was calculated to be 3689.83 $min^{-1}$. The relatively high TOF calculated here may be due to the limitation of pulse titration method for measuring CO-coverage for Pd catalysts (Prelazzi *et al.*, 1999) and lower CO-coverage measured due to Ni-Cu alloy formation. The yield of $CH_4$ was calculated to be 10.89 mol of $CH_4$/ kg of microalgae. Moreover, the overall yield of gases, char and tar on condensate and ash free basis was calculated to be 95%, 3.2% and 1%, respectively. Ni-Cu-Pd catalyst promoted methanation reaction via hydrogenation of CO and $CO_2$ resulting in low hydrogen-to-carbon monoxide ratio which is consistent with literature (Liu and Liu, 1999; Kitayama *et al.*, 1997). While the effect of Rh promoter was to enhance the reforming and WGS reactions, leading to high $H_2$ selectivity, the effect of Cu-Pd promoter was to enhance the methanation reaction. This compares favourably with the published literature. Raheem *et al.* (2017) reported gasification of *Chlorella vulgaris* with the efficiency of 75% and product gas composition consisting of 22.2% $CH_4$ and 24.2% $H_2$. Liu *et al.* (2017) reported gasification efficiency of 77.19% and product gas composition consisting of 9% $CH_4$ and 17% $H_2$ using chemical looping gasification of *Chlorella vulgaris*.

## 4.2 Ash transformation characteristics

Boström *et al.* (2010) classified the ash into two groups silica- and phosphorus-rich ash. Further it is also classified into subgroups such as high potassium or calcium containing ash based on the ratio of potassium to calcium. Woody biomass falls into the category of silica rich, high calcium containing ash (Boström *et al.*, 2010). Whereas, based on the composition described in the Table 3.1, microalgae can be classified as phospho-

rus rich, high potassium containing ash. Transformation of high silica containing ash is well reported in the literature. BostroÌĹm *et al.* (2009) and He *et al.* (2018) articulated that, the silicates of the alkali and alkaline earth metals (AAEM) are formed during ash transformation depending on the operating temperature of the reactor. However, the transformation of Phosphorous rich ash is not extensively reported in the literature. Skoglund (2014) has explained the potential reaction mechanism involved in the ash transformation. They have noted that, formation of AAEM phosphates is a three-step process consisting of oxidation, neutralization and phosphorylation. The Ellingham diagram for the participating elements shows that the reactivity of the potassium and magnesium is much higher compared to the silica and calcium (Grimm *et al.*, 2011, 2012b,a). The details pertaining to the reactions and their sequence leading to AAEM phosphate formation can be found elsewhere (Skoglund, 2014).

It was observed from the XRD pattern shown in Figure 4.6, that the crystalline ash was transformed into an amorphous slag. Table A.1 lists the compounds that were identified based on the XRD analysis of ash and slag. It was evident that, AAEM elements have transformed into their respective phosphates during the reaction. To confirm the transformation of AAEM elements, XPS analysis of slag was performed.

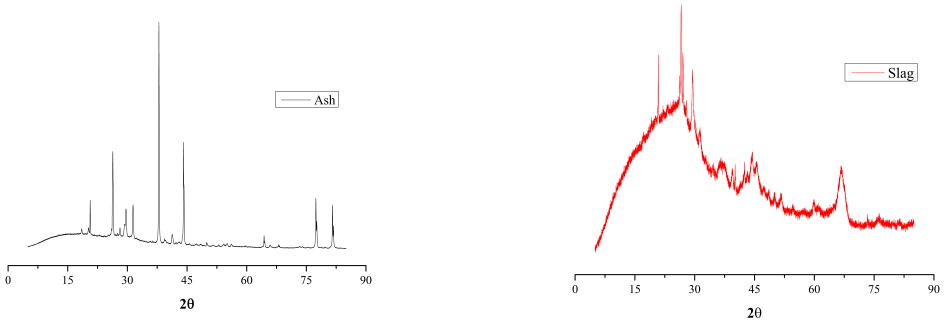


(a) Ash

(b) Slag

Figure 4.6: XRD pattern for ash and slag. (a) XRD of ash before reaction, (b) XRD of transformed ash (slag)

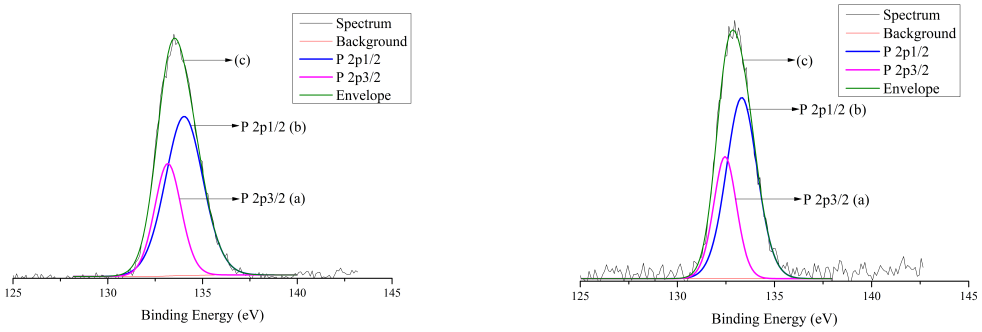


(a) Ash (b) Slag

Figure 4.7: XPS analysis of Phosphorus 2p to confirm a chemical shift after reaction. A) Phosphorus in ash and B) Phosphorus in slag

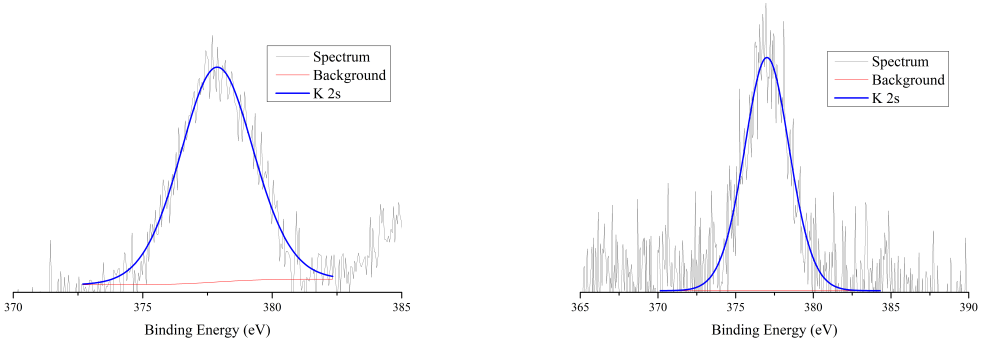


(a) Ash (b) Slag

Figure 4.8: XPS analysis of Potassium 2s to confirm a chemical shift after reaction. A) Potassium in ash and B) Potassium in slag

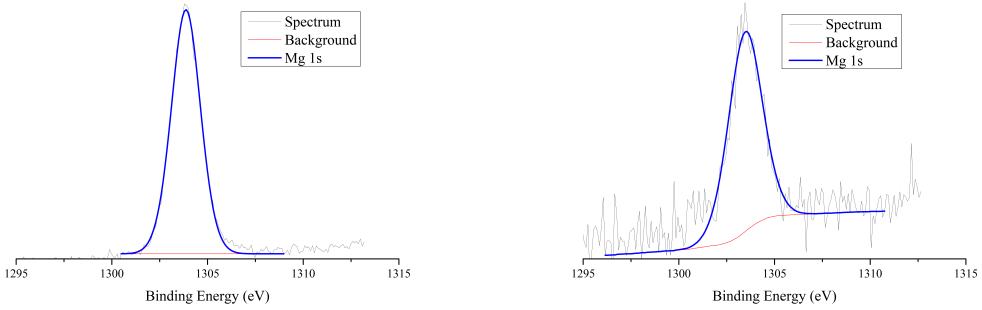


(a) Ash (b) Slag

Figure 4.9: XPS analysis of Magnesium 1s to confirm a chemical shift after reaction. A) Magnesium in ash and B) Magnesium in slag

Table 4.2: XPS analysis

| Element | Ash (eV) | Slag (eV) | Shift (eV) |
|---|---|---|---|
| P | 2p1/2: 133.67 | 2p1/2: 133.15 | 2p1/2: 0.52 |
| | 2p3/2: 132.81 | 2p3/2: 132.29 | 2p3/2: 0.52 |
| K | 2s: 377.42 | 2s: 376.86 | 2s: 0.56 |
| Mg | 1s: 1302.65 | 1s: 1303.42 | 1s: 0.77 |

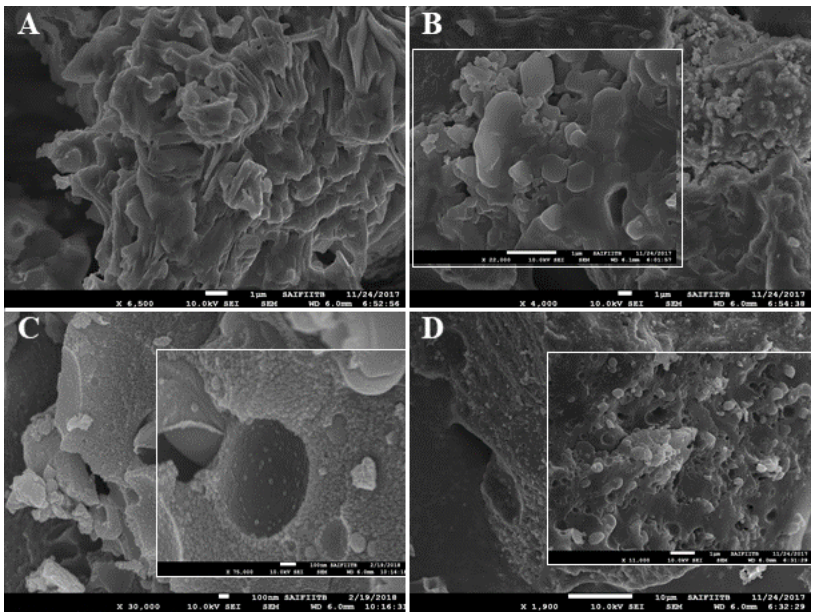


Figure 4.10: SEM Figures showing a morphological comparison of ash before reaction (A and B) and after reaction-slag (C and D).

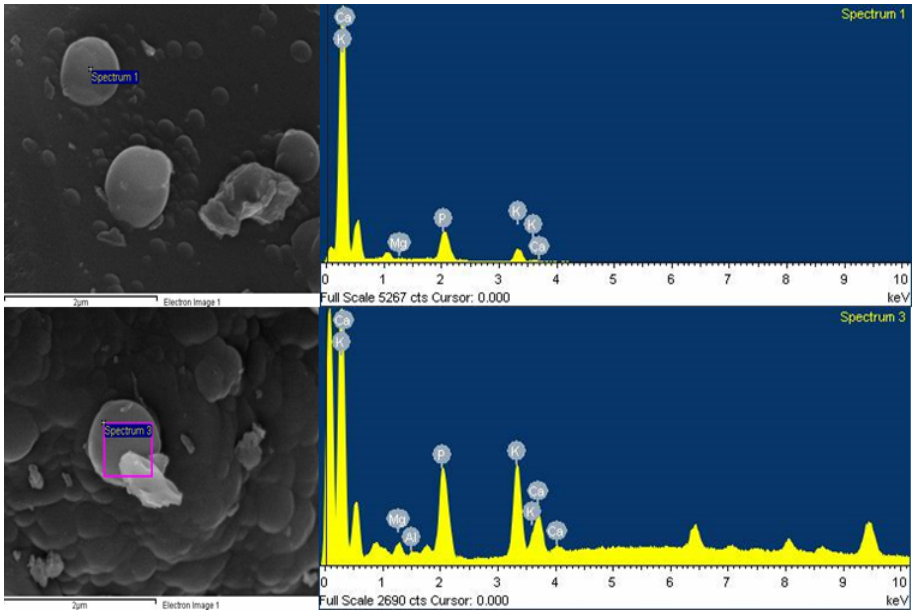


Figure 4.11: SEM EDX Figure showing the presence of Phosphorus, Calcium, Potassium and Magnesium on the spherical nanoparticles present in the slag

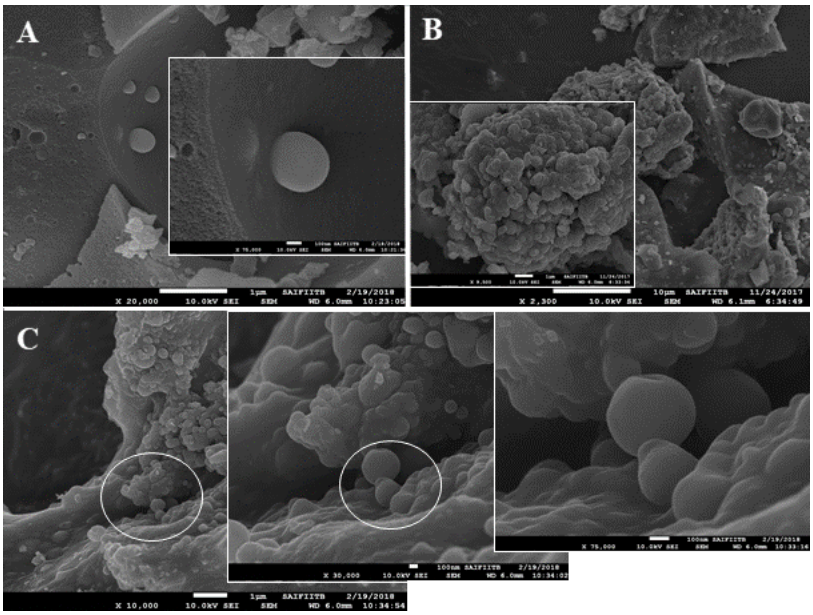


Figure 4.12: SEM Figure showing a evolution of highly porous structure of a slag. A) Nanoparticle– a fundamental unit of a bead B) Agglomeration of nanoparticles to form a bead and C) Steps in the evolution of a porous structure.

XPS profiles of Phosphorus, Potassium and Magnesium are shown in Figure 4.7, Figure 4.8 and Figure 4.9, respectively. A shift in the binding energy of the elements is observed and it is summarized in Table 4.2.Transformation in the chemical nature of the elements resulted into altered morphology, which was confirmed using FEG-SEM

analysis. Figure 4.10A and 4.10B shows non-porous surface with random arrangements of crystals and sheets. Whereas, Figure 4.10C and 4.10D shows a porous structure made up of small beads. Furthermore, as shown in Figure 4.11, SEM-EDX analysis has confirmed the presence of Ca, Mg, P and K in the naosphere formed during ash transformation.

We hypothesize that, an agglomeration of potassium- and magnesium- phosphate coated nano-spheres of calcium phosphates resulted into a porous morphology as shown in Figure 4.12. Moreover, the bed exhibits some catalytic properties due to its composition. Potassium is an electropositive element and it enhances the WGS reaction by dissociating CO from the adsorbed sites. This results into higher hydrogen selectivity in the gas. It also enhances the surface methanation reactions. In case of magnesium, though its role in tar reforming is briefly mentioned in the literature, the exact mechanism of magnesium catalysed gasification reactions is not extensively reported in the literature. The enhanced overall catalytic activity in a reactor could be a reason for tar free conversion of microalgae. The exact role of the ash transformation in reaction mechanism and the effect of operating parameters on the catalytic activity is discussed in the following sub-section.

## 4.3 Reaction mechanism

The RFV progresses through a series of chemical reactions. The sequence of these reactions is not fully understood. RFV was characterised by two different reaction mechanisms in the literature depending on the physical state of a feedstock [17, 19]. In case of liquid feedstock, such as soy oil, the dynamics of a simultaneously boiling and cracking of a droplet on a hot porous surface is a complex mechanism. The droplet partly behaves according to the 'Leidenfrost effect'. In conventional Leidenfrost effect a vapour layer forms around the droplet of volatile liquid as soon as it hits a hot surface. This layer insulates the droplet from the heat for a short period of time. RFV cannot be explained completely depending on this effect or film boiling, because; rapid heat transfer to the droplet will cool down the catalyst surface. In order to explain this phenomenon, Salge *et al.* (2006) postulated that, cold drop hits the hot catalytic surface and rebounds due to momentum transfer. A rapid heat flux causes the split and instantaneous vaporization followed by, oxidative pyrolysis; to form a layer of gases around the drop. Volatile organic compounds (VOC) and gases formed then react to maintain the temperature of the catalyst to sustain the steady state of the reactor.

In case of solid feedstock, such as cellulose, Colby *et al.* (2008) noted that, each step towards the conversion is complex combination of multi-step and multi-phase reaction with various modes of heat transfers. The process is complex due to simultaneous transfer

of mass and energy. Moreover, they postulated that the reaction starts only when the cellulose particles hits the catalyst sur face, because temperature in the reactor above catalyst is not sufficient for the pyrolysis of the particle. We observed that the postulation pertaining to the reaction mechanism explained by Colby *et al.* (2008) holds good in the case of ash free feedstock like cellulose. However, in case of ash rich feedstock such as microalgae, ash transformation characteristics plays a critical role in ensuring the suitability of the biomass for gasification.

Figure 4.13 shows the proposed mechanism for RFV of Phosphorus rich biomass. Figure 4.13A depicts the state of the catalyst surface during the initial hours of the experiment, where cold microalgae particles hit the hot catalyst surface and pyrolyse into gaseous compounds and ash. These gaseous compounds react on the surface and in the bed of the catalyst leaving behind the ash. Since, the temperature of the reaction is not high enough to melt the ash particles, they form phosphates or silicates of AAEM elements by absorbing the thermal energy (Skoglund, 2014). This chemical shift in the ash compounds leads to the formation of highly porous structure on top of the catalyst bed as shown in Figure 4.13B.

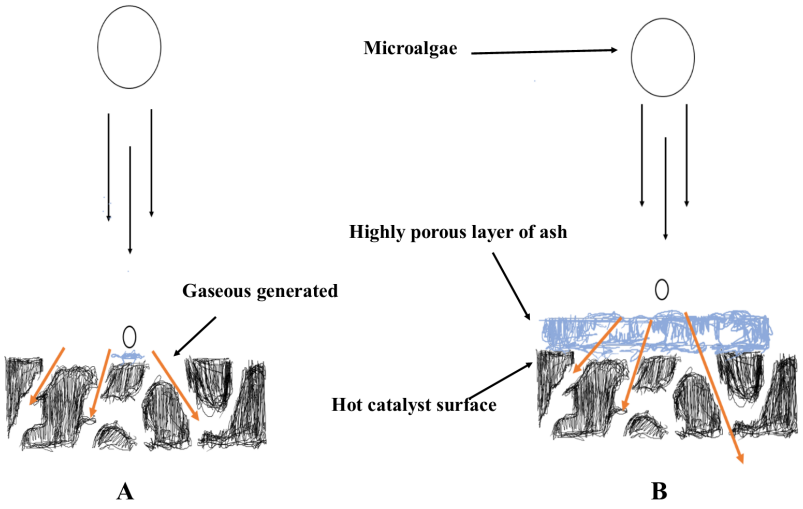


Figure 4.13: Proposed mechanism for reactive flash volatilization of microalgae. A shows the initial stages of RFV. B shows the formation of slag bed on top of the catalyst

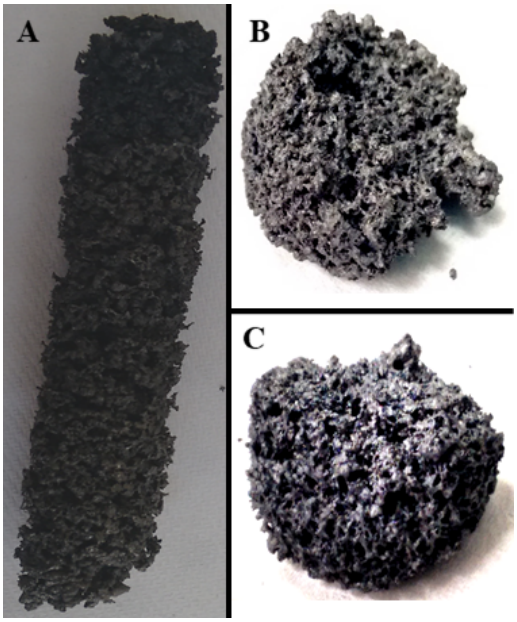


(a) Ash

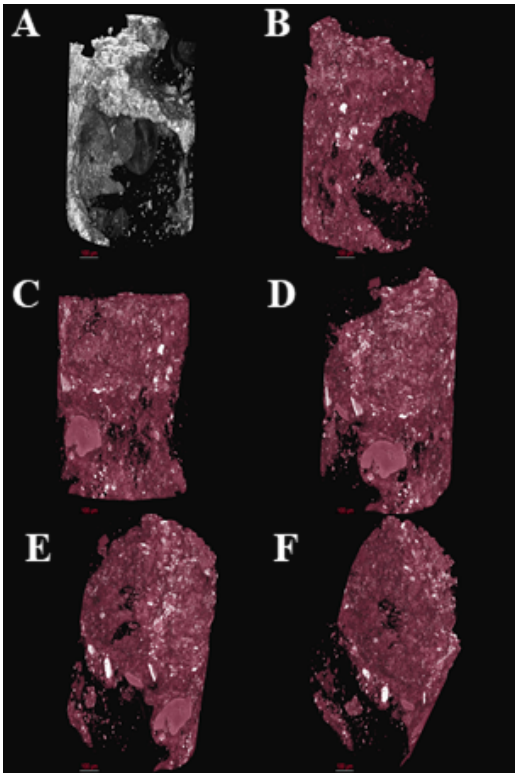


(b) Slag

Figure 4.14: Image showing a slag bed formed in the reactor during RFV of microalgae. (a) Optical image of the slag bed formed during RFV and (b) X-Ray CT image of the slag bed formed during RFV

The formation of porous bed on top of the catalyst was confirmed using an optical image and X-ray CT as shown in Figure 4.14a. Figures 4.14b (A) to 4.14b (F) represent an angular rotation of the sample along the Z-axis and it is clear from the figures that it is a porous, loosely held irregular arrangement of the slag particles. The bed formed due to the ash transformation conducts the heat upwards. This results into a temperature gradient across the slag bed. We hypothesized that, the moment microalgae come in the contact with a hot slag bed, it pyrolyses to form oils and gases. The gaseous compounds flow through the porous bed, and the oils are reformed into gases in the presence of steam as they trickled through the bed. The degradation of oils starts at around 420 °C , whereas, the reaction temperature in the centre of the catalyst bed is well in excess of 500 °C at all the conditions tested in this work (Marcilla *et al.*, 2009). The gases then come in contact with the catalyst leading to a further gas phase reaction, the gas phase selectivity depends upon the catalyst and the operating conditions.

## 4.4 Catalyst Stability

TEM and STEM-EDX was used to confirm the particle size and to map the distribution of the elements on the surface of the catalyst. Ni-Cu-Pd catalyst nanoparticles were in the range of 30 nm to 50 nm were present in the fresh catalyst (Figure 4.15a) and in case of Ni-Rh, the nanoparticles were in the range of 10 nm to 30 nm (Figure 4.16a). EDX of Ni and noble elements depicts the co-location of nanoparticles, possibly in the form of nano-alloy. However, synchrotron analysis of Extended X-ray Absorption Fine Structure (EXAFS) elucidation is required to confirm the alloy formation. Figure 4.15b shows that the particle size distribution of the used Ni-Cu-Pd catalyst is unchanged compared to the fresh catalyst, while in Figure 4.16b there is evidence of slight sintering on Ni-Rh nanoparticles. As shown in Figure 4.18 , the average rate of $H_2$ production was maintained at 7.38 mmol·min$^{-1}$·g-catalyst$^{-1}$ with a standard deviation of 0.55 mmol·min$^{-1}$·g-catalyst$^{-1}$, whereas, the average rate of $CH_4$ production was maintained at 0.63 mmol·min$^{-1}$·g-catalyst$^{-1}$ with a standard deviation of 0.13 mmol·min$^{-1}$·g-catalyst$^{-1}$ after 9 h and 13 h of operation, respectively. This proves that the Ni-Rh catalyst was stable for at least 9 h and Ni-Cu-Pd catalyst was stable for at least 13 h. Moreover, Figure 4.17 confirms the stability of the catalyst.

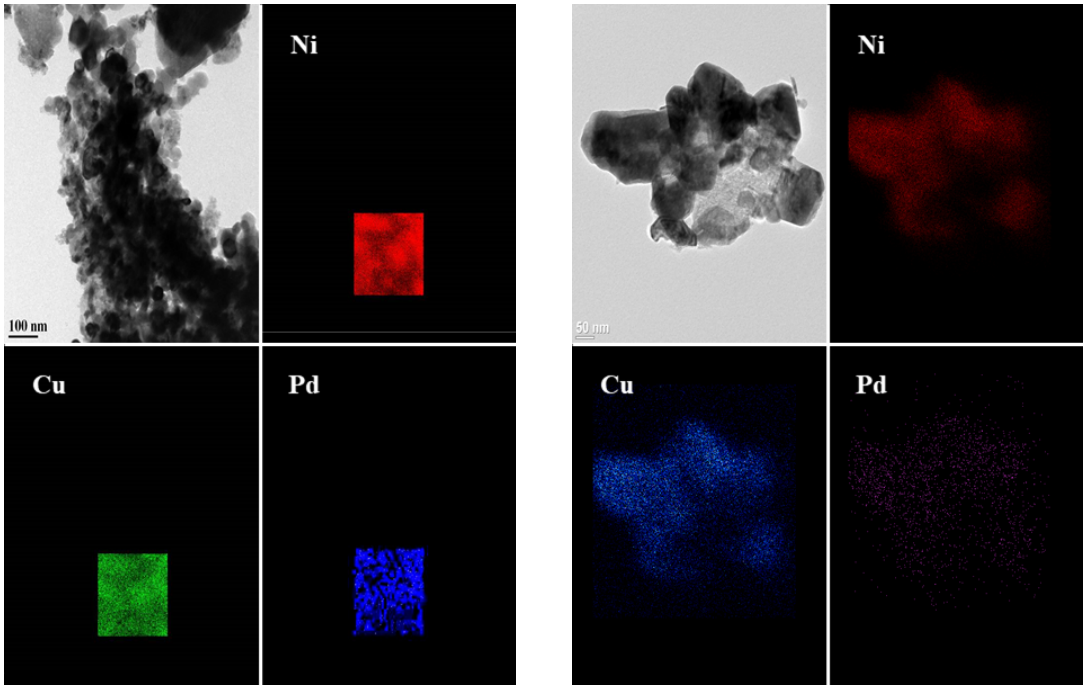


(a) Fresh catalyst (b) Used catalyst

Figure 4.15: STEM Figure of fresh and used Ni-Cu-Pd catalyst showing the presence of Nickel, Copper, and Palladium on the surface

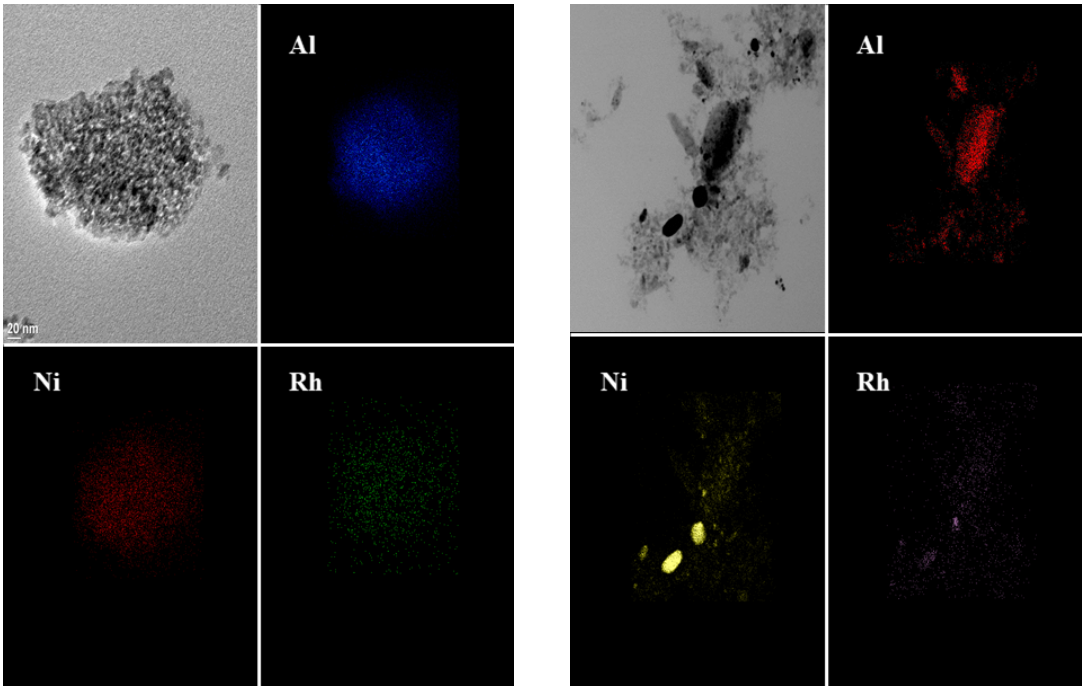


(a) Fresh catalyst (b) Used catalyst

Figure 4.16: STEM Figure of fresh and used Ni-Rh catalyst showing the presence of Nickel, Rhodium, and Aluminium on the surface

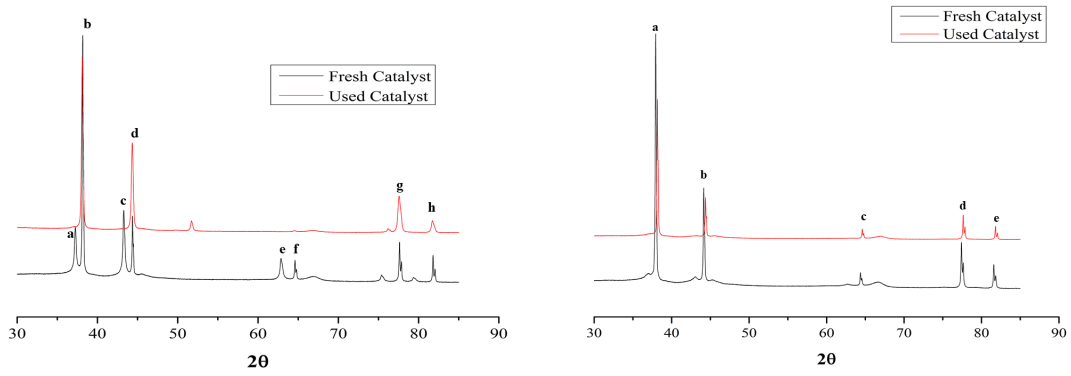


(a) Ni-Cu-Pd (b) Ni-Rh

Figure 4.17: XRD pattern for fresh and used catalyst

Table 4.3: XRD analysis of the catalyst

| Catalyst | Name of the compound | Peaks | JCPDS Number |
|---|---|---|---|
| Ni-Cu-Pd | Nickel Copper oxide | a, c, e | 78.0644, 78.0645 |
| | Nickel oxide | a, c, e | 44.1159 |
| | Aluminium Nickel | d, f, h | 44.1186 |
| | $\gamma$-alumina | b, g | 10.0425, 29.0063, 50.0741 |
| Ni-Rh | Aluminium Nickel | b, c, e | 44.1186 |
| | $\gamma$-alumina | a, d | 10.0425, 29.0063, 50.0741 |

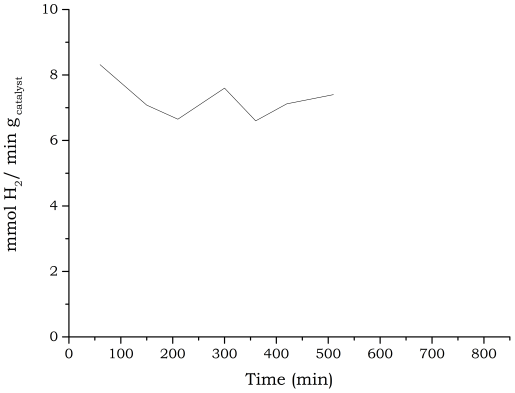


(a) Rate of hydrogen production

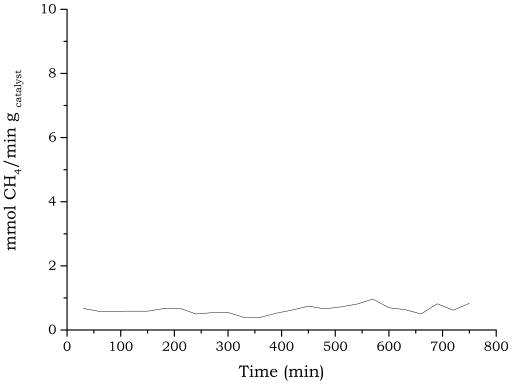


(b) Rate of methane production

Figure 4.18: Rate of hydrogen and methane production (operating conditions: feeding rate 7 g/h, Temp 650 °C for hydrogen and 600 °C for methane, C/S 0.12)

# Chapter 5

# Techno-Economic and Life Cycle Assessment

JSW Steel Ltd., the sponsoring agency for this work, emits 9100 tonne/day of $CO_2$ and it was assumed that all of it is sparged in the microalgal open pond system. Assuming microalgae can fix around 5% of the total $CO_2$ which is sparged in the open pond system (Klinthong *et al.*, 2015). After 17 day growth cycle, 307 tonne/day of microalgae was available for processing assuming microalgae has around 40.3% of carbon. This translated to microalgae production rate of 12790 kg/h.

## 5.1 Hydrogen production

Figures 5.1 and 5.2 show the major operational areas for hydrogen production viz. area 100H and area 200H. Microalgae undergoes thermochemical transformation to produce hydrogen-rich syngas in area 100H, and the gas undergoes further purification to produce 99.999% pure $H_2$ in area 200H.

### 5.1.1 Area 100H: Reactive flash Volatilization of microalgae

As shown in Figure 5.1 and Table A.2, 12790 kg/h of microalgae containing 60 wt.% moisture is gasified using 54120 kg/h steam as a gasifying agent at 650 °C in the presence of Ni-Rh/alumina catalyst. The steam is generated in the boiler using the waste gases from Pressure Swing Adsorption (PSA) having total calorific value of 78 GJ/h. A mixture of microalgae and super-heated steam is fed to the downdraft, slagging, and fixed bed catalytic reactor R1. Reactor R1 is operated under excess steam condition, which is corrosive for carbon steel. Therefore, as per the guidelines published by Keiser *et al.* (2018), it was assumed that the gasifier is made up of three different layers, namely,

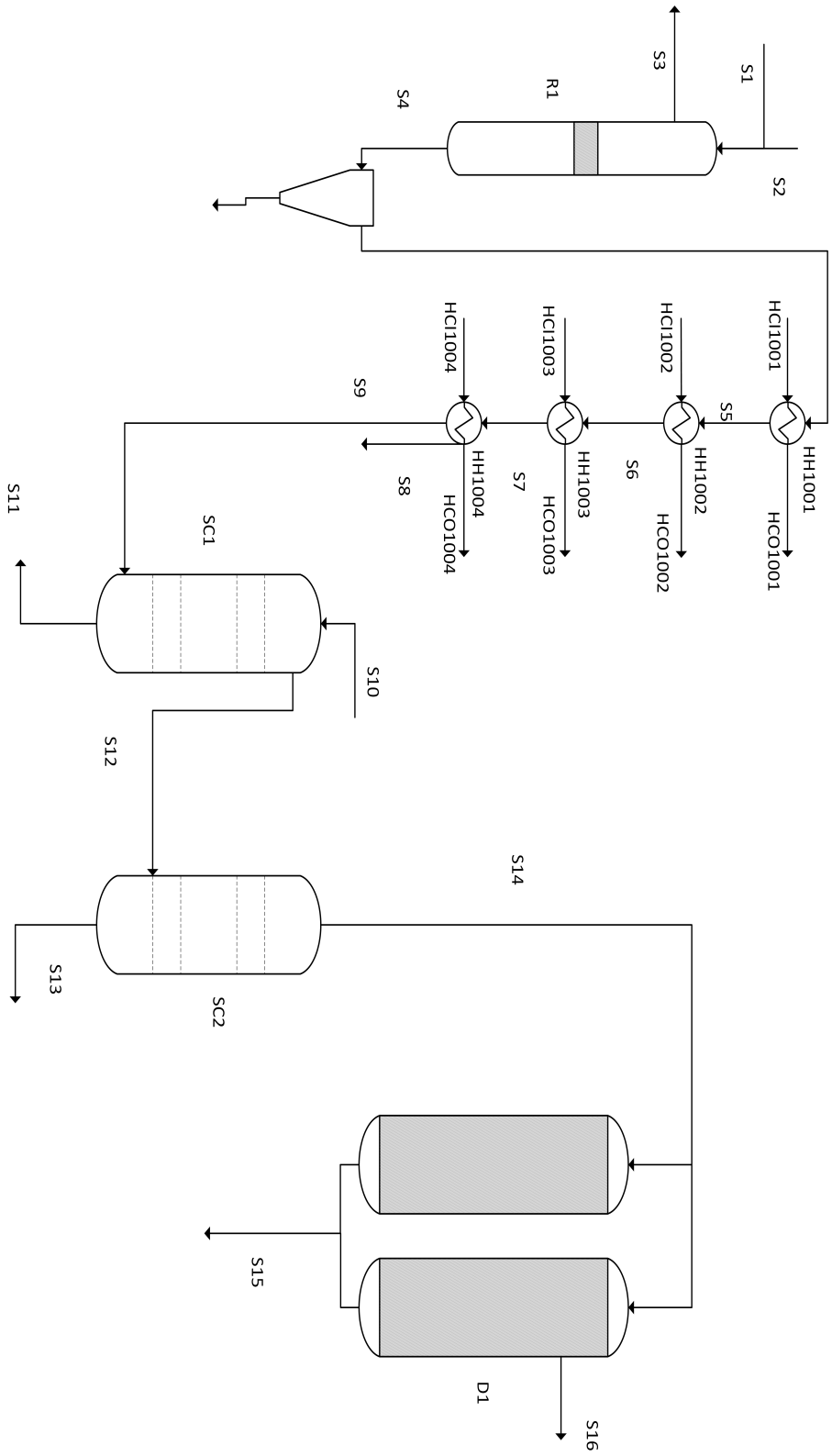


Figure 5.1: Area 100H Reactive flash volatilization of microalgae

Inconel, carbon steel and refractory lining from inside to outside, respectively. It is an overall endothermic reaction. The reactor is operated as an isothermal reactor, and the temperature inside the reactor is maintained by indirect heating using heat of combustion of the waste gases from PSA. The reactor was modelled as a RYield reactor in the ASPEN Plus® flowsheet. Equilibrium based model for reactor was not recommended because the difference in the composition calculated by equilibrium-based modelling and observed by experimentation was mentioned in the literature by Colby *et al.* (2008). Moreover, recent work by Tigabwa (2018) on ASPEN modelling of RFV showed that the equilibrium composition was not achieved during the reaction.The produced gas consists of 1339.60 kg/h of $H_2$, 1688.24 kg/h of CO, 13452.72 kg/h of $CO_2$, 693.85 kg/h of $CH_4$, 2095.00 kg/h of $NH_3$, 144 kg/h of $H_2S$ and 56981.56 kg/h of steam. The gas composition was based on the experimental studies for the optimal conditions previously explained. $NH_3$ is corrosive, and $H_2S$ poisons the shift catalyst, hence, it is necessary to scrub them. $NH_3$-scrubbers operates at 50 °C , so, the produced gas was passed through a series of heat exchangers to cool it down to 50 °C . Table A.6 enlists the details of the heat exchangers. HH1001, HH1002 and HH1003 are shell and tube heat exchangers, whereas, HH1004 is a convective air-cooled heat exchanger. The material of construction (MoC) for HH1001 is Cr-0.5Mo alloy since the temperature of the hot fluid is 650 °C which is beyond the safe operating temperature of carbon steel. However, the MoC for HH1002, HH1003, and HH1004 is carbon steel. The condensate collected from the HH1004 consisted of soluble tar, dissolved $NH_3$ and $H_2S$. It was treated using biological wastewater treatment process. The cooled gas was then allowed to react with 0.1 N $H_2SO_4$ in the acid scrubber to remove $NH_3$. The sour gas was treated using LO-CAT® technology to reduce the sulphur concentration of up to 10 ppmv in the sweet gas (Abdugaliev et al., 2003; Kolar et al., 2015), which is in the acceptable range for the shift catalysts Swanson *et al.* (2010) Temperature swing adsorption containing silica matrix was used to remove the moisture from the gas before the low-temperature (LT) shift. Moisture removal was necessary to ensure that traces of ammonia and sulfuric acid were removed completely. Microalgae has approximately 11% (w/w) ash, and during RFV it forms a porous catalytic bed on the top of the primary catalyst bed. Continuous accumulation of ash on top of the catalyst would result in clogging of the reactor. Hence, a mechanism of intermittent suction will be designed in the reactor to maintain the critical length of the ash bed such that, it will not clog the reactor and retains its catalytic property. Utilization of ash and char as a micronutrient fertilizer for plants is well reported in the literature (Piekarczyk et al., 2011). So, it was assumed that the extracted slag will be sold as the soil conditioner because the elemental analysis of microalgal ash confirmed that the ash was composed of alkali and

alkaline earth metals and did not contain any heavy elements. Stream S3 denotes the ash flow outside the reactor. Moreover, it was assumed that the transportation and the storage is buyer's responsibility.

### 5.1.2 Area 200H: LT-shift and hydrogen purification

As shown in Figure 5.2 and Table A.3, compressed gas at 25 bar pressure and 210 °C temperature was mixed with super-heated steam before the LT-shift reactor R2. The LT-shift reactor was used to convert excess CO into $H_2$ and $CO_2$ in the presence of catalyst. In this reactor, CO reacts with steam to form $CO_2$ and $H_2$ through water-gas-shift reaction. The LT-shift reactor was modelled as a tubular, fixed bed catalytic reactor. LK821-2 TOPSOE™catalyst having a bulk density of 2400 kg/m$^3$ was assumed for the LT-shift reaction. The weight of the catalyst and the size of the reactor was calculated using the reaction kinetics explained byByron *et al.* (2010) and sensitivity analysis performed using ASPEN Plus®. 26000 kg catalyst was required to convert 98% of CO. LT-Shift is an exothermic reaction; hence, a design of a jacket-cooled reactor was used for sizing and scaling up calculations of the R2 reactor. Hydrogen-rich syngas was then cooled to 50 °C using two heat exchangers in series prior to purification using PSA. It was assumed that the PSA operated in the range of 24 bar to 30 bar pressure and 40 °C to 45 °C temperature. The exact size and the nature of the matrix were as per the commercial specification. 99.999% pure hydrogen leaving from PSA was then compressed to 700 bars for further processing. The steam generated during the process was used to generate electricity using steam turbine. With the isentropic efficiency of 75%, 7800 kWh of the electricity was generated. The exit steam at 101 °C and 1 bar pressure was used as a gasifying agent to perform RFV after further processing.

## 5.2 Methane Production

Figures 5.3, 5.4 and 5.5 show the major operational areas for methane production. Microalgae undergoes thermochemical transformation to produce methane-rich syngas in area 100M. The produced gas undergoes upgrading through CO-methanation and LT-shift reaction in the area 200M, and $CH_4$ is purified using PSA in the area 300M.

### 5.2.1 Area 100M: Reactive flash volatilization of microalgae

As shown in Figure 5.3 and Table A.4, 12300 kg/hr of microalgae (on dry basis) was gasified at 600 °C in the presence of Ni-Cu-Pd/alumina catalyst using steam as the gasifying agent as explained earlier in the area 100H. Table A.7 enlists the details of the

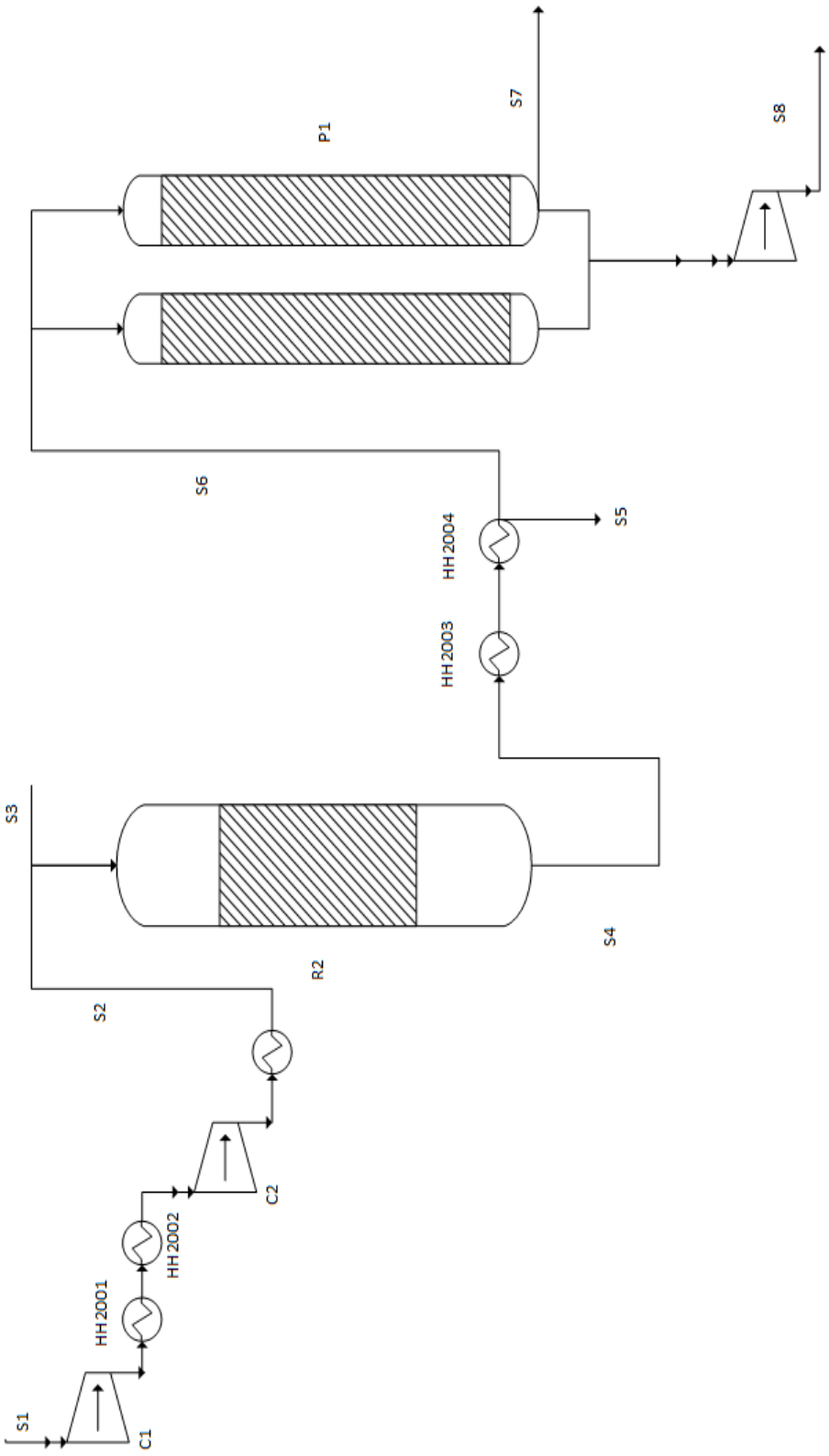


Figure 5.2: Area 200H LT shift and hydrogen purification

heat exchangers used to produce methane. The produced gas consisted of 367.64 kg/hr of $H_2$ (40% v/v), 6550.88 kg/hr of CO (22% v/v), 10294.24 kg/hr of $CO_2$ (22% v/v), 2139.04 kg/hr of $CH_4$ (16% v/v), 996.37 kg/hr of $NH_3$ and 52064.1 kg/hr of steam. The difference in the gas composition was attributed to the change in the operating temperature and catalyst.

### 5.2.2 Area 200M: CO-methanation and LT-shift

As shown in Figure 5.4 and Table A.5, the methane-rich syngas was compressed to 64 bar (260 °C ) with intercooled compressors in series. 3.9 MW power and 2958.38 kg/h of cooling water (30 °C ) was required at each stage to compress the produced gas. The compressed gas was then passed to CO-methanation rector. The reactor was modelled as using Langmuir-Hinshelwood-Hougen-Watson (LHHW) kinetics as explained by (Kopyscinski, 2010). Only 52% of CO was converted to methane due to limited availability of $H_2$. $H_2$ depleted gas was then passed through LT-shift reactor and remaining CO was converted to $CO_2$ and $H_2$ as explained earlier in the Area 200H.

### 5.2.3 Area 300M: Methane purification

As shown in Figure 5.5 and Table A.5, the compressed gas was flashed to 25 bar pressure and 45 °C temperature. The gaseous stream was then passed through PSA to separate $CH_4$. 3484.96 kg/hr of 99.999% pure $CH_4$ was produced when PSA was operated at 25 bar pressure.

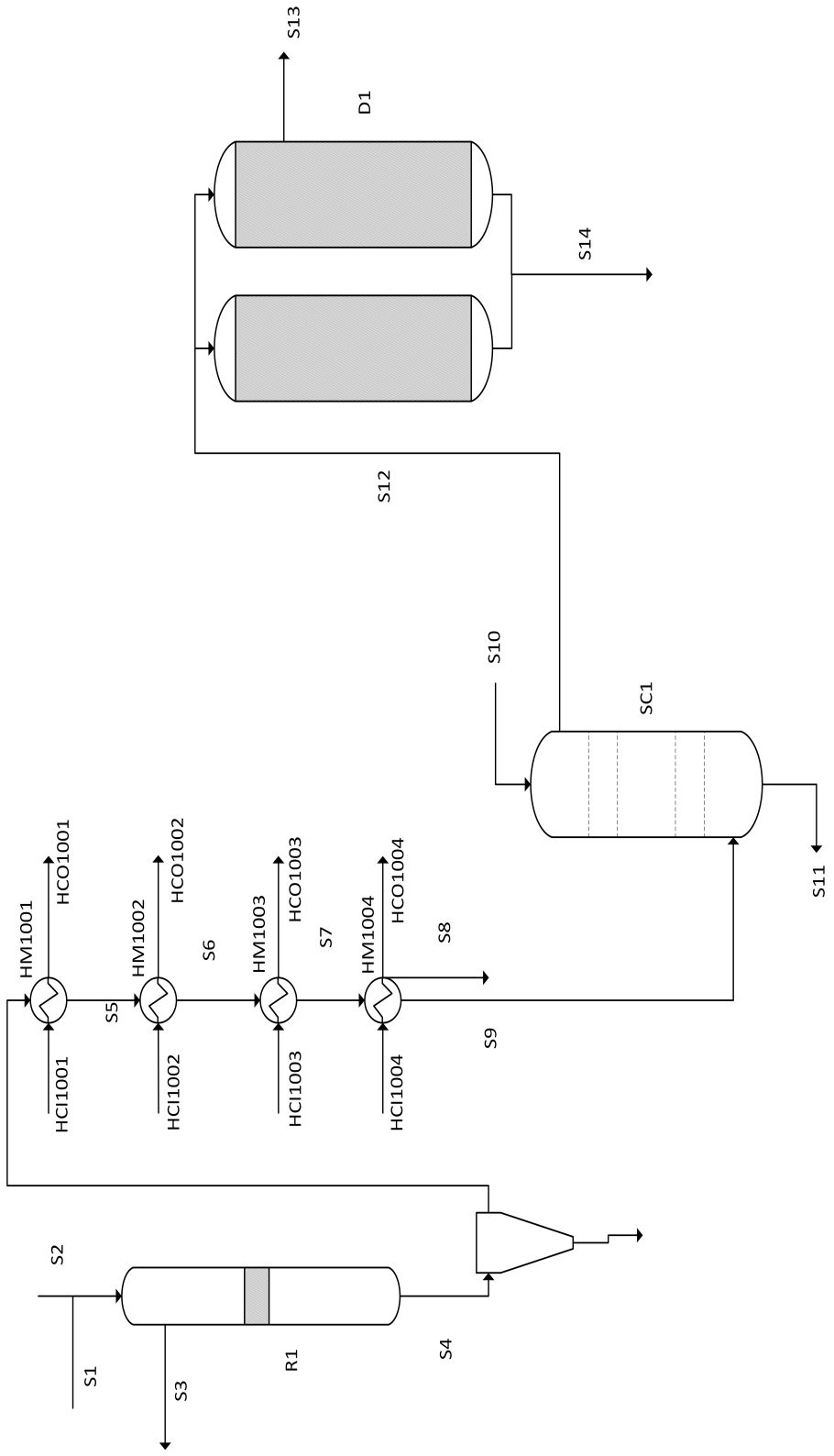


Figure 5.3: Area 100M Reactive flash volatilization of microalgae

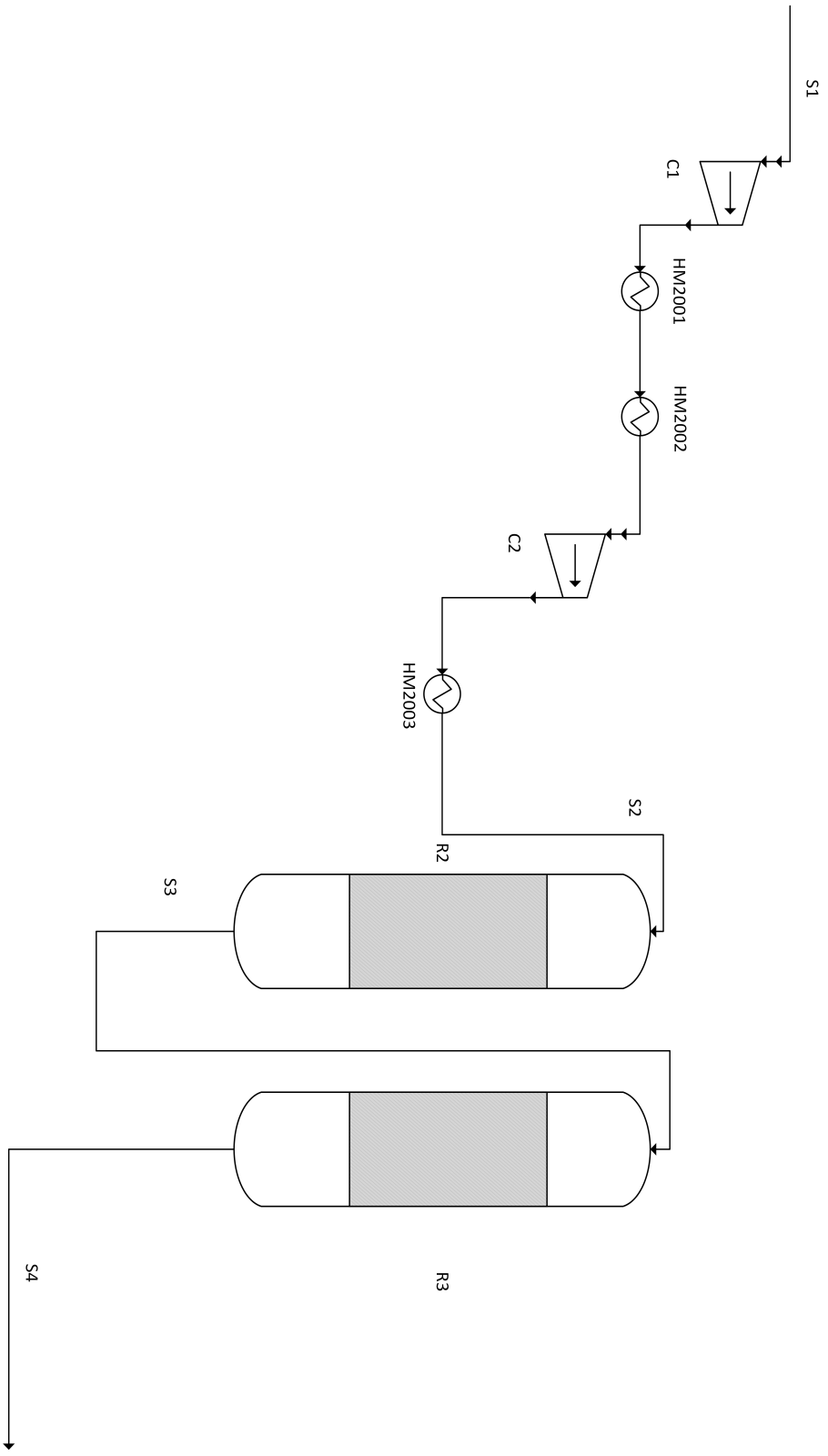


Figure 5.4: Area 200M CO methanation and LT shift

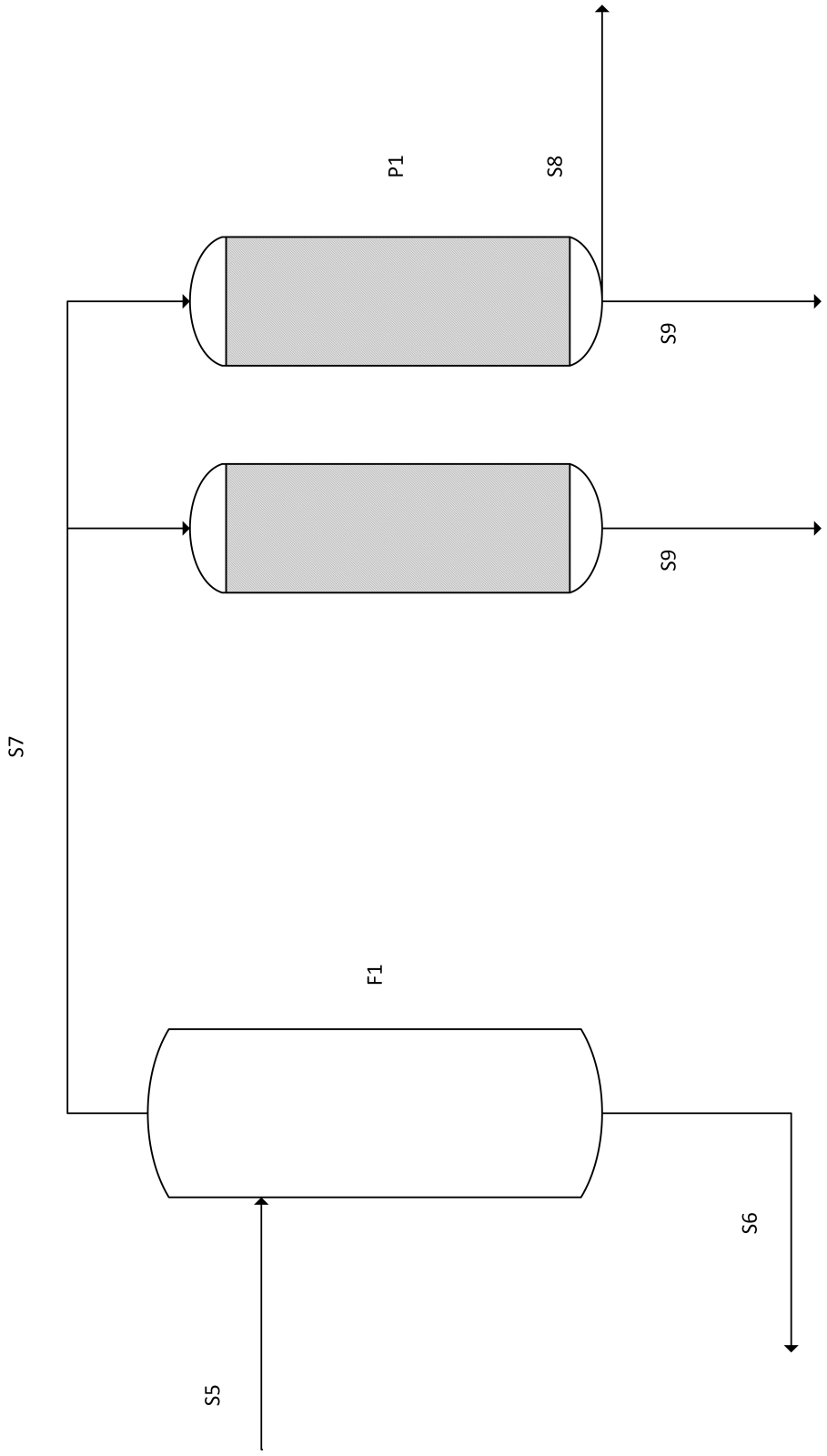


Figure 5.5: Area 300M Methane purification

## 5.3 TEA Methodology

The process flowsheets described in the previous section were used to perform detailed techno-economic and life cycle assessment calculations. This required detailed process input output data such as requirement of electricity, $H_2SO_4$, water and wastes generated. These data were generated using flowsheet simulation. The process flowsheets explained earlier were simulated using ASPEN Plus® Version 9. Peng-Robinson-Boston-Mathias (PR-BM) thermodynamic model was used for the process simulation. The RFV reactor was modelled as RYield reactor in ASPEN Plus ® since the yield of the products were available from experimental results. Low-Temperature shift and CO-methanation reactor was modeled as RPLUG reactor using kinetics from (Byron *et al.*, 2010) and (Kopyscinski, 2010), respectively.

The converged ASPEN Plus® simulation results provided the detailed input-output data for all the process and utility streams. ASPEN Plus® Exchanger Designer and Rating (EDR) program was used to design heat exchangers. Equipment sizing, utility requirements and cost evaluation was performed using reported literature and ASPEN Plus® Process Evaluation module.Capital investment and operating cost of LO-CAT ® and biological wastewater treatment was calculated based on the techno-economic analysis performed by Abdugaliev et al. (2003) and McMullen (2008), respectively. Whereas, capital investment expenditure of the PSA system was calculated through personal communication with the company. The costing and design of the gasifier was unique and could not be scaled up and evaluated by using ASPEN Plus®. It was designed by using the methodology explained by Bibber *et al.* (2007) and Swanson *et al.* (2010). Moreover, to evaluate the base case scenario, it was assumed that the performance of the lab scale reactor and the commercial reactor was the same. The installed cost of the gasifier and its accessories was calculated by using the following equation assuming n=0.8 (Swanson *et al.*, 2010).

$$\text{New Cost} = \text{Old Cost} \times \left(\frac{\text{New Size}}{\text{Old Size}}\right)^{n} \tag{5.1}$$

The installed cost of a heat exchanger was calculated by using the methodology suggested by Purohit (1983). Total capital investment (TCI) comprised of individual equipment cost, installation costs and indirect costs, was estimated by using the methodology suggested by Peters *et al.* (2003) assuming 8000 hr of plant operation per year. The total operating cost comprised of utility costs, maintenance cost, labour cost, facility development cost and the cost of microalgae, and was estimated based on the literature and ASPEN Plus® simulations.

The cost of hydrogen and methane is dynamic and driven by crude oil prices. Hence, instead of estimating the product value of these gases, the payback period and capital investment cost were calculated assuming the plant life of 20 years. 60% depreciation was accounted for the final calculation of the payback period as suggested by Swanson *et al.* (2010). The conversion rate of ₹ 65 per unit USD was used, and all the financial values were adjusted to 2017 by using chemical plant index (CPI). Additionally, to evaluate the India specific costing, it was assumed that the direct and indirect costs will be 40% less in India compared to the United States. Furthermore, it is assumed that the hydrogen or methane production facility is located in the Steel plant and some of the maintenance cost and labour cost will be shard with the steel plant. Cost of cooling water and electricity was assumed to be ₹ 0.03 per kg and ₹ 8.7 per kWh, respectively. It was also assumed that the $CO_2$ sequestered while growing microalgae will generate some credit from the carbon credit market. The cost of carbon credit varies significantly with country and time. Here, we considered a cost of $ 10 /tonne of carbon based on the technical report published by Mahindra Industries, which translated to ₹ 650 per tonne of carbon. The revenue obtained from selling these credits was considered in the economic calculations. The selling price of hydrogen and methane was assumed to be ₹ 650 per kg ($ 10 /kg) Eichman *et al.* (2016); Brown (2015) and ₹ 24 per kg ($ 0.4 /kg), respectively. It was assumed that the food grade $CO_2$ generated through PSA after separating $H_2$ was sold to the food industries at the price of ₹ 1.78 per kg. The price of food grade $CO_2$ was obtained through personal communication with the industry currently selling the $CO_2$. Commercial grade sulphur was produced as the product of LO-CAT® treatment process. It was sold to industry at the gate price of ₹ 15/kg ($0.23/kg). Moreover, slag generated during the process was sold as a soil conditioner at the gate price of ₹ 10/kg ($0.15/kg). The electricity produced using steam turbine was used to drive the compressors and excess electricity was connected to the grid. The selling price of the electricity was assumed to be ₹ 5/kWh ($0.076/kWh).

## 5.4 LCA methodology

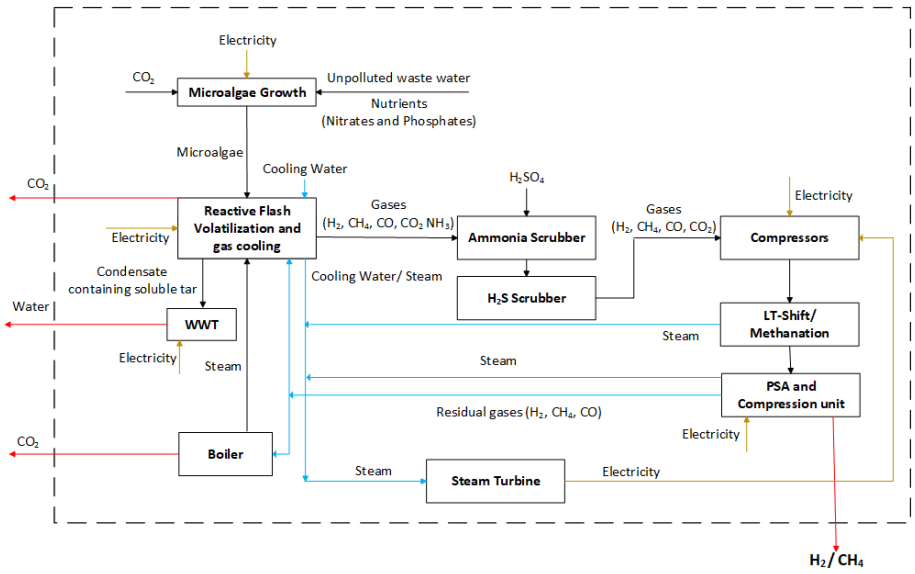


Figure 5.6: Boundary diagram for LCA analysis

To perform LCA, the system is broadly divided into two parts, microalgae growth and microalgae processing. The system boundary is illustrated in Figure 5.6 which contains, a) electricity requirements for paddle wheel, b) nutrients and water required for microalgae, c) process water required for cooling and RFV, d) electricity required to operate compressors and PSA, and e) emissions to the atmosphere due to indirect burning of gases. 1 kg of hydrogen or methane was considered as the functional unit of the LCA. OpenLCA ® V 1.7 was used to create the product system and link between various processes. Ecoinvent® V 3 database was used to collect the materials and energy associated with the individual process. The inventory data for inputs such as electricity was obtained from the Ecoinvent database. The International Reference Life Cycle Data System (ILCD) 2011 method was used to perform the impact assessment, and only mid-point indicators were calculated. Table 5.1 lists the inventory for hydrogen and methane production. Microalgae was cultivated in the open pond by using unpolluted wastewater as the growth media. Depending on the standard growth media requirements of Bold's Basal Medium (BBM), amount of sodium nitrate, potassium phosphate and calcium chloride were calculated. Paddlewheel was used to stir the media, and the electricity requirement of 0.1042 W/m$^2$ was assumed based on the literature (Davis *et al.*, 2016). The wet microalgal biomass containing 60% moisture obtained by sedimentation was used for RFV. It was assumed that 75% of the water separated at the harvesting stage is recycled back to the cultivation ponds. Further, it was assumed that the processing facility was located near the cultivation facility, and hence, transportation was not needed. The reactor was externally heated by using the

Table 5.1: LCA inventory to produce hydrogen and methane

| Components | Amount (per kg $H_2$) | Amount (per kg $CH_4$) |
|---|---|---|
| Calcium chloride | 0.59 kg | 0.12 kg |
| Carbon dioxide | 3.82 kg | 1.48 kg |
| Sodium nitrate | 2.96 kg | 0.58 kg |
| Sodium phosphate | 1.63 kg | 0.32 kg |
| Water for microalgae growth | 21.86 m3 | 4.24 m3 |
| Electricity for paddlewheel | 5.27 W | 1.02 W |
| $H_2SO_4$ | 3.4 gm | 0.66 gm |
| Process water | 0.16 m3 | 0.16 m3 |
| $CO_2$ emission | 3.24 kg | 0.49 kg |
| Electricity for RFV | 5.25 kW | 3.62 kW |
| Electricity for wastewater treatment | 4.0 kW | 1.53 kW |

waste gases from PSA. 3.24 kg of $CO_2$/ kg of $H_2$ and 0.49 kg of $CO_2$/ kg of $CH_4$ was emitted to the air during hydrogen and methane production, respectively. The amount of $CO_2$ was calculated assuming the complete combustion of waste gases from PSA to heat the gasifier and boiler. The total electricity requirement was calculated based on ASPEN PLUS® simulations. A combination of sources (65% hard coal, 20% hydro, 10% oil and 5% renewable) specific to Indian scenario was used to evaluate the impact. Lake water was used to generate the steam and as the cooling water for the heat exchangers. Both hydrogen and methane production processes generated multiple products. In hydrogen production process, ammonium sulphate and pure CO2 are the side products. In methane production, in addition to the above three, hydrogen is also a side product. Therefore, impact allocation needs to be performed. Economic impact allocation approach, where the impacts are divided based on the economic revenue generated, was used in this work. In the case of hydrogen production, out of total impact, 92% is due to hydrogen, 3.82% is due to ammonium sulphate, and 3.54% is due to $CO_2$. In the case of methane production, out of total impact, 41% is due to steam, 28% is due to methane, 11% due to ammonium sulphate, 10% is due to hydrogen, and 9% is due to $CO_2$.

## 5.5 Feasibility Assessment

At the plant entry gate, the cost of microalgae (60 wt.% moisture and 11 wt.% ash) was calculated to be ₹ 32/ kg ($ 0.5/ kg) based on the National Renewable Energy Lab‘s

(NREL) report on the cultivating microalgae (Davis *et al.*, 2016). The results showed that for the prevailing prices of the products, the payback period for hydrogen production plant was 3.78 years with the internal rate on the return of 22%. Moreover, the turnover ratio was calculated to be 0.75. The total capital investment (TCI) of ₹ 9.40 billion ($ 144.6 million) was estimated, and the detailed breakup of the direct-, indirect- and operating-cost involved is shown in the Table A.8, Table A.9 and Table A.10.

Table 5.2 shows the purchased cost of various equipment involved in hydrogen production. 11% of the TCI was attributed towards the cost of gasifier and its accessories such as boiler and feeder. Out of total operating cost of ₹ 0.5 million ($7,692), around 76%, was due to microalgae cultivation and around 23% was due to utilities (water, electricity and catalyst) used in the process. Table 5.3 shows the revenue share for hydrogen production. It is clear from Figure 5.7a that 90% of the revenue was generated from hydrogen. The $CO_2$ credit contributed to around 1% of total revenue. Though, hydrogen production using the proposed route is profitable, the turnover ratio, however, is a little on the lower side and many industries desire it to be 1 (Peters *et al.*, 2003). From that point of view, the proposed process is economically less attractive.

Table 5.4 shows the comparison of various processes to produce renewable hydrogen. Sarkar and Kumar (2010) have evaluated the cost of biohydrogen production via bio oil up-gradation for the year 2008. Bio oil originated from lignocellulosic biomass (wood chip, forest residue and agricultural waste) was considered for bio hydrogen production. They have reported that for a fixed IRR of 10%, and a TCI of $ 58 million the price of hydrogen was $2.4/kg of $H_2$ in the case of wood chips, $3.00/kg of $H_2$ in the case of forest residue and $4.32/kg of $H_2$ in the case of agricultural waste. The difference in the selling price of hydrogen is majorly due to the difference in the cost of biomass and the pressure of the hydrogen at which it is stored. The cost of wood chips was assumed to be $35/tonne (₹ 2.3/kg ) whereas, microalgae costs around ₹ 32/kg. Additionally, the cost of hydrogen at 700 bar is ₹ 650/kg ($10/kg). Zhang *et al.* (2013) have evaluated the comparative costs of biohydrogen production via bio oil gasification and bio oil reforming. They have noted that for a selling price of $ 3.3 per kg of $H_2$ and TCI of $ 241 million (bio oil gasification) and $ 184 million (bio oil reforming) IRR was 18.6% and 8.4%, respectively. The difference in the profit is mainly due to the difference in the selling price of the hydrogen. The cost of hydrogen at 700 bar is higher than at lower pressures (20 to 25 bar).

To evaluate the base case, it was assumed that the carbon composition (40.3% w/w) of microalgae and the performance of the reactor remains fix throughout the life of the plant. However, microalgae show seasonal variations in the carbon composition (32% (w/w) to 44% (w/w)) and performance of the reactor depends on various factors such as

life and the state of the catalyst, temperature of the reactor and carbon-to-steam ratio in the reactor. Moreover, the scale-up could affect the overall performance of the reactor. To evaluate the effect of various parameters on the payback period of hydrogen production, a parametric sensitivity analysis was performed.

Table 5.2: Cost of individual equipment involved in hydrogen production

| Area 100 | Million INR |
|---|---|
| Gasifier and accessories | 622 |
| HH1001 | 10 |
| HH1002 | 8.45 |
| HH1003 | 4.71 |
| HH1004 (Air cooled) | 47 |
| Ammonia separator | 0.58 |
| TSA | 156 |
| Area 200 | |
| C1 | 89.1 |
| C2 | 89.2 |
| HH2001 | 0.85 |
| HH2002 (Air Cooled) | 1.22 |
| HH2003 (Air Cooled) | 0.94 |
| LT Shift | 6.26 |
| HH2004 | 0.84 |
| HH2005 (Air Cooled) | 1.22 |
| PSA | 239 |
| Compressor assembly | 133.69 |
| Turbines | 20.8 |

Table 5.4: Comparison of renewable hydrogen production

| Parameters | Our study | Sarkar and Kumar | Zhang et al |
|---|---|---|---|
| Scale (tonne of feedstock/day) | 307 | 500 | 2000 |
| Feedstock | Microalgae | Wood chips, Agricultural residue Forest residue | Bio oil obtained from corn stover |
| Feedstock cost (₹/kg) | 32 | 2.3 | 5.4 |
| $H_2$ Cost (₹/kg) | 650 | 156 to 280 | 241 |

Table 5.3: Revenue generation from hydrogen and methane production

| Name | Total ($10^2$ INR/h) | |
|---|---|---|
| | Hydrogen Production | Methane Production |
| Hydrogen | 8054 | 307.3 |
| Methane | - | 836.4 |
| Steam | | 1248.8 |
| Ammonium Sulphate | 335.8 | 335.8 |
| $CO_2$ (Food grade) | 311.2 | 270.4 |
| $CO_2$ credit | 32 | 32 |

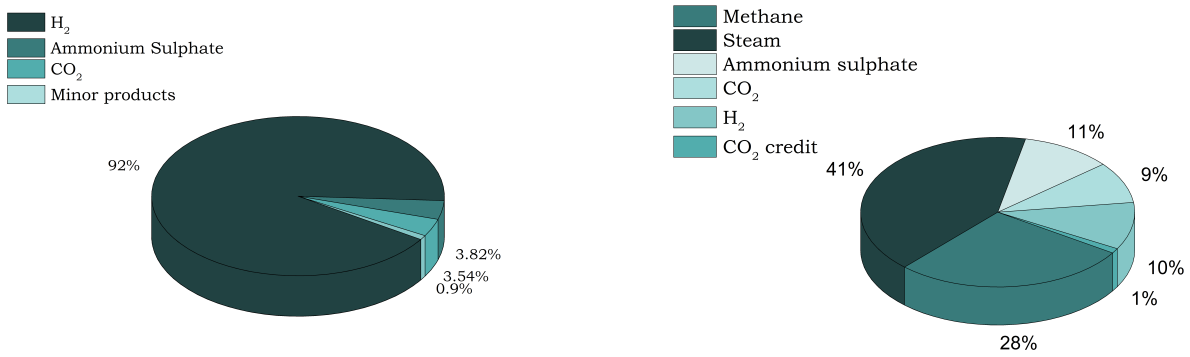


(a) Hydrogen Production

(b) Methane Production

Figure 5.7: Distribution of revenue generation from hydrogen and methane production

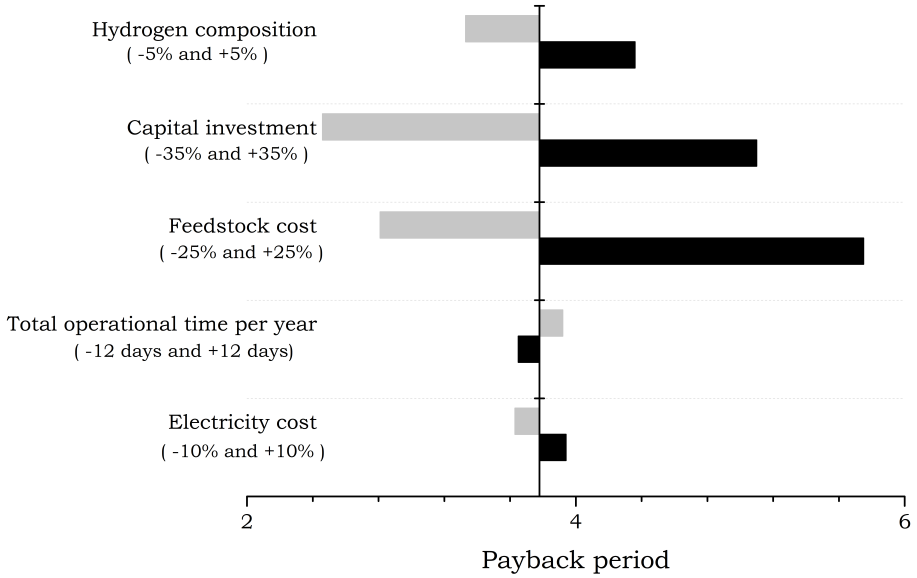


Figure 5.8: Sensitivity analysis of hydrogen production

The effects of various parameters on the payback period of hydrogen are plotted in Figure 5.8. To account for the change in the carbon composition, it was assumed that, the carbon distribution in the CO, $CO_2$ and $CH_4$ remains the same irrespective of the change in the carbon percentage of the microalgae. So, the amount of CO, $CO_2$ and $CH_4$ will increase when carbon content in the microalgae increases. Similarly, the amount of CO, $CO_2$ and $CH_4$ will decrease when the carbon content decreases. Additionally, it was observed during experiments that, the water-gas shift reaction would be favoured over methanation resulting in higher $H_2$ in the produced gas. This implies that proportional change in the carbon percentage translates indirectly to a proportional change in the hydrogen composition in the gas. To account for a change in the hydrogen composition, it was assumed that the carbon content in the microalgae remains unchanged, and the perturbations in the hydrogen composition are due to the proportional perturbations in the CO. Furthermore, the relative change in the composition of $H_2$ and CO is governed by the water-gas shift reaction.

The results showed that 5% change in the composition of hydrogen in the produced gas affected the payback period the most. This was caused by a cumulative effect attributed by a decrease in the revenue and an increase in the operational cost. Reduction in the hydrogen production directly affected the revenue generated since hydrogen is a low volume high-value product. Moreover, it increased the percentage of CO, and conversion of this unreacted CO contributed to increment in operating costs of LT-Shift. It was observed that the 5% decrease in hydrogen production increases the payback period by 25%. Among the other parameters studied here, 35% increase in the TCI increased the payback

period by 30%. Furthermore, it is clear from the trends that the cost of microalgae also affects the payback period significantly. 25% increase in the cost of microalgae increased the payback period by 77.5%. To account for the irregularities and possible shutdowns in the plant, total operational time per year was considered. It was observed that, 5% change (400 h) in the total operational time would not affect the payback period significantly compared to the change in other parameters.

The production of methane was however economically infeasible since the payback period was >20 y and it was in debt of ₹ 1.91 billion ($29.4 million). To produce methane, investment of ₹ 5.11 billion ($78.61 million) was estimated based on the economic analysis. Table A.11, Table A.12 and Table A.13 enlists various direct-, indirect-, and operational-costs incurred during methane production, respectively. Table 5.3 shows the total revenue generation from methane production. It is clear from Figure 5.7b that only 28% of the total revenue was contributed by methane. It can, therefore, be concluded that there are much cheaper options of methane, which make methane production from microalgae economically infeasible. Methane production was not considered for sensitivity analysis, because, TEA showed that the process is economically not feasible.

## 5.6 LCA analysis

Climate change, photochemical ozone formation, freshwater ecotoxicity, human toxicity (carcinogenic and non-carcinogenic), freshwater eutrophication, acidification potential and water depletion were the impact indicators for the LCA analysis as enlisted in the Table 5.5 for hydrogen and methane production.

Table 5.5: LCIA impacts for hydrogen and methane production

| Name | Unit | Hydrogen Production Impact | Methane Production Impact |
|---|---|---|---|
| Climate Change | kg $CO_2$ eq. | 7.56 | 1.18 |
| Freshwater ecotoxicity | CTUe | $5.32 \times 10^{1}$ | 7.65 |
| Photochemical ozone formation | kg $C_2H_4$ eq. | $2.52 \times 10^{-2}$ | $3.81 \times 10^{-3}$ |
| Human toxicity | CTUh | $7.67 \times 10^{-7}$ | $3.29 \times 10^{-7}$ |
| Freshwater eutrophication | Kg P eq. | $6.16 \times 10^{-3}$ | $8.74 \times 10^{-4}$ |

In the case of hydrogen production, it was observed that, the overall climate change impact was 8.24 kg $CO_2$-eq./kg $H_2$ produced. The overall value was a combination of negative emissions due to microalgae production (carbon sequestration) of 9.07 kg $CO_2$-eq./kg $H_2$ produced, and a positive emission due to electricity and nutrients (nitrates, phosphates and chlorides) 17.31 kg $CO_2$-eq./kg $H_2$ produced. Out of total positive impact

(emission) of 17.31 kg $CO_2$-eq., 54% was contributed by the electricity production and 46% was contributed by the nutrients production. If the economic impact allocation is preformed, then the climate change impact decreased to 7.56 kg $CO_2$-eq./kg $H_2$.

This indicated that most of the impacts were indirect in nature. It also pointed to the possibility of significantly reducing the GHG impact by using a different electricity source. The typical electricity available at grid in India has a life cycle impact of 1.17 kg $CO_2$-eq./kWh. However, hydro-electricity has the life cycle impact of only 0.006 kg $CO_2$-eq./kWh. In such a case, the net GHG emission (climate change impact) for hydrogen production would be 1.89 kg $CO_2$-eq./kg $H_2$. If the impact allocation is performed, the climate change impact decreased to 1.72kg $CO_2$-eq./kg $H_2$. It may be possible to further reduce the emissions by using wastewater as the source of nutrients for microalgae cultivation.

Cetinkaya *et al.* (2012) have compared various hydrogen production processes based on their environmental impacts and production capacity. They have observed that wind energy-driven water electrolysis has the least impact of 0.97 kg of $CO_2$ / kg of $H_2$, whereas, steam methane reforming has the highest impact of 11.9 kg $CO_2$ eq. / kg of $H_2$. Furthermore, Bhandari *et al.* (2014) have compiled the impacts for biomass gasification to produce hydrogen and biomass gasification driven water electrolysis to produce hydrogen. They have noted that around 2 kg of $CO_2$/ kg of $H_2$ was produced during hydrogen production directly from biomass gasification. Whereas, in the case of gasification driven water electrolysis, the impact was reported to be 4 kg of $CO_2$/ kg of $H_2$.

Azadi *et al.* (2014) have compared the alternative microalgae processing technologies such as; HTL, anaerobic digestion, gasification for power generation and gasification followed by Fischer-Tropsch conversion based on the GHG emissions. They have assumed that the microalgae was primarily processed for FAME production, and the oil extracted microalgae was processed using the above-mentioned technologies. Furthermore, they have assumed that products of these processing technologies were used to meet the energy demands of the respective processes. Considering the scenario as mentioned above, GHG emission of HTL, anaerobic digestion, gasification for power generation, and gasification followed by Fischer-Tropsch conversion was 41 g $CO_2$-eq./MJ of biodiesel, 86 g $CO_2$-eq./MJ of biodiesel, 109 g $CO_2$-eq./MJ of biodiesel, and 124 g $CO_2$-eq./MJ of biodiesel, respectively. Whereas, in the case of RFV of microalgae to produce hydrogen, GHG emissions was calculated to be 69 g $CO_2$-eq./MJ of hydrogen.

A similar trend was observed for the total freshwater ecotoxicity of $5.92 \times 10^2$ CTUe / kg $H_2$ produced. It was expressed in terms of the comparative toxic unit for aquatic ecotoxicity impacts (CTUe). This unit accounts for potentially affected fractions of species

per unit mass of chemical released into water or soil. Leaching of zinc, copper and nickel into the water during coal combustion and nutrients production was responsible for the freshwater ecotoxicity. Chromium VI was responsible for human toxicity. It was observed that total human toxicity was negligible. Impact on photochemical ozone formation was calculated to be 0.029 kg $C_2H_4$ eq. / kg $H_2$ produced. Non-methane volatile organic compounds and NOx produced during the coal combustion were responsible for affecting the ozone formation.

In the case of methane production, Table 5.5 enlists all the impacts. The total climate change impact of 1.18 kg $CO_2$ eq. / kg $CH_4$ (84.94 g $CO_2$ eq./ MJ) produced was observed during methane production using microalgae. In contrast to, natural gas mining which has an overall impact of 55 g $CO_2$ eq. / MJ (Clark *et al.*, 2012). Jury *et al.* (2010) reported the overall impact of 60 g $CO_2$ eq. / MJ for methane production using crop fermentation. Moreover, the overall impact of 7.5 g $CO_2$ eq. / MJ was reported by RamÃŋrez-Arpide, et al. (2018) to produce methane using fermentation of cow dung and nopal cladodes. Methane production showed the negligible human toxicity ($3.29 \times 10^{-7}$ CTUh) and Freshwater eutrophication ($8.74 \times 10^{-4}$ kg P eq.) impact.

## 5.7 Scale-up challenges

To perform base case techno-economic feasibility calculations, we have made some assumptions pertaining to cultivating microalgae, $CO_2$ sequestration and process design. These challenges and some ways to overcome them are discussed below.

### 5.7.1 Microalgae cultivation

Microalgae grow as a dilute solution. When cultivated in the open pond system, the typical concentration of microalgae is in the range of 0.5 g/l to 2 g/l. In our base case TE calculations, we have accounted for the cost of microalgae assuming an open pond system. Moreover, we have also assumed that the cultivation site is close to the plant; therefore, the transportation cost is negligible. Depending on the $CO_2$ sequestration ability of *Scenedesmus sp.* and standard open pond dimensions, around 30000 hectares of land is required to cultivate microalgae. This vast land requirement would be one of the limitations during scale-up. This limitation can be overcome by cultivating microalgae using photobioreactor (PBR). Furthermore, the concentration of microalgae cultivated in the PBR is higher compared to an open pond system. However, the initial capital investment for PBR would be higher compared to an open pond system, and as a consequence, the cost of microalgae cultivated in the PBR will be higher.

### 5.7.2 $CO_2$ sequestration

To perform TE analysis, we have assumed that the exhaust gas from JSW steel plant is used as a source of $CO_2$ to cultivate microalgae. A way to perform this $CO_2$ sparging should be envisioned. There are 2 plausible solutions a) barren land should be available to construct an establishment for the cultivation of microalgae such that $CO_2$ along with other flue gases could be sparged directly into cultivation media or b) a $CO_2$ separation and sequestration process should be set up, and the $CO_2$ should be transported to a microalgae cultivation site. The first option is difficult to execute because mostly power plants and steel processing plants have constructed their establishments and land acquisition in the densely populated country like India is troublesome. In such a scenario, the second option appears more feasible. However, it will result in more capital investment and operating costs. Therefore, the payback period will increase, and IRR will decrease.

### 5.7.3 Process design

To accommodate the limited land availability constraint on the microalgae cultivation, we can scale down the process such that only available microalgae can be processed. This scale down will not affect RFV reactor and LT-shift reactor sizing. However, $H_2$ separation will be difficult. Techno-economics of PSA is highly dependent on $H_2$ flow. Below 10000 $NM^3/h$, operating PSA becomes economically infeasible, and hence it cannot be used. To separate $H_2$ where $H_2$ gas flow is below 10000 $NM^3/h$, palladium membrane is used. Commercial membrane-based gas separation technology for $H_2$ is not available yet. Therefore, designing such a process will not be cost-effective, and as a consequence, overall $H_2$ production process will not be techno-economically feasible. Furthermore, this TE calculation assumes that the $H_2$ production facility is located in a Steel manufacturing plant. Hence, the cost of maintenance and labour is shared with the Steel manufacturing plant. In the case of stand alone plant the payback period of the plant will be 4.25 years.

# Chapter 6

# Conclusion and Prospects

Hydrogen and methane are the clean sources of fuel and green chemical synthesis only if they are produced from renewable resources. At present, 96% of the hydrogen and 100% methane is produced using non-renewable resources. Microalgae is a leading candidate to produce renewable hydrogen. However, most of the microalgae-based fuel production efforts were directed towards microalgal oil. Recently, some efforts were made to convert entire microalgae into fuel using hydrothermal liquefaction. However, harsh operating condition limits its commercial potential. Therefore, a strong need of the novel catalytic thermochemical process to convert entire microalgae into hydrogen was observed.

We have developed a novel catalytic, single-step, and tar-free conversion process for microalgae. In the presence of Ni-Rh/ alumina catalyst at 650 °C and CSR of 0.12, 65% hydrogen was produced. Whereas, in the presence of Ni-Cu-Pd/alumina catalyst at 600 °C and CSR of 0.12, 16% methane was produced. A detail, surface reconstruction study of Ni-Cu-Pd catalyst is required to analyse the effect of loading on the morphology of the metal nanoparticles. Although, surface reconstruction of Ni is well known, a combined effect of metals on the crystal morphology and catalysis is missing in the literature. Understanding the surface reconstruction effect can increase the tunability of the process.

Microalgae has around 11% ash, most of which is alkali and alkaline earth metals (AAEM). The role of AAEM was extensively reported in the literature. However, the synergistic effect of AAEM and phosphorus was missing in the literature. We reported that the microalgal ash gets transformed into a catalytic bed during the reaction by forming agglomerates of potassium and magnesium coated calcium phosphate nano-spheres. Moreover, the catalyst bed helps to maintain the clean catalyst surface. Although the effect of AAEM as a promoter is well reported in the literature, it would be interesting to see the effect of these AAEM as a support for metal catalysts. An operando study would be necessary to analyse the exact reaction mechanism.

We have made an effort to establish the trade-off between economics and environmental impacts of renewable hydrogen and methane production using microalgae. The hydrogen production was economically feasible, assuming a market price of ₹ 650 per kg. A payback period of 3.78 years, with 22% IRR was estimated through a detailed techno-economic analysis. Hydrogen composition and cost of microalgae production played a crucial role in determining the payback period.

Two major assumptions were made during TEA calculations; first, A design of slagging bed gasifier with intermittent suction to maintain the critical height of slag bed, and second, the microalgae was harvested using sedimentation and the excess water was used as the gasifying agent. The second assumption is valid for freshwater microalgae because the amount of minerals are limited. However, microalgae can be grown into saline water, and with our limited understanding of the effect of the minerals on the catalytic activity, it is not possible to extrapolate the same assumption for saltwater microalgae. A detailed experimental analysis is required to understand the effect of minerals on the catalytic activity. In the case of the first assumption, a new design of gasifier considering the pressure drop and gaseous flows inside the slag bed is recommended.

LCA analysis of hydrogen production showed that the climate change impact of hydrogen production using RFV of microalgae was 36.47% lower (7.56 kg $CO_2$ eq.) compared to steam reforming of methane (11.9 kg $CO_2$ eq.), as well as proposed renewable hydrogen production technologies. It was observed that the majority of the emissions were due to electricity production. A futuristic simulation of hydro-electricity based RFV of microalgae; to produce hydrogen, showed the impact of 1.2 kg $CO_2$ eq./kg of $H_2$. Comparing various microalgae processing technologies by performing a superstructure optimisation will provide further insights into process selection. Deciding a suitable alternative is completely dependent on the government policies and global energy outline.

# Appendix A

# Supporting Information

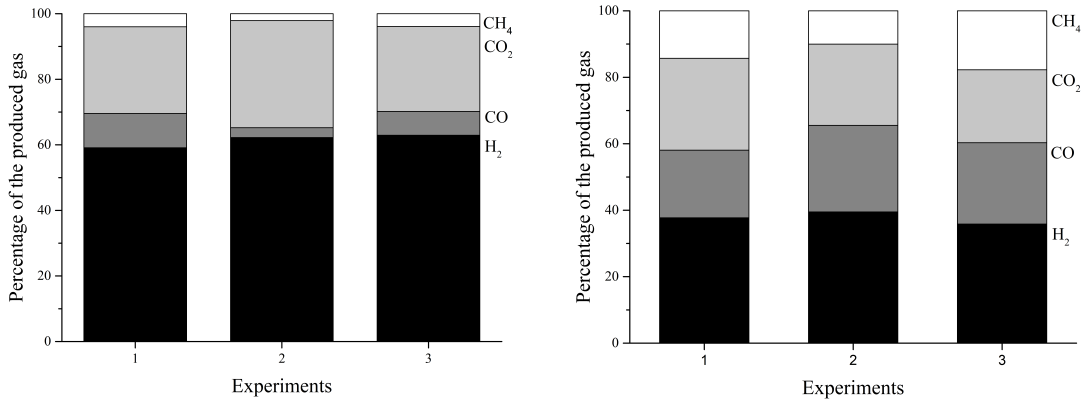


(a) Ni-Rh (b) Ni-Cu-Pd

Figure A.1: Performance evaluation of the reactor (a) Operating conditions :– Temp: 650 °C , feeding rate: 7g/h, Bi-metallic catalyst: Ni-Rh/$Al_2O_3$ (b) Operating conditions :– Temp: 600 °C , feeding rate: 7g/h, Tri-metallic catalyst: Ni-Cu-Pd/$Al_2O_3$

Figure A.1 shows the reproducibility of the results. In the case of Ni-Rh catalyst, experiment 1 was performed for 4 h, experiment 2 was performed for 3.5 h, and experiment 3 was performed for 9 h to evaluate the catalytic activity of the catalyst. Similarly, for Ni-Cu-Pd catalyst, experiment 1 was performed for 3.5 h, experiment 2 was performed for 3 h, and experiment 3 was performed for 13 h to evaluate the catalytic activity of the catalyst. The average value of these 3 experiments is reported in the section 4.1.4, for Ni-Rh catalyst the average composition of 65% ± 5.02 hydrogen was observed and for Ni-Cu-Pd catalyst the average composition of 16% ± 4.6 methane was observed.

Table A.1: Elements present in the slag after reaction

| Name of the compound | JCPDS Number |
|---|---|
| Aluminium Phosphate | 47.0599, 47.0603, 47.0325, 45.0455, 15.0273 |
| Aluminium Calcium | 14.0428 |
| Aluminium | 04.0787 |
| Calcium | 10.0348 |
| Monocalcium Aluminate | 23.1036 |
| Calcium Aluminium Phosphate Silicate | 36.0108 |
| Calcium Magnesium Phosphate | 11.0234 |
| Calcium Phosphate | 15.0204, 50.0584 |
| Dicalcium oxocalcium silicate | 16.0406 |
| Magnesium Aluminium Phosphate | 35.0244 |
| Magnesium Phosphate | 35.0134, 43.0225, 32.0626, 27.1273 |
| Potassium Aluminium Silicate | 31.0965, 50.0436 |
| Potassium Calcium Phosphate | 03.0316, 33.1002 |
| Silicon Phosphate | 39.0189, 22.1274, 22.1320, 11.1167 |
| Potassium Oxide | 30.0794 |
| SAPO 20,30,41 | 47.0634, 47.0632, 47.0616 |
| Zeolite SSZ 28 | 49.0915 |

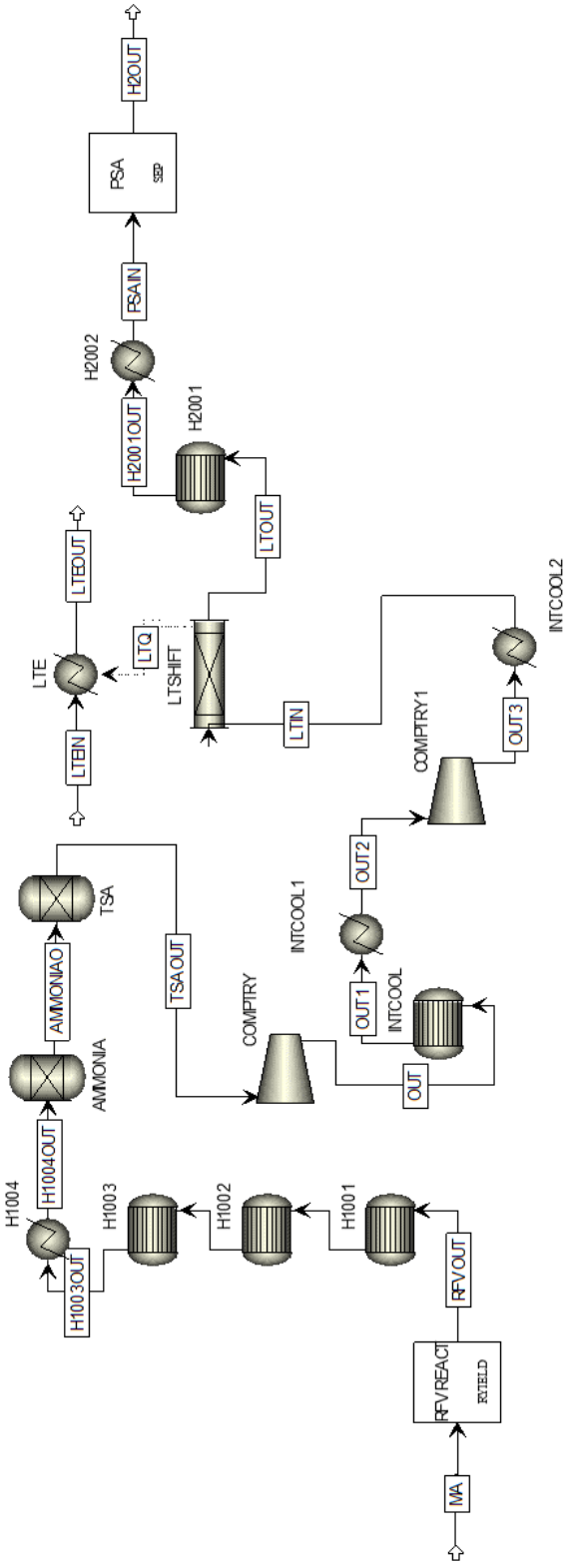


Figure A.2: ASPEN plus process flow diagram for hydrogen production

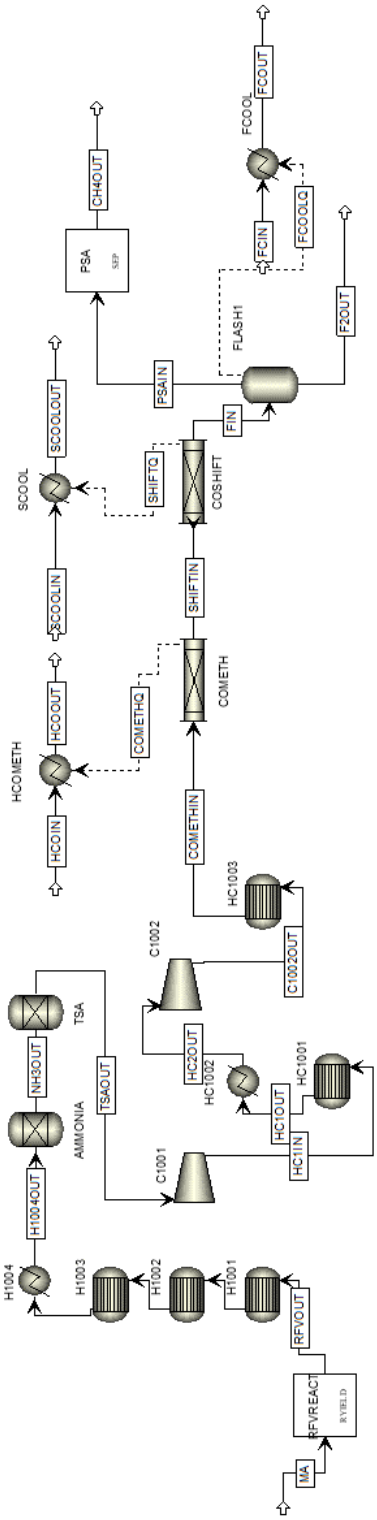


Figure A.3: ASPEN plus process flow diagram for methane production

Table A.2: Stream table for Area 100H

| Components | S1 | S2 | S3 | S4 | S5 | S6 | S7 | S8 | S9 | S10 | S11 | S12 | S13 | S14 | S132 | S142 | HCI1001 | HCI1002 | HCI1003 | HCI1004 | HCO1001 | HCO1002 | HCO1003 | HCO1004 |
|---|---|---|---|---|---|---|---|---|---|---|---|---|---|---|---|---|---|---|---|---|---|---|---|---|
| Temp ( °C ) | 25 | 160 | 650 | 650 | 420 | 270 | 110 | 50 | 50 | 25 | 50 | 50 | 50 | 50 | | 50 | 30 | 30 | 30 | 30 | 420 | 250 | 105 | 45 |
| Pressure (Bar) | 1 | 1 | 1 | 1 | 1 | 1 | 1 | 1 | 1 | 1 | 1 | 1 | 1 | 1 | | 1 | 40 | 40 | 1 | | 40 | 40 | 1 | |
| Microalgae (kg/h) | 12790 | 0 | 0 | 0 | 0 | 0 | 0 | 0 | 0 | 0 | 0 | 0 | 0 | 0 | 0 | 0 | 0 | 0 | 0 | 0 | 0 | 0 | 0 | 0 |
| Steam (kg/hr) | 0 | 63950 | 0 | 0 | 0 | 0 | 0 | 0 | 0 | 0 | 0 | 0 | 0 | 0 | 0 | 0 | 0 | 0 | 0 | 0 | 0 | 0 | 0 | 0 |
| Slag (kg/hr) | 0 | 0 | 345.33 | 0 | 0 | 0 | 0 | 0 | 0 | 0 | 0 | 0 | 0 | 0 | 0 | 0 | 0 | 0 | 0 | 0 | 0 | 0 | 0 | 0 |
| H2 (kg/hr) | 0 | 0 | 0 | 1339.6 | 1339.6 | 1339.6 | 1339.6 | 0 | 1339.6 | 0 | 0 | 1339.6 | 0 | 1339.6 | 0 | 1339.6 | 0 | 0 | 0 | 0 | 0 | 0 | 0 | 0 |
| H2 (kmol/hr) | | | | 669.8 | 669.8 | 669.8 | 669.8 | 0 | 669.8 | 0 | 0 | 669.8 | 0 | 669.8 | | 669.8 | | | | | | | | |
| CO (kg/hr) | 0 | 0 | 0 | 1688.24 | 1688.24 | 1688.24 | 1688.24 | 0 | 1688.24 | 0 | 0 | 1688.24 | 0 | 1688.24 | 0 | 1688.24 | 0 | 0 | 0 | 0 | 0 | 0 | 0 | 0 |
| CO (kmol/hr) | | | | 60.29 | 60.29 | 60.29 | 60.29 | | 60.29 | | | 60.29 | | 60.29 | | 60.29 | | | | | | | | |
| CO2 (kg/hr) | 0 | 0 | 0 | 13452.72 | 13452.72 | 13452.72 | 13452.72 | 0 | 13452.72 | 0 | 0 | 13452.72 | 0 | 13452.72 | 0 | 13452.72 | 0 | 0 | 0 | 0 | 0 | 0 | 0 | 0 |
| CO2 (kmol/hr) | | | | 305.74 | 305.74 | 305.74 | 305.74 | | 305.74 | | | 305.74 | | 305.74 | | 305.74 | | | | | | | | |
| CH4 (kg/hr) | 0 | 0 | 0 | 693.85 | 693.85 | 693.85 | 693.85 | 0 | 693.85 | 0 | 0 | 693.85 | 0 | 693.85 | 0 | 693.85 | 0 | 0 | 0 | 0 | 0 | 0 | 0 | 0 |
| CH4 (kmol/hr) | | | | 43.36 | 43.36 | 43.36 | 43.36 | | 43.36 | | | 43.36 | | 43.36 | | 43.36 | | | | | | | | |
| NH3 (kg/hr) | 0 | 0 | 0 | 2095 | 2095 | 2095 | 2095 | 679.2 | 1415.8 | 0 | 0 | 0 | 0 | 0 | 0 | 0 | 0 | 0 | 0 | 0 | 0 | 0 | 0 | 0 |
| NH3 (kmol/hr) | | | | 123.24 | 123.24 | 123.24 | 123.24 | 39.95 | 83.28 | | | | | | | | | | | | | | | |
| H2O (kg/hr) | 0 | 0 | 0 | 56981.56 | 56981.56 | 56981.56 | 58340.79 | 52121 | 4860.53 | 0 | 0 | 4860.53 | 0 | 5573.65 | 5573.65 | 0 | 0 | 0 | 0 | 0 | 0 | 0 | 0 | 0 |
| Cooling water (kg/hr) | 0 | 0 | 0 | 0 | 0 | 0 | 0 | 0 | 0 | 0 | 0 | 0 | 0 | 0 | 0 | 0 | 12524.5 | 24908.3 | 9469.91 | 0 | 12524.5 | 24908.3 | 9469.91 | 0 |
| Air | 0 | 0 | 0 | 0 | 0 | 0 | 0 | 0 | 0 | 0 | 0 | 0 | 0 | 0 | 0 | 0 | 0 | 0 | 0 | 0 | 0 | 0 | 0 | 0 |
| H2SO4 (kg/hr) | 0 | 0 | 0 | 0 | 0 | 0 | 0 | 0 | 0 | 2.3 | 0 | 0 | 0 | 0 | 0 | 0 | 0 | 0 | 0 | 0 | 0 | 0 | 0 | 0 |
| H2S | 0 | 0 | | 144 | 144 | 144 | 150 | 99.32 | 44.68 | 0 | 0 | 44.68 | 0 | 0 | 0 | 0 | 0 | 0 | 0 | 0 | 0 | 0 | 0 | 0 |
| Sulphur | 0 | 0 | 0 | 0 | 0 | 0 | 0 | 0 | 0 | 0 | 0 | 0 | 44.68 | 0 | 0 | 0 | 0 | 0 | 0 | 0 | 0 | 0 | 0 | 0 |
| Ammonium Sulphate (kg/hr) | 0 | 0 | 0 | 0 | 0 | 0 | 0 | 0 | 0 | 0 | 1412.24 | 0 | 0 | 0 | 0 | 0 | 0 | 0 | 0 | 0 | 0 | 0 | 0 | 0 |

Table A.3: Stream table for Area 200H

| Components | S1 | S2 | S3 | S4 | S5 | S6 | S7 | S8 |
|---|---|---|---|---|---|---|---|---|
| Temp (ÂřC) | 50 | 210 | 250 | 250 | 45 | 45 | 45 | 45 |
| Pressure (Bar) | 1 | 25 | 25 | 25 | 1 | 25 | 25 | 700 |
| Microalgae (kg/h) | 0 | 0 | 0 | 0 | 0 | 0 | 0 | 0 |
| Steam (kg/hr) | 0 | 0 | 1800 | 0 | 0 | 0 | 0 | 0 |
| Slag (kg/hr) | 0 | 0 | 0 | 0 | 0 | 0 | 0 | 0 |
| H2 (kg/hr) | 1339.6 | 1339.6 | 0 | 1457.76 | 0 | 1457.76 | 218.65 | 1239.1 |
| H2 (kmol/hr) | 669.8 | 669.8 | | 728.88 | | 728.88 | 109.32 | 619.5 |
| CO (kg/hr) | 1688.24 | 1688.24 | 0 | 33.88 | 0 | 33.88 | 33.88 | 0 |
| CO (kmol/hr) | 60.29 | 60.29 | | 1.21 | | 1.21 | 1.21 | |
| CO2 (kg/hr) | 13452.72 | 13452.72 | 0 | 16052.08 | 0 | 16052.08 | 16052.08 | 0 |
| CO2 (kmol/hr) | 305.74 | 305.74 | | 364.82 | | 364.82 | 364.82 | |
| CH4 (kg/hr) | 693.85 | 693.85 | 0 | 693.85 | 0 | 693.85 | 693.85 | 0 |
| CH4 (kmol/hr) | 43.36 | 43.36 | | 43.36 | | 43.36 | 43.36 | |
| NH3 (kg/hr) | 0 | 0 | 0 | 0 | 0 | 0 | 0 | 0 |
| H2O (kg/hr) | 0 | 0 | 0 | 736.56 | 287.26 | 449.28 | 449.28 | 0 |
| Cooling water (kg/hr) | 0 | 0 | 0 | 0 | 0 | 0 | 0 | 0 |
| Air | 0 | 0 | 0 | 0 | 0 | 0 | 0 | 0 |
| H2SO4 (kg/hr) | 0 | 0 | 0 | 0 | 0 | 0 | 0 | 0 |
| H2S (kg/hr) | 0 | 0 | 0 | 0 | 0 | 0 | 0 | 0 |
| Ammonium Sulphate (kg/hr) | 0 | 0 | 0 | 0 | 0 | 0 | 0 | 0 |

Table A.4: Stream table for Area 100M

| Components | S1 | S2 | S3 | S4 | S5 | S6 | S7 | S8 | S9 | S10 | S11 | S12 | S13 | S14 | HCI1001 | HCI1002 | HCI1003 | HCI1004 | HCO1001 | HCO1002 | HCO1003 | HCO1004 |
|---|---|---|---|---|---|---|---|---|---|---|---|---|---|---|---|---|---|---|---|---|---|---|
| Temp (ÂřC) | 25 | 160 | 600 | 600 | 420 | 270 | 110 | 50 | 50 | 25 | 50 | 50 | | 50 | 30 | 30 | 30 | 30 | 400 | 250 | 105 | 45 |
| Pressure (Bar) | 1 | 1 | 1 | 1 | 1 | 1 | 1 | 1 | 1 | 1 | 1 | 1 | | 1 | 40 | 40 | 1 | | 40 | 40 | 1 | |
| Microalgae (kg/h) | 12790 | 0 | 0 | 0 | 0 | 0 | 0 | 0 | 0 | 0 | 0 | 0 | 0 | 0 | 0 | 0 | 0 | 0 | 0 | 0 | 0 | 0 |
| Steam (kg/hr) | 0 | 63950 | 0 | 0 | 0 | 0 | 0 | 0 | 0 | 0 | 0 | 0 | 0 | 0 | 0 | 0 | 0 | 0 | 0 | 0 | 0 | 0 |
| Slag (kg/hr) | 0 | 0 | 404.14 | 0 | 0 | 0 | 0 | 0 | 0 | 0 | 0 | 0 | 0 | 0 | 0 | 0 | 0 | 0 | 0 | 0 | 0 | 0 |
| H2 (kg/hr) | 0 | 0 | 0 | 382.29 | 382.29 | 382.29 | 382.29 | 0 | 382.29 | 0 | 0 | 382.29 | 0 | 382.29 | 0 | 0 | 0 | 0 | 0 | 0 | 0 | 0 |
| CO (kg/hr) | 0 | 0 | 0 | 6881.85 | 6881.85 | 6881.85 | 6881.85 | 0 | 6881.85 | 0 | 0 | 6861.85 | 0 | 6861.85 | 0 | 0 | 0 | 0 | 0 | 0 | 0 | 0 |
| CO2 (kg/hr) | 0 | 0 | 0 | 10704.34 | 10704.34 | 10704.34 | 10704.34 | 0 | 10704.34 | 0 | 0 | 10704.34 | 0 | 10704.34 | 0 | 0 | 0 | 0 | 0 | 0 | 0 | 0 |
| CH4 (kg/hr) | 0 | 0 | 0 | 2224.25 | 2224.25 | 2224.25 | 2224.25 | 0 | 2224.25 | 0 | 0 | 2224.25 | 0 | 2224.25 | 0 | 0 | 0 | 0 | 0 | 0 | 0 | 0 |
| NH3 (kg/hr) | 0 | 0 | 0 | 1036.06 | 1036.06 | 1036.06 | 1036.06 | 365.21 | 670.85 | 0 | 0 | 0 | 0 | 0 | 0 | 0 | 0 | 0 | 0 | 0 | 0 | 0 |
| H2O (kg/hr) | 0 | 0 | 0 | 54138.19 | 54138.19 | 54138.19 | 54138.19 | 50012.86 | 4125.33 | 0 | 0 | 4602.33 | 4602.33 | 0 | 0 | 0 | 0 | 0 | 0 | 0 | 0 | 0 |
| Cooling water (kg/hr) | 0 | 0 | 0 | 0 | 0 | 0 | 0 | 0 | 0 | 0 | 0 | 0 | 0 | 0 | 8930.12 | 22741.8 | 8597.75 | 0 | 8930.12 | 22741.8 | 8597.75 | 0 |
| Air | 0 | 0 | 0 | 0 | 0 | 0 | 0 | 0 | 0 | 0 | 0 | 0 | 0 | 0 | 0 | 0 | 0 | 0 | 0 | 0 | 0 | 0 |
| H2SO4 (kg/hr) | 0 | 0 | 0 | 0 | 0 | 0 | 0 | 0 | 0 | 2.3 | 0 | 0 | 0 | 0 | 0 | 0 | 0 | 0 | 0 | 0 | 0 | 0 |
| Ammonium Sulphate (kg/hr) | 0 | 0 | 0 | 0 | 0 | 0 | 0 | 0 | 0 | 0 | 645.15 | 0 | 0 | 0 | 0 | 0 | 0 | 0 | 0 | 0 | 0 | 0 |

Table A.5: Stream table for Area 200M and Area 300M

| Components | S1 | S2 | S3 | S4 | S5 | S6 | S7 | S8 | S9 |
|---|---|---|---|---|---|---|---|---|---|
| Temp (ÂřC) | 50 | 260 | 260 | 260 | 260 | 45 | 45 | 45 | 45 |
| Pressure (Bar) | 1 | 64 | 64 | 64 | 64 | 24 | 24 | 24 | 24 |
| Microalgae (kg/h) | 0 | 0 | 0 | 0 | 0 | 0 | 0 | 0 | 0 |
| Steam (kg/hr) | 0 | 0 | 0 | 0 | 0 | 0 | 0 | 0 | 0 |
| Slag (kg/hr) | 0 | 0 | 0 | 0 | 0 | 0 | 0 | 0 | 0 |
| H2 (kg/hr) | 382.29 | 382.29 | 0 | 111.25 | 111.25 | 0 | 111.25 | 16.69 | 94.56 |
| CO (kg/hr) | 6861.85 | 6861.85 | 3119.48 | 4.2 | 4.2 | 0 | 4.2 | 4.2 | 0 |
| CO2 (kg/hr) | 10704.34 | 10704.34 | 10294.24 | 15189.24 | 15189.24 | 0 | 15189.24 | 15189.24 | 0 |
| CH4 (kg/hr) | 2224.25 | 2224.25 | 4100 | 4100 | 4100 | 0 | 4100 | 615.04 | 3484.96 |
| NH3 (kg/hr) | 0 | 0 | 0 | 0 | 0 | 0 | 0 | 0 | 0 |
| H2O (kg/hr) | 0 | 0 | 2206.08 | 203.58 | 203.58 | 146.88 | 56.7 | 56.7 | 0 |
| Cooling water (kg/hr) | 0 | 0 | 0 | 0 | 0 | 0 | 0 | 0 | 0 |
| Air | 0 | 0 | 0 | 0 | 0 | 0 | 0 | 0 | 0 |
| H2SO4 (kg/hr) | 0 | 0 | 0 | 0 | 0 | 0 | 0 | 0 | 0 |
| Ammonium Sulphate (kg/hr) | 0 | 0 | 0 | 0 | 0 | 0 | 0 | 0 | 0 |

Table A.6: Details of heat exchanger to produce hydrogen from microalgae using reactive flash volatilization

| Heat Exchanger | Type | Configuration | Material of construction | Area (m2) |
|---|---|---|---|---|
| HH1001 | S&T | BEU | Cr-0.5Mo | 521.9 |
| HH1002 | S&T | BEU | Carbon Steel | 604 |
| HH1003 | S&T | BEM | Carbon Steel | 348.7 |
| HH1004 | Air cooled | | Carbon Steel | 43.4 |

Table A.7: Details of heat exchanger to produce methane from microalgae using reactive flash volatilization

| Heat Exchanger | Type | Configuration | Material of construction | Area (m2) |
|---|---|---|---|---|
| HM1001 | S&T | BEU | Cr-0.5Mo | 448.8 |
| HM1002 | S&T | BEU | Carbon Steel | 385.4 |
| HM1003 | S&T | BEM | Carbon Steel | 354.4 |
| HM1004 | Air cooled | | Carbon Steel | 48.1 |

Table A.8: Direct costs involved in hydrogen production

| Direct costs | Cost (Million INR) |
|---|---|
| Purchased equipment delivered | 1398.23 |
| Purchased equipment installation | 657.17 |
| Instrumentation and control | 251.68 |
| Piping | 922.83 |
| Electrical | 153.80 |
| Building | 251.68 |
| Yard Improvement | 139.82 |
| Service facilities | 987.76 |
| Land | 83.89 |
| Total Direct Plant cost | 4837.88 |

Table A.9: Indirect costs involved in hydrogen production

| Indirect Cost | Cost (Million INR) |
|---|---|
| Engineering and supervision | 461.42 |
| Construction Expenses | 573.27 |
| Contractor's fee | 349.56 |
| Contingency | 587.26 |
| Total indirect cost | 1971.50 |

Table A.10: Operating costs involved in hydrogen production

| Component | Cost (INR/h) |
|---|---|
| Microalgae (32 INR/kg) | 393600 |
| Operating Labour | 522 |
| Operating Supervision | 78.41 |
| Utilities | 121150 |
| Maintenance cost equipment | 890 |
| Operating supplies | 135 |
| Overhead cost | 750 |
| Total | 517135 |

Table A.11: Direct costs involved in methane production

| Direct costs | Cost (Million INR) |
|---|---|
| Purchased equipment delivered | 1399.19 |
| Purchased equipment installation | 657.62 |
| Instrumentation and control | 251.85 |
| Piping | 923.46 |
| Electrical | 153.91 |
| Building | 251.85 |
| Yard Improvement | 139.92 |
| Service facilities | 979.43 |
| Land | 83.95 |
| Total Direct Plant cost | 4841.18 |

Table A.12: Indirect costs involved in methane production

| Indirect Cost | Cost (Million INR) |
|---|---|
| Engineering and supervision | 461.73 |
| Construction Expenses | 573.67 |
| Contractor's fee | 349.80 |
| Contingency | 587.66 |
| Total indirect cost | 1972.85 |

Table A.13: Operating costs involved in hydrogen production

| Component | Cost (INR/h) |
|---|---|
| Microalgae (32 INR/kg) | 393600 |
| Operating Labour | 523 |
| Operating Supervision | 79 |
| Utilities | 119173 |
| Maintenance cost equipment | 1233 |
| Operating supplies | 185 |
| Overhead cost | 917 |
| Total | 515710 |

# References


Abu El-Rub, Z., Bramer, E. A., and Brem, G., 2004, "Review of catalysts for tar elimination in biomass gasification processes," *Industrial & engineering chemistry research* **43**, 6911–6919.

Acar, C., and Dincer, I., 2014, "Comparative assessment of hydrogen production methods from renewable and non-renewable sources," *International journal of hydrogen energy* **39**, 1–12.

Acar, C., Dincer, I., and Naterer, G. F., 2016, "Review of photocatalytic water-splitting methods for sustainable hydrogen production," *International Journal of Energy Research* **40**, 1449–1473.

Adnan, M. A., and Hossain, M. M., 2018, "Co2 gasification of microalgae (n. oculata)–a thermodynamic study," in *MATEC Web of Conferences*, Vol. 154 (EDP Sciences). p. 01002.

Agrawal, A., and Chakraborty, S., 2013, "A kinetic study of pyrolysis and combustion of microalgae chlorella vulgaris using thermo-gravimetric analysis," *Bioresource technology* **128**, 72–80.

Appels, L., Lauwers, J., Degrève, J., Helsen, L., Lievens, B., Willems, K., Van Impe, J., and Dewil, R., 2011, "Anaerobic digestion in global bio-energy production: potential and research challenges," *Renewable and Sustainable Energy Reviews* **15**, 4295–4301.

Arnold, R., and Hill, J., 2019, "Catalysts for gasification: a review," *Sustainable energy & fuels* **3**, 656–672.

Arregi, A., Amutio, M., Lopez, G., Bilbao, J., and Olazar, M., 2018, "Evaluation of thermochemical routes for hydrogen production from biomass: A review," *Energy conversion and management* **165**, 696–719.

Azadi, P., Brownbridge, G., Mosbach, S., Inderwildi, O., and Kraft, M., 2015, "Simulation and life cycle assessment of algae gasification process in dual fluidized bed gasifiers," *Green Chemistry* **17**, 1793–1801.

Azadi, P., Brownbridge, G., Mosbach, S., Smallbone, A., Bhave, A., Inderwildi, O., and Kraft, M., 2014, "The carbon footprint and non-renewable energy demand of algae-derived biodiesel," *Applied energy* **113**, 1632–1644.

Aznar, M. P., Caballero, M. A., Gil, J., Martin, J. A., and Corella, J., 1998, "Commercial steam reforming catalysts to improve biomass gasification with steam- oxygen mixtures. 2. catalytic tar removal," *Industrial & engineering chemistry research* **37**, 2668–2680.

Bakhtyari, A., Makarem, M. A., and Rahimpour, M. R., 2017, "Hydrogen production through pyrolysis," (Springer New York). pp. 1–28.

Bali, N., Prasad, P. M., and Antelo, M., 2019, "Sustainable performance-oriented production practices in the indian iron and steel industry: An empirical investigation," *Journal of Cleaner Production*

Benemann, J. R., and Oswald, W. J., 1996, *Systems and economic analysis of microalgae ponds for conversion of CO {sub 2} to biomass. Final report*, Tech. Rep. (California Univ., Berkeley, CA (United States). Dept. of Civil Engineering).

Bhandari, R., Trudewind, C. A., and Zapp, P., 2014, "Life cycle assessment of hydrogen production via electrolysis–a review," *Journal of cleaner production* **85**, 151–163.

Bibber, L. V., Shuster, E., Haslbeck, J., Rutkowski, M., Olson, S., and Kramer, S., 2007, "Baseline technical and economic assessment of a commercial scale fischer-tropsch liquids facility," *US Department of Energy, National Energy Technology Laboratory [DOE/NETL-2007/1260]*

Biller, P., Riley, R., and Ross, A., 2011, "Catalytic hydrothermal processing of microalgae: decomposition and upgrading of lipids," *Bioresource technology* **102**, 4841–4848.

Boström, D., Boström, M., Skoglund, N., Boman, C., Backman, R., Öhman, M., and Grimm, A., 2010, "Ash transformation chemistry during energy conversion of biomass," in *Impacts of Fuel Quality on Power Production & Environment: 29/08/2010-03/09/2010*

BostroÌĹm, D., Eriksson, G., Boman, C., and Ohman, M., 2009, "Ash transformations in fluidized-bed combustion of rapeseed meal," *Energy & Fuels* **23**, 2700–2706.

Brennan, L., and Owende, P., 2010, "Biofuels from microalgaeâĂŤa review of technologies for production, processing, and extractions of biofuels and co-products," *Renewable and sustainable energy reviews* **14**, 557–577.

British Petroleum, 2018, "Bp statistical review of world energy 2018,"

Brown, E., 2015, "Joint agency staff report on assembly bill 8: Assessment of time and cost needed to attain 100 hydrogen refueling stations in california," *California Energy Commission: Sacramento, CA, USA*

Brownbridge, G., Azadi, P., Smallbone, A., Bhave, A., Taylor, B., and Kraft, M., 2014, "The future viability of algae-derived biodiesel under economic and technical uncertainties," *Bioresource technology* **151**, 166–173.

Burdon, R., Palmer, G., and Chakraborty, S., 2019, "National hydrogen strategy-submission,"

Byron, S. R., Loganathan, M., and Shantha, M. S., 2010, "A review of the water gas shift reaction kinetics," *International Journal of Chemical Reactor Engineering* **8**

Caballero, M. A., Aznar, M. P., Gil, J., Martín, J. A., Francés, E., and Corella, J., 1997, "Commercial steam reforming catalysts to improve biomass gasification with steam-oxygen mixtures. 1. hot gas upgrading by the catalytic reactor," *Industrial & engineering chemistry research* **36**, 5227–5239.

Caballero, M. A., Corella, J., Aznar, M.-P., and Gil, J., 2000, "Biomass gasification with air in fluidized bed. hot gas cleanup with selected commercial and full-size nickel-based catalysts," *Industrial & Engineering Chemistry Research* **39**, 1143–1154.

Cavinato, C., Ugurlu, A., de Godos, I., Kendir, E., and Gonzalez-Fernandez, C., 2017, "Biogas production from microalgae," in *Microalgae-Based Biofuels and Bioproducts* (Elsevier). pp. 155–182.

Cetinkaya, E., Dincer, I., and Naterer, G., 2012, "Life cycle assessment of various hydrogen production methods," *International journal of hydrogen energy* **37**, 2071–2080.

Chaiprasert, P., and Vitidsant, T., 2009, "Effects of promoters on biomass gasification using nickel/dolomite catalyst," *Korean journal of chemical engineering* **26**, 1545–1549.

Chan, F. L., and Tanksale, A., 2014a, "Catalytic steam gasification of cellulose using reactive flash volatilization," *ChemCatChem* **6**, 2727–2739.

Chan, F. L., and Tanksale, A., 2014b, "Review of recent developments in ni-based catalysts for biomass gasification," *Renewable and Sustainable Energy Reviews* **38**, 428–438.

Chan, F. L., and Tanksale, A., 2016, "Catalytic steam gasification of pinewood and eucalyptus sawdust using reactive flash volatilization," *Applied Catalysis B: Environmental* **187**, 310–327.

Cherad, R., Onwudili, J., Biller, P., Williams, P., and Ross, A., 2016, "Hydrogen production from the catalytic supercritical water gasification of process water generated from hydrothermal liquefaction of microalgae," *Fuel* **166**, 24–28.

Chisti, Y., 2007, "Biodiesel from microalgae," *Biotechnology advances* **25**, 294–306.

Chisti, Y., 2008, "Biodiesel from microalgae beats bioethanol," *Trends in biotechnology* **26**, 126–131.

Chu, S., Cui, Y., and Liu, N., 2017, "The path towards sustainable energy," *Nature materials* **16**, 16–22.

Clark, C. E., Han, J., Burnham, A., Dunn, J. B., and Wang, M., 2012, *Life-cycle analysis of shale gas and natural gas.*, Tech. Rep. (Argonne National Lab.(ANL), Argonne, IL (United States)).

Colby, J. L., Dauenhauer, P. J., and Schmidt, L. D., 2008, "Millisecond autothermal steam reforming of cellulose for synthetic biofuels by reactive flash volatilization," *Green Chemistry* **10**, 773–783.

Conti, J., Holtberg, P., Diefenderfer, J., LaRose, A., Turnure, J. T., and Westfall, L., 2016, *International energy outlook 2016 with projections to 2040*, Tech. Rep. (USDOE Energy Information Administration (EIA), Washington, DC (United States âĂę).

Corella, J., Orío, A., and Aznar, P., 1998, "Biomass gasification with air in fluidized bed: reforming of the gas composition with commercial steam reforming catalysts," *Industrial & Engineering Chemistry Research* **37**, 4617–4624.

Cowan, A. J., Tang, J., Leng, W., Durrant, J. R., and Klug, D. R., 2010, "Water splitting by nanocrystalline tio2 in a complete photoelectrochemical cell exhibits efficiencies limited by charge recombination," *The Journal of Physical Chemistry C* **114**, 4208–4214.

Crabtree, G. W., Dresselhaus, M. S., and Buchanan, M. V., 2004, "The hydrogen economy," *Physics today* **57**, 39–44.

Dauenhauer, P. J., 2008, "Millisecond autothermal catalytic reforming of carbohydrates for synthetic fuels by reactive flash volatilization,"

Davis, R., Aden, A., and Pienkos, P. T., 2011, "Techno-economic analysis of autotrophic microalgae for fuel production," *Applied Energy* **88**, 3524–3531.

Davis, R., Markham, J., Kinchin, C., Grundl, N., Tan, E. C., and Humbird, D., 2016, *Process design and economics for the production of algal biomass: algal biomass production in open pond systems and processing through dewatering for downstream conversion*, Tech. Rep. (National Renewable Energy Lab.(NREL), Golden, CO (United States)).

Demirbaş, A., 2002, "Gaseous products from biomass by pyrolysis and gasification: effects of catalyst on hydrogen yield," *Energy Conversion and Management* **43**, 897–909.

Deshpande, A., and Gupta, N. M., 2010, "Critical role of particle size and interfacial properties in the visible light induced splitting of water over the nanocrystallites of supported cadmium sulphide," *international journal of hydrogen energy* **35**, 3287–3296.

Dincer, I., 2012, "Green methods for hydrogen production," *International journal of hydrogen energy* **37**, 1954–1971.

Dincer, I., and Acar, C., 2015, "Review and evaluation of hydrogen production methods for better sustainability," *International journal of hydrogen energy* **40**, 11094–11111.

Dismukes, G. C., Carrieri, D., Bennette, N., Ananyev, G. M., and Posewitz, M. C., 2008, "Aquatic phototrophs: efficient alternatives to land-based crops for biofuels," *Current Opinion in Biotechnology* **19**, 235–240.

Drapcho, C. M., Nhuan, N. P., and Walker, T. H., 2008, *Biofuels engineering process technology* (McGraw-Hill New York, NY, USA:).

Duman, G., Uddin, M. A., and Yanik, J., 2014, "Hydrogen production from algal biomass via steam gasification," *Bioresource technology* **166**, 24–30.

Eichman, J., Townsend, A., and Melaina, M., 2016, *Economic assessment of hydrogen technologies participating in California electricity markets*, Tech. Rep. (National Renewable Energy Lab.(NREL), Golden, CO (United States)).

El-Emam, R. S., and Özcan, H., 2019, "Comprehensive review on the techno-economics of sustainable large-scale clean hydrogen production," *Journal of Cleaner Production* **220**, 593–609.

Fraga, A.-R., Gaines, A. F., and Kandiyoti, R., 1991, "Characterization of biomass pyrolysis tars produced in the relative absence of extraparticle secondary reactions," *Fuel* **70**, 803–809.

Fricke, K., Santen, H., Wallmann, R., Hüttner, A., and Dichtl, N., 2007, "Operating problems in anaerobic digestion plants resulting from nitrogen in msw," *Waste Management* **27**, 30–43.

Fu, J., Lu, X., and Savage, P. E., 2010, "Catalytic hydrothermal deoxygenation of palmitic acid," *Energy & Environmental Science* **3**, 311–317.

Gao, Y., Wang, X.-H., Yang, H.-P., and Chen, H.-P., 2012, "Characterization of products from hydrothermal treatments of cellulose," *Energy* **42**, 457–465.

Glavič, P., and Lukman, R., 2007, "Review of sustainability terms and their definitions," *Journal of cleaner production* **15**, 1875–1885.

González-Fernández, C., Sialve, B., Bernet, N., and Steyer, J.-P., 2012, "Impact of microalgae characteristics on their conversion to biofuel. part ii: Focus on biomethane production," *Biofuels, Bioproducts and Biorefining* **6**, 205–218.

Grima, E. M., Belarbi, E.-H., Fernández, F. A., Medina, A. R., and Chisti, Y., 2003, "Recovery of microalgal biomass and metabolites: process options and economics," *Biotechnology advances* **20**, 491–515.

Grimm, A., OÌĺhman, M., Lindberg, T., Fredriksson, A., and BostroÌĺm, D., 2012a, "Bed agglomeration characteristics in fluidized-bed combustion of biomass fuels using olivine as bed material," *Energy & Fuels* **26**, 4550–4559.

Grimm, A., Skoglund, N., BostroÌĺm, D., Boman, C., and OÌĺhman, M., 2012b, "Influence of phosphorus on alkali distribution during combustion of logging residues and wheat straw in a bench-scale fluidized bed," *Energy & Fuels* **26**, 3012–3023.

Grimm, A., Skoglund, N., BostroÌĺm, D., and OÌĺhman, M., 2011, "Bed agglomeration characteristics in fluidized quartz bed combustion of phosphorus-rich biomass fuels," *Energy & Fuels* **25**, 937–947.

Guo, J., Lou, H., Zhao, H., Chai, D., and Zheng, X., 2004, "Dry reforming of methane over nickel catalysts supported on magnesium aluminate spinels," *Applied Catalysis A: General* **273**, 75–82.

Harrison, K. W., Remick, R., Hoskin, A., and Martin, G., 2010, *Hydrogen production: fundamentals and case study summaries*, Tech. Rep. (National Renewable Energy Lab.(NREL), Golden, CO (United States)).

Hayward, D. O., and Trapnell, B. M. W., 1964, *Chemisorption* (Butterworths London).

He, Z., Lane, D. J., Saw, W. L., van Eyk, P. J., Nathan, G. J., and Ashman, P. J., 2018, "Ash–bed material interaction during the combustion and steam gasification of australian agricultural residues," *Energy & Fuels* **32**, 4278–4290.

Homs, N., Montané, D., and de la Piscina, P. R., 2018, "Biohydrogen and biomethane production," in *Sustainable Catalysis for Biorefineries*, pp. 300–339.

Huber, G. W., Cortright, R. D., and Dumesic, J. A., 2004, "Renewable alkanes by aqueous-phase reforming of biomass-derived oxygenates," *Angewandte Chemie International Edition* **43**, 1549–1551.

IEA Bioenergy, 2019, "Lessons learned about thermal biomass gasification,"

Johnson, M. C., and Tester, J. W., 2013, "Lipid transformation in hydrothermal processing of whole algal cells," *Industrial & Engineering Chemistry Research* **52**, 10988–10995.

Jüntgen, H., 1981, "Reactivities of carbon to steam and hydrogen and applications to technical gasification processesâĂŤa review," *Carbon* **19**, 167–173.

Jury, C., Benetto, E., Koster, D., Schmitt, B., and Welfring, J., 2010, "Life cycle assessment of biogas production by monofermentation of energy crops and injection into the natural gas grid," *Biomass and Bioenergy* **34**, 54–66.

Kalinci, Y., Hepbasli, A., and Dincer, I., 2009, "Biomass-based hydrogen production: a review and analysis," *International journal of hydrogen energy* **34**, 8799–8817.

Kayhanian, M., 1999, "Ammonia inhibition in high-solids biogasification: an overview and practical solutions," *Environmental Technology* **20**, 355–365.

Keiser, J. R., Lewis Sr, S. A., Connatser, R. M., Leonard, D. N., and Brady, M. P., 2018, *Materials Issues In Biomass Gasification*, Tech. Rep. (Oak Ridge National Lab.(ORNL), Oak Ridge, TN (United States)).

Kiel, J., Van Paasen, S., Neeft, J., Devi, L., Ptasinski, K., Janssen, F., Meijer, R., Berends, R., Temmink, H., Brem, G., *et al.*, 2004, "Primary measures to reduce tar formation in fluidised-bed biomass gasifiers," *ECN, ECN-C-04-014*

Kirkels, A. F., and Verbong, G. P., 2011, "Biomass gasification: Still promising? a 30-year global overview," *Renewable and Sustainable Energy Reviews* **15**, 471–481.

Kirubakaran, V., Sivaramakrishnan, V., Nalini, R., Sekar, T., Premalatha, M., and Subramanian, P., 2009, "A review on gasification of biomass," *Renewable and Sustainable Energy Reviews* **13**, 179–186.

Kitayama, Y., Watanabe, Y., Muramatsu, K., and Kodama, T., 1997, "Catalytic reduction of carbon dioxide on niîŮÿ cu alloys," *Energy* **22**, 177–182.

Klassen, V., Blifernez-Klassen, O., Wibberg, D., Winkler, A., Kalinowski, J., Posten, C., and Kruse, O., 2017, "Highly efficient methane generation from untreated microalgae biomass," *Biotechnology for biofuels* **10**, 186.

Klinthong, W., Yang, Y.-H., Huang, C.-H., and Tan, C.-S., 2015, "A review: microalgae and their applications in co2 capture and renewable energy," *Aerosol Air Qual Res* **15**, 712–742.

Kopyscinski, J., 2010, "Production of synthetic natural gas in a fluidized bed reactor," *Disseration ETH Zurich*

Krishnan, V., Thachanan, S., Matsumura, Y., and Uemura, Y., 2016, "Supercritical water gasification on three types of microalgae in the presence and absence of catalyst and salt," *Procedia engineering* **148**, 594–599.

Kumar, S. S., 2019, "Hydrogen production by pem water electrolysis–a review," *Materials Science for Energy Technologies*

Li, C., and Chen, Y.-W., 1995, "Temperature-programmed-reduction studies of nickel oxide/alumina catalysts: effects of the preparation method," *Thermochimica Acta* **256**, 457–465.

Li, M., 2019, "Syngas production from algae biomass gasification: the case of china," *Energy Sources, Part A: Recovery, Utilization, and Environmental Effects* **41**, 1474–1482.

Liobikienė, G., and Butkus, M., 2017, "The european union possibilities to achieve targets of europe 2020 and paris agreement climate policy," *Renewable Energy* **106**, 298–309.

Liu, G., Liao, Y., Wu, Y., Ma, X., and Chen, L., 2017, "Characteristics of microalgae gasification through chemical looping in the presence of steam," *International Journal of Hydrogen Energy* **42**, 22730–22742.

Liu, Y., and Liu, D., 1999, "Study of bimetallic cu–ni/$\gamma$-al2o3 catalysts for carbon dioxide hydrogenation," *International Journal of Hydrogen Energy* **24**, 351–354.

López-González, D., Fernandez-Lopez, M., Valverde, J., and Sanchez-Silva, L., 2014, "Comparison of the steam gasification performance of three species of microalgae by thermogravimetric–mass spectrometric analysis," *Fuel* **134**, 1–10.

Lü, F., Ji, J., Shao, L., and He, P., 2013, "Bacterial bioaugmentation for improving methane and hydrogen production from microalgae," *Biotechnology for biofuels* **6**, 92.

Manabe, A., Kashiwase, M., Hashimoto, T., Hayashida, T., Kato, A., Hirao, K., Shimomura, I., and Nagashima, I., 2013, "Basic study of alkaline water electrolysis," *Electrochimica Acta* **100**, 249–256.

Marcilla, A., Gómez-Siurana, A., Gomis, C., Chápuli, E., Catalá, M. C., and Valdés, F. J., 2009, "Characterization of microalgal species through tga/ftir analysis: Application to nannochloropsis sp.." *Thermochimica Acta* **484**, 41–47.

Mata, T. M., Martins, A. A., and Caetano, N. S., 2010, "Microalgae for biodiesel production and other applications: a review," *Renewable and sustainable energy reviews* **14**, 217–232.

Miao, X., Wu, Q., and Yang, C., 2004, "Fast pyrolysis of microalgae to produce renewable fuels," *Journal of analytical and applied pyrolysis* **71**, 855–863.

Milne, T. A., Evans, R. J., and Abatzaglou, N., 1998, *Biomass Gasifier"Tars": Their Nature, Formation, and Conversion*, Tech. Rep. (National Renewable Energy Laboratory, Golden, CO (US)).

Murali, G., and Shastri, Y., 2019, "Life-cycle assessment-based comparison of different lignocellulosic ethanol production routes," *Biofuels*, 1–11.

Mussgnug, J. H., Klassen, V., Schlüter, A., and Kruse, O., 2010, "Microalgae as substrates for fermentative biogas production in a combined biorefinery concept," *Journal of biotechnology* **150**, 51–56.

Nisamaneenate, J., Atong, D., and Sricharoenchaikul, V., 2012, "Steam reforming of tar model compound using pd catalyst on alumina tube," *Environmental technology* **33**, 2497–2505.

Nishikawa, J., Nakamura, K., Asadullah, M., Miyazawa, T., Kunimori, K., and Tomishige, K., 2008, "Catalytic performance of ni/ceo2/al2o3 modified with noble metals in steam gasification of biomass," *Catalysis today* **131**, 146–155.

Okolie, J. A., Rana, R., Nanda, S., Dalai, A. K., and Kozinski, J. A., 2019, "Supercritical water gasification of biomass: a state-of-the-art review of process parameters, reaction mechanisms and catalysis," *Sustainable energy & fuels* **3**, 578–598.

Ou, L., Thilakaratne, R., Brown, R. C., and Wright, M. M., 2015, "Techno-economic analysis of transportation fuels from defatted microalgae via hydrothermal liquefaction and hydroprocessing," *Biomass and Bioenergy* **72**, 45–54.

Parthasarathy, P., and Narayanan, K. S., 2014, "Hydrogen production from steam gasification of biomass: influence of process parameters on hydrogen yield–a review," *Renewable energy* **66**, 570–579.

Peters, M. S., Timmerhaus, K. D., West, R. E., Timmerhaus, K., and West, R., 2003, *Plant design and economics for chemical engineers*, Vol. 4 (McGraw-Hill New York).

Prelazzi, G., Cerboni, M., and Leofanti, G., 1999, "Comparison of h2adsorption, o2adsorption, h2titration, and o2titration on supported palladium catalysts," *Journal of Catalysis* **181**, 73–79.

Profeti, L. P., Ticianelli, E. A., and Assaf, E. M., 2009, "Production of hydrogen via steam reforming of biofuels on ni/ceo 2–al 2 o 3 catalysts promoted by noble metals," *International Journal of Hydrogen Energy* **34**, 5049–5060.

Purohit, G., 1983, "Estimating costs of shell-and-tube heat exchangers," *Chemical engineering* **90**, 56–67.

Raheem, A., Dupont, V., Channa, A. Q., Zhao, X., Vuppaladadiyam, A. K., Taufiq-Yap, Y.-H., Zhao, M., and Harun, R., 2017, "Parametric characterization of air gasification of chlorella vulgaris biomass," *Energy & Fuels* **31**, 2959–2969.

Rittmann, B. E., 2008, "Opportunities for renewable bioenergy using microorganisms," *Biotechnology and bioengineering* **100**, 203–212.

Rizwan, M., Lee, J. H., and Gani, R., 2013, "Optimal processing pathway for the production of biodiesel from microalgal biomass: A superstructure based approach," *Computers & Chemical Engineering* **58**, 305–314.

Rizwan, M., Lee, J. H., and Gani, R., 2015, "Optimal design of microalgae-based biorefinery: Economics, opportunities and challenges," *Applied Energy* **150**, 69–79.

Rizzo, A. M., Prussi, M., Bettucci, L., Libelli, I. M., and Chiaramonti, D., 2013, "Characterization of microalga chlorella as a fuel and its thermogravimetric behavior," *Applied energy* **102**, 24–31.

Rosenberg, J. N., Oyler, G. A., Wilkinson, L., and Betenbaugh, M. J., 2008a, "A green light for engineered algae: redirecting metabolism to fuel a biotechnology revolution," *Current opinion in Biotechnology* **19**, 430–436.

Rosenberg, J. N., Oyler, G. A., Wilkinson, L., and Betenbaugh, M. J., 2008b, "A green light for engineered algae: redirecting metabolism to fuel a biotechnology revolution," *Current Opinion in Biotechnology* **19**, 430 – 436.

Ruth, M., 2011, *Hydrogen Production Cost Estimate Using Biomass Gasification: Independent Review*, Tech. Rep. (National Renewable Energy Lab.(NREL), Golden, CO (United States)).

Salge, J., Dreyer, B., Dauenhauer, P., and Schmidt, L., 2006, "Renewable hydrogen from nonvolatile fuels by reactive flash volatilization," *Science* **314**, 801–804.

Sanchez-Silva, L., López-González, D., Garcia-Minguillan, A., and Valverde, J., 2013, "Pyrolysis, combustion and gasification characteristics of nannochloropsis gaditana microalgae," *Bioresource technology* **130**, 321–331.

Santos, N. O., Oliveira, S. M., Alves, L. C., and Cammarota, M. C., 2014, "Methane production from marine microalgae isochrysis galbana," *Bioresource technology* **157**, 60–67.

Sarkar, S., and Kumar, A., 2010, "Large-scale biohydrogen production from bio-oil," *Bioresource technology* **101**, 7350–7361.

Sehested, J., 2006, "Four challenges for nickel steam-reforming catalysts," *Catalysis Today* **111**, 103–110.

Sen Gupta, S., Shastri, Y., and Bhartiya, S., 2016, "Model-based optimisation of biodiesel production from microalgae," *Computers & Chemical Engineering* **89**, 222–249.

Sen Gupta, S., Shastri, Y., and Bhartiya, S., 2017, "Optimization of integrated microalgal biorefinery producing fuel and value-added products," *Biofuels, Bioproducts and Biorefining* **11**, 1030–1050.

Shaner, M. R., Atwater, H. A., Lewis, N. S., and McFarland, E. W., 2016, "A comparative technoeconomic analysis of renewable hydrogen production using solar energy," *Energy & Environmental Science* **9**, 2354–2371.

Sialve, B., Bernet, N., and Bernard, O., 2009, "Anaerobic digestion of microalgae as a necessary step to make microalgal biodiesel sustainable.." *Biotechnology advances* **27**, 409–416.

Sirdeshpande, A., and Preston, W. E., 2011 Mar. 17, "Integrated hydromethanation combined cycle process," uS Patent App. 12/882,408.

Skoglund, N., 2014, *Ash chemistry and fuel design focusing on combustion of phosphorus-rich biomass*, Ph.D. thesis (Umeå universitet).

Spath, P. L., Mann, M. K., and Amos, W. A., 2003, "Update of hydrogen from biomass – determination of the delivered cost of hydrogen,"

Sutton, D., Kelleher, B., and Ross, J. R., 2001, "Review of literature on catalysts for biomass gasification," *Fuel processing technology* **73**, 155–173.

Swanson, R., Platon, A., Satrio, J., Brown, R., and Hsu, D., 2010, "Techno-economic analysis of biofuels production based on gasification,"

Tanksale, A., Beltramini, J., Dumesic, J., and Lu, G., 2008, "Effect of pt and pd promoter on ni supported catalystsâĂŤa tpr/tpo/tpd and microcalorimetry study," *Journal of Catalysis* **258**, 366–377.

Tanksale, A., Beltramini, J. N., and Lu, G. M., 2010, "A review of catalytic hydrogen production processes from biomass," *Renewable and Sustainable Energy Reviews* **14**, 166–182.

Tapia-Venegas, E., Ramirez-Morales, J. E., Silva-Illanes, F., Toledo-Alarcón, J., Paillet, F., Escudie, R., Lay, C.-H., Chu, C.-Y., Leu, H.-J., Marone, A., *et al.*, 2015, "Biohydrogen production by dark fermentation: scaling-up and technologies integration for a sustainable system," *Reviews in Environmental Science and Bio/Technology* **14**, 761–785.

Taylor, B., Xiao, N., Sikorski, J., Yong, M., Harris, T., Helme, T., Smallbone, A., Bhave, A., and Kraft, M., 2013, "Techno-economic assessment of carbon-negative algal biodiesel for transport solutions," *Applied energy* **106**, 262–274.

Tigabwa, Y. A., 2018, "Kinetic study of reactive flash volatilization of biomass,"

Tiong, L., Komiyama, M., Uemura, Y., and Nguyen, T. T., 2016, "Catalytic supercritical water gasification of microalgae: Comparison of chlorella vulgaris and scenedesmus quadricauda," *The Journal of Supercritical Fluids* **107**, 408–413.

Tsukahara, K., and Sawayama, S., 2005, "Liquid fuel production using microalgae," *J Jpn Pet Inst* **48**, 251.

Turn, S., Kinoshita, C., Zhang, Z., Ishimura, D., and Zhou, J., 1998, "An experimental investigation of hydrogen production from biomass gasification," *International journal of hydrogen energy* **23**, 641–648.

Van Druten, G., and Ponec, V., 2000, "Hydrogenation of carbonylic compounds: Part i: Competitive hydrogenation of propanal and acetone over noble metal catalysts," *Applied Catalysis A: General* **191**, 153–162.

Wang, H., and Ruckenstein, E., 2000, "Carbon dioxide reforming of methane to synthesis gas over supported rhodium catalysts: the effect of support," *Applied Catalysis A: General* **204**, 143–152.

Wang, K., Brown, R. C., Homsy, S., Martinez, L., and Sidhu, S. S., 2013, "Fast pyrolysis of microalgae remnants in a fluidized bed reactor for bio-oil and biochar production," *Bioresource technology* **127**, 494–499.

Wang, T., Chang, J., Wu, C., Fu, Y., and Chen, Y., 2005, "The steam reforming of naphthalene over a nickel–dolomite cracking catalyst," *Biomass and Bioenergy* **28**, 508–514.

Ward, A., Lewis, D., and Green, F., 2014, "Anaerobic digestion of algae biomass: a review," *Algal Research* **5**, 204–214.

Wheeler, C., Jhalani, A., Klein, E., Tummala, S., and Schmidt, L., 2004, "The water–gas-shift reaction at short contact times," *Journal of catalysis* **223**, 191–199.

Wijffels, R. H., 2008, "Potential of sponges and microalgae for marine biotechnology," *Trends in biotechnology* **26**, 26–31.

Xie, L.-F., Duan, P.-G., Jiao, J.-L., and Xu, Y.-P., 2019, "Hydrothermal gasification of microalgae over nickel catalysts for production of hydrogen-rich fuel gas: effect of zeolite supports," *International Journal of Hydrogen Energy* **44**, 5114–5124.

Yang, H., Yan, R., Chen, H., Lee, D. H., Liang, D. T., and Zheng, C., 2006, "Pyrolysis of palm oil wastes for enhanced production of hydrogen rich gases," *Fuel processing technology* **87**, 935–942.

Zhang, Y., Brown, T. R., Hu, G., and Brown, R. C., 2013, "Comparative techno-economic analysis of biohydrogen production via bio-oil gasification and bio-oil reforming," *Biomass and bioenergy* **51**, 99–108.